

Please respect publisher's rights and refer only to the official version

dpnote-dirac-paper T<sub>E</sub>X 2022-06-08 12:17 ©2022 Iwai, Sadovskii & Zhilinskii  
Journal of Geometric Mechanics 2020, 12(3): 455-505 doi: 10.3934/jgm.2020021  
preprint at <http://purple.univ-littoral.fr/~sadvovski/downloads/dpD2019.pdf>

# Angular momentum coupling, Dirac oscillators, and quantum band rearrangements in the presence of momentum reversal symmetries

T. Iwai<sup>1</sup>, D. A. Sadovskii<sup>2</sup>, and B. I. Zhilinskii<sup>2</sup>

<sup>1</sup>*Department of Applied Mathematics and Physics, Kyoto University, Kyoto 606, Japan*

<sup>2</sup>*Department of Physics, Université du Littoral—Côte d'Opale, 59140 Dunkerque, France*

submitted September 27, 2019; revised February 27, 2020; published July 15, 2020 ([online](#))

## Abstract

We investigate the elementary rearrangements of energy bands in slow-fast one-parameter families of systems whose fast subsystem possesses a half-integer spin. Beginning with a simple case without any time-reversal symmetries, we analyze and compare increasingly sophisticated model Hamiltonians with these symmetries. The models are inspired by the time-reversal modification of the Berry phase setup which uses a family of quadratic spin-quadrupole Hamiltonians of [Mead, Phys. Rev. Lett. **59**, 161–164 (1987); Avron *et al*, Commun. Math. Phys. **124**(4), 595–627 (1989)]. An explicit correspondence between the typical quantum energy level patterns in the energy band rearrangements of the finite particle systems with compact slow phase space and those of the Dirac oscillator is found in the limit of linearization near the conical degeneracy point of the semi-quantum eigenvalues.

Special issue in honor of *James Montaldi*, edited by *Luis García-Naranjo*.

© American Institute of Mathematical Sciences

With 12 figures, 0 tables, and 45 bibliography entries. ms Id 190927-Zhilinskii

## 1 Introduction

The interest in the geometric and topological properties of parametric families of quantum Hamiltonians was largely stimulated by the seminal paper of Michael Berry [1984], who analyzed the evolution of the spin states with spin  $S = \frac{1}{2} \approx \|\mathbf{S}\|$  in the presence of the magnetic field  $\mathbf{B}$ . The system is governed by the linear Hamiltonian

$$\hat{H} = \mathbf{B} \cdot \hat{\mathbf{S}}. \quad (1.1)$$

When  $\mathbf{B}$  is made to vary adiabatically slowly, following a closed path in the regular domain  $\mathbb{R}_B^3 \setminus \{0\}$  of the parameter space, the eigenstates of (1.1) acquire a *geometric phase* [Berry, 1984, Wilczek and Shapere, 1989]. This phase can be seen as both a consequence and an indicator of the nontrivial topology of the system. To examine the topology more fully, we study the two eigenstate bundles defined by the eigenvalues  $\lambda_{1,2}(\mathbf{B})$  with  $S = \frac{1}{2}$ . Away from the degeneracy at  $\mathbf{B} = 0$ , and more specifically, over any sphere  $\mathbb{S}^2$  surrounding the origin in  $\mathbb{R}_B^3$ , and in particular over  $\{\mathbf{B}, \|\mathbf{B}\| = 1\}$ , we find that  $\lambda(\mathbf{B})$  define regular complex line bundles with Chern index  $c_1 = 1$  or  $-1$ .

## 1.1 Formal and dynamical control parameters. Their number

We like to point out that the parameters  $B$  in (1.1) can be chosen and changed at will within their domain and without any feedback from the system with Hamiltonian (1.1). In other words,  $B$  are not influenced in any way by the dynamics of the system. We will call such control parameters *formal*, *plain*, or *tuning*. Their physical origins should not obscure their formal character<sup>1</sup>. At the same time, parameters whose evolution is governed by the Hamiltonian of the system itself, i.e., whose (adiabatically slow) variation provokes a feedback from the fast system, will be called *dynamical*. In our work, we focus on slow–fast systems<sup>2</sup> with dynamical parameters. Dynamical parameters play the role of control parameters only in the semi-quantum system (see sec. 1.3). At the same time, they are dynamical variables of the complete system and of its slow subsystem.

The eigenstates of systems with a finite number of states, such as the system with Hamiltonian (1.1), are given by the eigenvectors of Hermitian matrices. The codimension of degeneracy of two eigenvalues of a general Hermitian matrix, regardless the dimension of the matrix itself (in other words, for any spin), is *three* [von Neumann and Wigner, 1929, Arnold, 1995, Iwai and Zhilinskiĭ, 2011]. So in the particular case of (1.1) and for  $S = \frac{1}{2}$ , the eigenvalues of the  $2 \times 2$  Hermitian matrix become degenerate in one single point  $B = 0$ . We conclude that in general, we may be interested in systems with one slow degree of freedom (two dynamical parameters) and one formal control parameter (see examples in sec. 1.3). In the presence of additional symmetries (sec. 2.3, 4, 5), the matrix of the quantum Hamiltonian and its spectrum may have specific additional properties. In particular, the minimal number of semi-quantum states (the dimension of the matrix) required to observe typical spectra, the kind of degeneracy, and the codimension may vary.

## 1.2 Semiclassical eigenstate bundles

It is important to notice that in general, with regard to parameters of the system, we distinguish two kinds of semi-quantum eigenstate bundles which we will denote  $\Lambda$  and  $\Delta$ . The base space of  $\Lambda$  is always the slow classical phase space  $P$  whose coordinates are dynamical parameters. This  $P$  is not necessarily a sphere, and it may not even be compact. The  $\Lambda$  bundle can be called *global*. The base space of  $\Delta$  is a sphere surrounding the degeneracy point in the total (dynamical-formal) control parameter space. The  $\Delta$  bundle is considered in the geometric phase framework. We may call it *local*. In the example in sec. 2.1,  $\Lambda$  and  $\Delta$  are the same bundle, while in sec. 2.2 they are rather different. In sec. 3 and 4, both  $\Lambda$  and  $\Delta$  are bundles over a sphere, but one is parameterized by dynamical parameters, while the other—by formal and dynamical control parameters. In the space of all parameters, the base spaces of  $\Lambda$  and  $\Delta$  intersect (appendix A.4). They have common closed loops parameterized entirely by dynamical variables for fixed formal control parameters. Furthermore, such loops may be periodic orbits of the slow classical system. Such periodic orbits exhibit *dynamical geometric phase* given by the Chern index of  $\Delta$ . Semiclassical quantization [Fuchs et al., 2010, Appendix A] provides one possible manifestation of such phase.

We observe further that global bundles  $\Lambda$  form continuous parametric families with regard to regular values of tuning control parameter(s)  $\mu$ , while there is one single local  $\Delta$  bundle for each degeneracy point (tuning parameters are often chosen so that degeneracies occur for critical value  $\mu = 0$ ). When tuning parameters  $\mu$  have several disconnected open domains of regular values (such as, in the simplest case, two

1 intervals with  $\mu < 0$  and  $\mu > 0$ ), the  $c_1$  indices of  $\Lambda$  bundles on each domain may  
 2 differ and the difference(s)  $\delta c_1$  or *delta-Chern* characterize the degeneracy point(s). At  
 3 the same time, the  $c_1$  indices of  $\Delta$  bundles contribute to  $\delta c_1$  (appendix A.4). While  
 4 the  $\Delta$  bundle construction ignores any differences between the dynamical and formal  
 5 control parameters,  $\Lambda$  bundles have an important dynamical interpretation. Their index  
 6 characterizes the number of slow quantum states which can be supported on  $P$  and this  
 7 relates  $\delta c_1$  to the number of redistributed quantum states, see more in sec. 1.3.

### 8 **1.3 Quantum, semi-quantum, and classical**

9 Dynamical parameterization enhances considerably the object of our study and places  
 10 it at crossroads of several powerful mathematical theories. It becomes universally im-  
 11 portant to many physical applications.

12 Within the geometric phase setup, we obtain a “fast” quantum system on a finite  
 13 Hilbert space  $\mathcal{H}_{\text{fast}}$  of low dimension (e.g., two for  $S = \frac{1}{2}$ ). The Hamiltonian of  
 14 this system is a combination of operators acting on  $\mathcal{H}_{\text{fast}}$  with coefficients depending  
 15 on classical dynamical variables  $(q, p)$  of the “slow” system and, possibly, additional  
 16 formal control parameters  $\mu$  which are also meant to be varied adiabatically slowly  
 17 (see footnote 2). The eigenstates are obtained as eigenvectors of a low-dimensional  
 18 Hermitian matrix whose eigenvalues  $\lambda(q, p)$  play the role of classical Hamiltonians  
 19 governing the dynamics of the slow system corresponding to each fast eigenstate. We  
 20 call this description *semi-quantum*.

21 At the same time, the fast and slow systems can be both treated as quantum and  
 22 can be described using the Hilbert space  $\mathcal{H}_{\text{fast}} \times \mathcal{H}_{\text{slow}}$ . Since the slow system has  
 23 a close and well defined classical limit,  $\mathcal{H}_{\text{slow}}$  is typically a much larger space, and,  
 24 if the underlying slow classical phase space is non-compact,  $\mathcal{H}_{\text{slow}}$  is infinite (Dirac  
 25 equation, Dirac oscillator in sec. 2.2). Different time-scales (footnote 2) result in a  
 26 specific structure of the energy spectrum and the localization patterns of the quantum  
 27 states of such system. The spectrum consists of *bands* with relatively large density and  
 28 number of states. Transitions between the states within a band correspond to excitations  
 29 in the slow degree of freedom, and, in most basic situations, energy alone is enough  
 30 to separate the bands: the in-band splittings are considerably smaller than the gaps  
 31 between the bands. In regular cases, the number of energy bands equals the number of  
 32 semi-quantum eigenvalues. When the latter have a degeneracy, the bands merge and  
 33 exchange energy levels. The reason for this exchange is in the nature of the dynamical  
 34 parameterization of the fast system. Near the degeneracy point, due to the interaction  
 35 between the two subsystems, the separation of the slow and fast dynamics becomes  
 36 blurred, and certain states localized near the degeneracy may change their character  
 37 and switch bands. We conclude that the degeneracy of semi-quantum eigenvalues is  
 38 the cause of both the geometric phase and this *redistribution phenomenon*.

39 To realize how considerable the relation and the interplay between the geometric  
 40 phase and the energy level redistribution is, we like to go a bit further into the structure  
 41 of the bands. For nondegenerate (typical) singularities, the number of the exchanged  
 42 states is much smaller than that of the states in the bands. In fact, most of the levels  
 43 are never exchanged and continue always within the same band. We call them “bulk”  
 44 states. Their number is given roughly by the symplectic volume of the underlying com-  
 45 pact slow classical phase space and may be obtained using an appropriate quantization  
 46 scheme (sec. 2.1). In the non-compact setting, this can be generalized using fractional  
 47 formal Chern number (A.25) in Appendix A.3. The few levels that can and do get ex-  
 48 changed are the “edge” states. In this context, the *correlation diagrams* showing how

1 levels continue when parameters cross the degeneracy point become very instrumental  
2 and are employed throughout the article (sec. 3, 4, and 5). The Chern index charac-  
3 terizing the bundle  $\Lambda$  of semi-quantum eigenvalues over the slow phase space gives,  
4 essentially, the number of missing/excessive edge states [Faure and Zhilinskiĭ, 2000,  
5 2001, 2002a, Iwai and Zhilinskiĭ, 2011, 2013, 2015, 2017]. More specifically, this in-  
6 dex gives the quantity by which the actual number of states in the band differs from  
7 that given by the symplectic volume of the underlying classical phase space. The same  
8 index, but computed for bundle  $\Delta$  gives the geometric phase, and it can be con-  
9 jectured that computation for all local  $\Delta$  bundles gives the number of redistributed states.  
10 For further generalization of the analysis of the redistribution phenomenon, an applica-  
11 tion of the Atiyah-Singer index theorem [Atiyah et al., 1975a,b, 1976] and geometric  
12 quantization principles Fedosov [1996] seems to be relevant.

13 The last but not the least, although being the least exploited in our present work,  
14 comes the fully classical description. Singularities of the slow-fast classical mechanical  
15 system with several (at least two) degrees of freedom are related to the semi-quantum  
16 degeneracies and, therefore, to the edge state redistribution. In particular, if the slow-  
17 fast system is integrable, such singularities are at the origin of *Hamiltonian monodromy*  
18 [Sadovskii and Zhilinskiĭ, 1999].

## 19 1.4 Main purpose and outline

20 Dynamical modifications of the original setup (1.1) open a large domain of diverse and  
21 versatile mathematical theory and applications which go far beyond the original geo-  
22 metric phase analysis. The latter remains, however, a vital organizing tool in the study  
23 of different dynamical parametric systems. Our main interest in this work is in the phe-  
24 nomenon of redistribution between the energy bands in the slow-fast systems [Faure  
25 and Zhilinskiĭ, 2001], and so we focus primarily on the full quantum system and its  
26 relation to the semi-quantum description. Among different symmetry properties which  
27 can be appropriate for concrete physical systems there is one particular property, the  
28 time reversal invariance (see note 5), which is considered as rather general due to its  
29 relevance across a very wide class of physical systems. In this work, we focus on time-  
30 reversal-invariant dynamical modifications. We also prefer uncovering systems which  
31 are fundamental and important to atomic and molecular (finite particle) applications.  
32 As a consequence, we analyze semi-quantum systems with compact slow phase spaces  
33 (such as the simple angular momentum coupling system in sec. 2.1) and relate them to  
34 non-compact examples (such as the Dirac oscillator in sec. 2.2) through linearization  
35 (sec. 2.1.4) and local description near the degeneracy of their semi-quantum eigen-  
36 values. The linearized systems with non-compact slow phase spaces may in turn be of  
37 importance to other fields, notably in solid state physics. The eventual distant but much  
38 desired outcome of this approach is a universal theory of redistribution phenomena.

39 In the context of sec. 1.3, the interest in finding dynamical equivalents of time-  
40 reversal invariant modifications by Mead [1987], Avron et al. [1988] of the original  
41 geometric phase setup (1.1) is quite substantial. As we explain in sec. 2.3, the system  
42 with the quadratic spin-quadrupole Hamiltonian of [Mead, 1987, Avron et al., 1988]  
43 has co-dimension 5, and, therefore, its dynamical analogues can have a slow phase  
44 space  $P$  of maximal dimension 4, i.e., four dynamical and one formal control param-  
45 eter. In our present work, however, we remain at the level of systems with only two dy-  
46 namical parameters (one slow degree freedom). Furthering substantial understanding  
47 of such systems allows uncovering possible consequences of the additional symmetries  
48 imposed by Mead [1987], Avron et al. [1988] and is a necessary precursor investigation

1 in preparation for larger dynamical models (sec. 6).

2 We outline the plan of the article. In sec. 2 we discuss two basic dynamical modifi-  
3 cations of (1.1) along with its time-reversal modification by Avron et al. [1988, 1989].  
4 In sec. 3 we return to the historically first simple dynamical modification of (1.1) sug-  
5 gested very early in 1988 by Pavlov-Verevkin et al. [1988] and analyzed further in  
6 [Sadovskii and Zhilinskiĭ, 1999, Faure and Zhilinskiĭ, 2000, Iwai and Zhilinskiĭ, 2011].  
7 Here we uncover the exact relation of this system to the Dirac oscillator.

8 The progression of different systems analyzed further in the paper is chosen so  
9 that the description of preceding simpler systems in sec. 2 and 3 helps towards under-  
10 standing subsequent systems, with increasingly smaller effort, through linearization,  
11 deformation, and discrete symmetry reduction. So turning to time-reversal-invariant  
12 systems in sec. 4, we come up with an angular momentum system whose Hamiltonian  
13 can be regarded as the most basic time-reversal deformation of the spin-orbit coupling  
14 term in sec. 2.1, itself the most natural and basic dynamical modification of the original  
15 Hamiltonian (1.1). It turns out that there is a 1:2 correspondence between this system  
16 and the non-symmetric case in sec. 3 and its Dirac oscillator linearization. As a conse-  
17 quence, Chern indices  $c_1$  and their change  $\delta c_1$  can be deduced essentially from the  
18 results in sec. 3. Otherwise, Chern indices can be computed directly for our model  
19 systems as detailed in Appendix A.

20 Finally, in sec. 5, we consider dynamical modifications of quadratic spin systems in  
21 [Mead, 1987, Avron et al., 1988, 1989] with spin  $\frac{3}{2}$ . We continue using angular momen-  
22 tum slow systems. Our particular modification has the time-reversal invariance group  
23 of order four including both the  $\mathcal{T}_S$ -symmetry of quadratic spin systems (sec. 2.3) and  
24 the  $\mathcal{T}$ -symmetry of systems with two angular momenta (sec. 2.1 and 4). Furthermore,  
25 like in all our spin- $\frac{1}{2}$  systems (sec. 2.1, 3, and 4), we have only one slow degree of  
26 freedom, which is, in this case, not the maximal possibility. With the minimal number  
27 of dynamical parameters, the redistribution phenomena in such quadratic spin-orbit  
28 systems turn out to be in 1:2 correspondence with the preceding spin- $\frac{1}{2}$   $\mathcal{T}$ -invariant  
29 system in sec. 4. However, while four individual levels get exchanged between the  
30 bands, the total number of states in the bands remains unchanged, i.e., redistributions  
31 occur “both ways” and the bulk phenomenon amounts to 0. The detailed Chern index  
32 analysis reflects the topological origins of this arrangement.

## 33 2 Three basic examples

34 We begin with simple modifications of the original setup with Hamiltonian (1.1) which  
35 illustrate sec. 1.1 and 1.3. The details in each example are instructive to follow. They  
36 help understanding the key elements in the analysis of the systems in sec. 3, 4, and 5.

### 37 2.1 Spin-orbit coupling

38 One of the simplest and most direct dynamical analogues of (1.1) is the Hamiltonian

$$39 \hat{H} = N \cdot \hat{S}, \quad (2.1a)$$

40 where  $N$  represents the mechanical angular momentum of the system. In atomic  
41 physics, this momentum is called orbital and denoted by  $L$ , but for us its physical  
42 origin can lie elsewhere, e.g., it can be associated with a degenerate molecular vibra-  
43 tion, or with the overall rotation of a molecule. Nevertheless, for brevity, we like to call  
44 the right hand side of (2.1a) the *spin-orbit coupling* term.

As discussed in sec. 1.3, dynamically parameterized semi-quantum Hamiltonian (2.1a), is accompanied by the fully quantum Hamiltonian

$$\hat{H} = \hat{\mathbf{N}} \cdot \hat{\mathbf{S}}, \quad (2.1b)$$

and the fully classical Hamiltonian

$$H = \mathbf{N} \cdot \mathbf{S}. \quad (2.1c)$$

Since both  $\|\mathbf{N}\|$  and  $\|\mathbf{S}\|$  Poisson commute with (2.1c), we can fix respective values<sup>3</sup> of  $N$  and  $S$  when analyzing systems with Hamiltonians (2.1). This means that the classical (slow) phase space of the semi-quantum system is the 2-sphere  $\mathbb{S}_N^2$ , the set of all orientations<sup>4</sup> of  $\mathbf{N}$ . Furthermore, the phase space of the fully classical system is  $\mathbb{S}^2 \times \mathbb{S}^2$ , while the  $(2S + 1)(2N + 1)$ -dimensional Hilbert space of the corresponding fully quantum system

$$\mathcal{H}_{S,N} = \mathcal{H}_S \otimes \mathcal{H}_N$$

is spanned by eigenfunctions  $|S, \sigma\rangle|N, \eta\rangle$  of  $\hat{S}_1$  and  $\hat{N}_1$ , such that

$$\hat{S}_1|S, \sigma\rangle|N, \eta\rangle = \sigma|S, \sigma\rangle|N, \eta\rangle \quad \text{and} \quad \hat{N}_1|S, \sigma\rangle|N, \eta\rangle = \eta|S, \sigma\rangle|N, \eta\rangle$$

with  $\sigma = -S, -S + 1, \dots, S - 1, S$  and  $\eta = -N, -N + 1, \dots, N - 1, N$ . The above basis implies well separated fast and slow subsystems and is called *uncoupled*.

### 2.1.1 The semi-quantum system with spin $\frac{1}{2}$

For a given fast system with spin  $S$ , the semi-quantum Hamiltonian (2.1a) becomes a  $(2S + 1)$ -dimensional Hermitian matrix defined on  $\mathbb{S}_N^2$ . Rewriting (2.1a) in terms of  $\text{so}(3)$  ladder operators

$$N_{\pm} = N_2 \pm iN_3 \quad \text{and} \quad \hat{S}_{\pm} = \hat{S}_2 \pm i\hat{S}_3, \quad (2.2)$$

we can find its matrix from the action of  $\hat{S}_{\pm}$  on  $|S, \sigma\rangle$ . Specifically, using

$$\langle \frac{1}{2}, \frac{1}{2} | \hat{S}_+ | \frac{1}{2}, -\frac{1}{2} \rangle = \langle \frac{1}{2}, -\frac{1}{2} | \hat{S}_- | \frac{1}{2}, \frac{1}{2} \rangle = \sqrt{(S + \frac{1}{2})(S - \frac{1}{2} + 1)} = 1,$$

we arrive at the  $S = \frac{1}{2}$  spinor representation of (2.1a)

$$\hat{H} = \frac{1}{2} \begin{pmatrix} -N_1 & N_+ \\ N_- & N_1 \end{pmatrix} \quad (2.3)$$

in the basis  $\{|\frac{1}{2}, -\frac{1}{2}\rangle, |\frac{1}{2}, \frac{1}{2}\rangle\}$ .

Coordinates on  $\mathbb{S}_N^2$  are dynamical parameters of (2.1a), while the third control parameter  $N$  (see footnote 3) is formal. In the particular example (2.1), the spherical symmetry results in the conservation of the norm  $\|\mathbf{J}\|$  of the total angular momentum

$$\mathbf{J} = \mathbf{N} + \mathbf{S},$$

and in constant eigenvalues of (2.3)

$$\lambda_{1,2}(N) = \pm \frac{1}{2}N. \quad (2.4)$$

The slow dynamics is trivial. The degeneracy of the two constant eigenvalues (2.4) themselves is, in turn, achieved for  $N = 0$ .

### 2.1.2 Topologically nontrivial energy bands

Even though the slow dynamics is trivial, the topology of the parametric semi-quantum system with Hamiltonian (2.3) is not: just like in the original Berry system with Hamiltonian (1.1), the two semi-quantum eigenfunction bundles  $\Lambda_{1,2}$  over  $\mathbb{S}_N^2$  have Chern indices  $\pm 1$ , see Appendix A.1. It is important to uncover how the spectrum of the fully quantum Hamiltonian (2.1b) reflects this. The  $\text{SO}(3)$  isotropy of (2.1b) means that the spectrum is joint with operator  $\|\hat{\mathbf{J}}\|$ , and that the eigenstates are labeled by the respective quantum number  $J$  along with  $N$  and  $S$ . Rewriting (2.1b) as

$$\hat{H} = \frac{1}{2} \hat{\mathbf{J}}^2 - \frac{1}{2} (\hat{\mathbf{N}}^2 + \hat{\mathbf{S}}^2),$$

we can see immediately that its spectrum is given by

$$\frac{1}{2} (J(J+1) - N(N+1) - S(S+1))$$

and that for given constant  $N$  and  $S$ , this spectrum has  $(2J+1)$ -degenerated discrete multiplets corresponding to possible values  $|N-S|, |N-S|+1, \dots, N+S$  of  $J$ . The spectrum domain  $[-(N+1)S, NS]$  is delimited by the energies of multiplets with  $J = N-S$  and  $N+S$ , respectively. So, in particular, the upper and lower multiplets of the  $S = \frac{1}{2}$  system consist of  $2N+2$  and  $2N$  levels, respectively. In the limit  $N \gg 1$ , as detailed further in sec. 2.3.3, the energies of multiplets are pseudo-symmetric with respect to energy 0.

The two multiplets of the  $S = \frac{1}{2}$  system are the *energy bands* corresponding to the two semi-quantum eigenvalues  $\lambda_{1,2}(N)$ . Recall that a multiplet of an isolated system with fixed norm  $N$  of angular momentum  $N$  has  $2N+1$  levels. This number corresponds to the symplectic volume of the underlying classical phase space  $\mathbb{S}_N^2$  (plus a quantum correction due to sphere's curvature). The number of levels  $\mathcal{N}_{1,2}$  in the two bands of the  $S = \frac{1}{2}$  system differs from  $2N+1$  by  $\pm 1$ . The difference  $2N+1 - \mathcal{N}_{1,2}$  equals the values of Chern indices  $c_1$  of  $\Lambda_{1,2}$ , see Appendix A. This is not coincidental. The bands of the coupled system reflect the nontrivial topology of the semi-quantum description [Faure and Zhilinskiĭ, 2000, Iwai and Zhilinskiĭ, 2011].

### 2.1.3 Possible deformations

In order to have the nontrivial slow dynamics and split energy bands, the spherical isotropy of (2.1) should be removed. At the same time, there is an option of retaining its time-reversal<sup>5</sup> invariance

$$\mathcal{T} : (S, N) \rightarrow (-S, -N), \tag{2.5}$$

under which *both* angular momenta  $N$  and  $S$  change sign. In sec. 3 we revisit the simple system [Pavlov-Verevkin et al., 1988] with  $\text{SO}(3)$  broken down to its  $\text{SO}(2)$  subgroup (axial symmetry) and no  $\mathcal{T}$ -symmetry, while in sec. 4, we introduce an axially symmetric and  $\mathcal{T}$ -equivariant deformation of (2.1). In both cases, we have slow dynamics. The semi-quantum eigenvalues are not constant over the phase space  $\mathbb{S}_N^2$ , and the latter is foliated with typical constant level sets being periodic orbits  $\mathbb{S}^1$ . The degeneracy of the bands may still occur locally, at certain points on  $\mathbb{S}_N^2$ . This brings us to the next section.

## 2.1.4 Describing and linearizing the slow dynamics

The dynamics of a classical slow system on  $\mathbb{S}_N^2$  with Hamiltonian  $\lambda : \mathbb{S}_N^2 \rightarrow \mathbb{R}$  can be described using the Poisson algebra  $\mathfrak{so}(3)$  generated by  $(N_1, N_2, N_3)$  to obtain the Euler-Poisson equations of motion  $\dot{\mathbf{N}} = \{\mathbf{N}, \lambda(\mathbf{N})\}$  and  $\dot{N} = 0$ . A generic semi-quantum Hermitian  $2 \times 2$  matrix, such as the one we will encounter in sec. 3, has three real control parameters [von Neumann and Wigner, 1929, Arnold, 1995]. This means that the degeneracy of the eigenvalues  $\lambda$  does typically occur in an isolated point  $x \in \mathbb{S}_N^2$  and for an isolated value of the third formal control parameter. The local study near  $x$  uncovers universal features of quantum, semi-quantum, and classical slow-fast systems with one slow degree of freedom undergoing degeneracy of their semi-quantum eigenvalues. In other words, while such systems may be very different globally, they are equivalent in their behaviour near the isolated degeneracy point. For the semi-quantum systems, the local study of slow dynamics is based on the linearized equations of slow motion at  $x$ .

In the subsequent sections, we deform (2.1) so that the semi-quantum eigenvalues of the deformed systems have generic degeneracies at one or both poles of the slow phase space  $\mathbb{S}_N^2$ , and we study the respective linearizations. At the north pole with  $N_1 = N$ , the Poisson bracket  $\{N_2, N_3\} = N_1 = N$  suggests that in the most basic, lowest order (linear) approximation, the local symplectic coordinates  $(q, p)$  of the chart  $\mathbb{R}_{q,p}^2$  at this pole should be chosen as

$$(q, p) = (N_2, N_3)/\sqrt{N} + O((q, p)^2), \quad (2.6a)$$

while at the origin  $(q, p) = 0$  of the chart, we have

$$N_1/N = 1 + O((q, p)^2). \quad (2.6b)$$

The south pole linearization with  $N_1 = -N$  differs in the definition of coordinates  $(q, p)$  as summarized below

$N_1/N$	$\{N_2, N_3\}$	$(q, p)$	$N_{\pm}$	$N_1$	
+1	+N	$(N_2, N_3)/\sqrt{N}$	$a^{\mp}\sqrt{2N}$	$N - n$	(2.7)
-1	-N	$(N_3, N_2)/\sqrt{N}$	$\pm i a^{\pm}\sqrt{2N}$	$n - N$	

with standard oscillator creation-annihilation operators

$$a^{\dagger} = a^+ := \frac{q - ip}{\sqrt{2}} = \bar{z}/\sqrt{2} \quad \text{and} \quad a = a^- := \frac{q + ip}{\sqrt{2}} = z/\sqrt{2}. \quad (2.8)$$

Replacing  $N_1$  and  $N_{\pm}$  in (2.3) according to (2.7) gives the spinor forms of (2.1a) linearized near each pole. Specifically, at the pole with  $N_1 \approx N$  we compute

$$\hat{H}|_{N_1=N} = \mu(2\mu, \sqrt{2}q, \sqrt{2}p) \cdot \hat{\mathbf{S}} = \mu \begin{pmatrix} -\mu & a^- \\ a^+ & \mu \end{pmatrix} \quad \text{with} \quad \mu = \frac{\sqrt{N}}{\sqrt{2}}. \quad (2.9)$$

The linearized spinor form (2.9) is the most basic universal local representation of any dynamical analogue of the geometric phase setup with Hamiltonian (1.1).

Linearization is deeply related to the slow phase space localization (footnote 11) of the quantum eigenstates. In the full quantum description, the slow phase space becomes a set of coherent states localized at points on  $\mathbb{S}_N^2$  [Zhang et al., 1990], i.e., a set of functions  $|N, N\rangle$  with all possible orientations of  $N$ . Since the slow dynamics for



1 Hamiltonian (2.1) is trivial, we can associate every state in the  $2J + 1$  degenerate mul-  
 2 tiplet of the full quantum system with a specific localized coherent state. Linearization  
 3 (2.9) describes what happens to this localized state when formal control parameter  $\mu$  is  
 4 varied. In sec. 3 and later, such description will apply to the exceptional *edge* state(s).  
 5 We like also to note that linearization (2.9) can be used to calculate the Chern indices  
 6  $c_1$  of the semi-quantum eigenfunction bundle  $\Lambda_{1,2}$  over  $\mathbb{S}_{N>0}^2$ . The specific “excep-  
 7 tional point” (see Appendix A.1) where we linearize is coordinate-dependent, but the  
 8 existence of such point (for any coordinates) reflects the non-triviality of  $\Lambda$ .

## 9 2.2 Dirac oscillator

10 The one-dimensional (1D) Dirac oscillator [Moshinsky and Szczepaniak, 1989], a vari-  
 11 ation on the theme of the Dirac equation, is the basic dynamical modification of the  
 12 geometric phase setup with Hamiltonian (1.1). Using variables (2.8) and spin  $S = \frac{1}{2}$ ,  
 13 the semi-quantum Hamiltonian of this system can be written as

$$14 \quad \hat{H} = \mu \begin{pmatrix} -1 & 0 \\ 0 & 1 \end{pmatrix} + \begin{pmatrix} 0 & a^\dagger \\ a & 0 \end{pmatrix}. \quad (2.10)$$

15 The dynamical parameters  $(q, p)$  of (2.10) are symplectic coordinates on the noncom-  
 16 pact phase space  $\mathbb{R}_{(q,p)}^2$ . We notice immediately that for a particular value of  $\mu$ , this  
 17 Hamiltonian corresponds to the linearized spin-orbit Hamiltonian (2.9). In fact, we  
 18 will see that linearization of the angular momentum system in sec. 3 provides the cor-  
 19 respondence for the entire family (2.10). The eigenvalues of (2.10)

$$20 \quad \lambda_{1,2} = \pm \sqrt{n + \mu^2}$$

21 with classical oscillator action<sup>6</sup>

$$22 \quad n = \frac{1}{2}(q^2 + p^2) \geq 0,$$

23 are distinct as long as we stay away from  $\mu = q = p = 0$ , where they vanish. The ad-  
 24 ditional third formal control parameter  $\mu$  is needed to have a handle on the sole degener-  
 25 eracy point of  $\lambda_{1,2}$ . The slow dynamics in  $\mathbb{R}_{(q,p)}^2$  consists of motion along the circular  
 26 orbits with constant  $n$  and a single equilibrium at  $n = 0$  (and  $\mu \neq 0$ ). The equations of  
 27 motions for  $(q, p)$  are defined by the Hamiltonian function  $\lambda_{1,2}$ , cf. sec. 2.1.4.

28 The major flaw of the previous example in sec. 2.1, is that the degeneracy of its  
 29 semi-quantum eigenvalues is not generic dynamically because it coincides with the  
 30 whole slow phase space contracting to one point (a singularity of the slow dynamical  
 31 system). In particular, this means that the typical energy level redistribution cannot  
 32 be observed with such parameterization. The Dirac oscillator with Hamiltonian (2.10)  
 33 poses no such problem. Its degeneracy occurs at a regular point  $n = \mu = 0$ .

34 The indices  $c_1 = \pm 1$  of the  $\Delta_{1,2}$  bundles over the 2-sphere in the parameter space  
 35  $\mathbb{R}_{(\mu,q,p)}^3$  encircling the origin give the number of levels which the two energy bands of  
 36 the full quantum system gain/lose as  $\mu$  varies through 0. In other words,  $c_1$  gives the  
 37 number of redistributed levels  $\delta\mathcal{N}$ . The construction and analysis of  $\Delta_{1,2}$  is analogous  
 38 to that in the original geometric phase setup [Simon, 1983, Wilczek and Shapere, 1989]  
 39 because the operator form of (2.10)

$$40 \quad \hat{H} = 2\mu \hat{S}_1 + \sqrt{2}q \hat{S}_2 - \sqrt{2}p \hat{S}_3 = 2\mu \hat{S}_1 + a_- \hat{S}_+ + a_+ \hat{S}_-,$$

1 where we used cyclic components in (2.2) and (2.8), reproduces (1.1) with  $\mathbf{B} =$   
2  $(2\mu, \sqrt{2}q, -\sqrt{2}p)$ . The relation between  $\mathbf{B}$  and the concrete parameters of the system  
3 defines the sign in the relation between  $c_1$  and  $\delta\mathcal{N}$ , see appendices A.2–A.3. On the  
4 other hand, comparing the spectra of (2.9) and (2.10), these indices can be computed  
5 essentially in the same way as for the  $\Lambda$  bundles of the spin-orbit system in sec. 2.1  
6 at constant  $N > 0$  which in turn go back to the original geometric phase setup (with  
7  $\mathbf{B} = \mathbf{N}$ ), see appendix A.1 and A.4. A different calculation, using  $\Lambda_{1,2}$  bundles for  
8  $\mu < 0$  and  $\mu > 0$  with specific boundary conditions [Iwai and Zhilinskiĭ, 2016] yields  
9 the same result as “delta-Chern”  $\delta c_1$  by taking the difference of indices before and after  
10 degeneracy for the non-compact classical phase space, see appendix A.3.

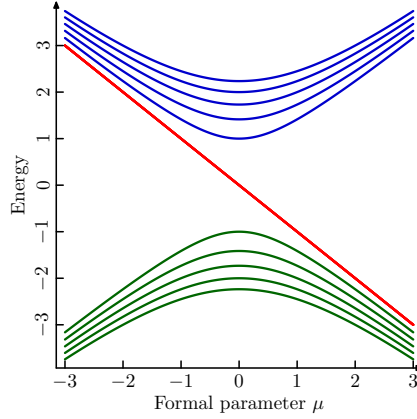


**Figure 1:** Spectrum of the Dirac oscillator with  $S = \frac{1}{2}$  as function of formal control parameter  $\mu$ . The energies of the bulk states (blue and green) and of the edge state (red) are given by (2.12).

11 The quantum spectrum of (2.10) can be computed straightforwardly after we realize  
12 that the system has a Lie symmetry with generator  $\hat{n} + \hat{S}_1$ . Using harmonic oscillator  
13 wavefunctions  $|n\rangle$  with  $n \in \mathbb{Z}_{\geq 0}$  as a basis in the infinite-dimensional Hilbert space  
14  $\mathcal{H}_{\text{slow}}$ , we can split  $\mathcal{H}_{S=\frac{1}{2}} \times \mathcal{H}_{\text{slow}}$  into a union of two-dimensional subspaces of eigen-  
15 functions of  $\hat{n} + \hat{S}_1$  with the same positive half-integer eigenvalue  $k$ ,

$$16 \quad \psi_k = \sum_{\sigma} c_{\sigma,k} |S, \sigma\rangle |k - \sigma\rangle \quad \text{with } S = \frac{1}{2}, \sigma = \pm \frac{1}{2}, \text{ and } k > 0,$$

17 and an exceptional sole function

$$18 \quad \psi_{-\frac{1}{2}} = |\frac{1}{2}, -\frac{1}{2}\rangle |0\rangle.$$

19 Replacing (2.8) for their quantum analogs and recalling the action of operators

$$20 \quad \hat{a}^\dagger |n-1\rangle = \sqrt{n} |n\rangle \quad \text{and} \quad \hat{a} |n\rangle = \sqrt{n} |n-1\rangle, \quad (2.11)$$

21 we compute the action of (2.10) on  $\psi_k$  and find its eigenvalues

$$22 \quad \lambda_{-\frac{1}{2}} = -\mu, \quad \lambda_k = \pm \sqrt{\mu^2 + n}, \quad \text{with } n = k + \frac{1}{2} \in \mathbb{Z}_{>0}. \quad (2.12)$$

23 As illustrated in fig. 1, the bulk states  $\psi_k$  with  $k > 0$  have a pseudo-symmetric spectrum  
24 with upper (positive) and lower (negative) bands separated by at least 2. The edge

1 state  $\psi_{-\frac{1}{2}}$  passes between the bands when the formal control parameter  $\mu$  changes  
 2 sign. We recognize the redistribution phenomenon described in sec. 1.3 and note the  
 3 universality of the eigenvalue expression (2.12) which is encountered, with variations  
 4 and iterations, across many fields, notably in quantum Hall effect [Haldane, 1988] and  
 5 spin-orbit coupling [Pavlov-Verevkin et al., 1988]. Multiplying (2.10) by  $-1$  alternates  
 6 the “direction” in which the edge state transfers as  $\mu$  increases through 0 (top down in  
 7 fig. 1). Parameterizations in sec. 3 and 4 result in the opposite direction, while both  
 8 directions occur simultaneously in sec. 5 as two copies of (2.10) with different signs  
 9 appear in the linearized semi-quantum  $4 \times 4$  matrix Hamiltonian.

10 It is also remarkable that for large  $n$ , when small quantum corrections to the classi-  
 11 cal action can be ignored (footnote 6), the quantum bulk energies  $\lambda_k$  match the eigen-  
 12 values  $\pm\sqrt{\mu^2 + I}$  of the semi-quantum Hamiltonian (2.10), i.e., the semi-quantum  
 13 energies. Examining the semiclassical description of the two classical dynamical sys-  
 14 tems on the slow phase space  $\mathbb{R}_{q,p}^2$  whose Hamiltonians are given by the eigenvalues  
 15 of (2.10), we can reveal the reasons why the classical action  $I$  is quantized as  $\tilde{n} + 1$   
 16 with  $\tilde{n} \in \mathbb{R}_{\geq 0}$ , i.e., with a quantum correction of 1. In such systems, phase corrections  
 17 combine the usual WKB contribution of  $\pi$  and the geometric phase shift [Fuchs et al.,  
 18 2010, Appendix A].

### 19 2.3 Spin-quadrupole system and its dynamical modification

20 The quadratic spin-quadrupole interaction Hamiltonian

$$21 \quad \hat{H} = \hat{S}Q\hat{S} \quad (2.13)$$

22 with five-parameter traceless symmetric matrix  $Q$  representing *electric quadrupole* is  
 23 of particular interest to our present study. Being invariant under reversal symmetry

$$24 \quad \mathcal{T}_S : \hat{S} \rightarrow -\hat{S}, \quad (2.14)$$

25 Hamiltonian (2.13) was proposed by Mead [1987], Avron et al. [1988, 1989] as a time-  
 26 reversal (cf. footnote 5) modification of (1.1). Our study of  $\mathcal{T}$ -invariant slow-fast sys-  
 27 tems is motivated by an attempt to find a dynamical equivalent of the geometric phase  
 28 analysis in [Mead, 1987, Avron et al., 1988, 1989].

29 Drawing the parallel with (1.1) requires, naturally, to consider states with half-  
 30 integer spin. For such states, the presence of time-reversal invariance of (2.13) has  
 31 one important consequence, known as *Kramers degeneracy* [Kramers, 1930, Wigner,  
 32 1932]: all quantum levels of the system form strictly degenerate doublets whose com-  
 33 ponents are related by the symmetry operation (2.14). It follows that unveiling the  
 34 spectrum of (2.13) requires more states in the fast subsystem. The minimal number  
 35 of these states is four. They can be realized as four spin components with  $S = \frac{3}{2}$   
 36 which combine into two Kramers degenerate pairs<sup>7</sup>. So just like (1.1), Hamiltonian  
 37 (2.13) for  $S = \frac{3}{2}$  has typically two distinct eigenvalues  $\lambda_{1,2}(Q)$ . These eigenvalues  
 38 will correspond to the semi-quantum eigenvalues, and comparing to the linear system  
 39 with Hamiltonian (2.1), we will have again two quantum bands, but each will now be  
 40 doubly degenerate.

41 The matrix of Hamiltonian (2.13) in the spinor basis

$$42 \quad \left\{ \left| \frac{3}{2}, \frac{1}{2} \right\rangle, \left| \frac{3}{2}, -\frac{1}{2} \right\rangle, \left| \frac{3}{2}, \frac{3}{2} \right\rangle, \left| \frac{3}{2}, -\frac{3}{2} \right\rangle \right\} \quad (2.15)$$

1 is of the general *quaternionic* form

$$2 \quad \begin{pmatrix} g & 0 & -c + id & a - ib \\ 0 & g & a + ib & c + id \\ -c - id & a - ib & -g & 0 \\ a + ib & c - id & 0 & -g \end{pmatrix} = \begin{pmatrix} G & M \\ M^\dagger & -G \end{pmatrix} \quad (2.16)$$

3 with eigenvalues

$$4 \quad \lambda_\pm(Q) = \pm \sqrt{g^2 + d^2 + c^2 + b^2 + a^2}$$

5 of multiplicity 2, and so it follows that the codimension now is 5. In the parameter space  
6  $\mathbb{R}^5$ , the sole degeneracy point 0 is now surrounded by  $\mathbb{S}^4$ . The second Chern index  $c_2$  is  
7 required to characterize the respective eigenstate bundles  $\Delta_{1,2}$ . A dynamical extension  
8 of (2.13) can have a slow subsystem with two degrees of freedom and, therefore, four  
9 dynamical and one formal control parameter. On the other hand, adding several formal  
10 control parameters, we can continue with one slow degree of freedom (sec. 5). Unless  
11 the slow phase space is flat, correspondence with [Mead, 1987, Avron et al., 1989] will  
12 require linearization and local analysis.

### 13 2.3.1 Time reversal symmetries

14 In comparison to (2.1), the spin-quadrupole Hamiltonian (2.13) has one clear and es-  
15 sential difference: the reversal operation (2.14) acts *exclusively* on spin components  
16 and does not affect the five formal control parameters of the system, the components  
17 of the electric quadrupole  $Q$ . As a consequence, (2.13) is quadratic in  $\mathcal{S}$ . On the other  
18 hand, our dynamical parameters  $N$  are engaged by time reversal (2.5). This makes us  
19 to distinguish reversal operations

$$20 \quad \mathcal{T}_S : (N, \mathcal{S}) \rightarrow (N, -\mathcal{S}), \quad \mathcal{T}_N : (N, \mathcal{S}) \rightarrow (-N, \mathcal{S}), \quad \text{and} \quad \mathcal{T} = \mathcal{T}_S \wedge \mathcal{T}_N$$

21 generating an order-4 group  $Z_2 \times Z_2$ . Since (2.1) and its  $\mathcal{T}$ -equivariant deforma-  
22 tions in sec. 4 are not  $\mathcal{T}_S$ -invariant, they cannot be dynamical analogues of (2.13). We  
23 should turn to terms of degree 2 in  $\mathcal{S}$ , and furthermore, we can introduce “dynamical  
24 quadrupole”  $Q$  (sec. 2.3.2) as a symmetric rank-2 tensor constructed of slow variables.  
25 Depending on the choice of the slow subsystem and on the particular construction,  
26 the resulting system may also come out fully  $\mathcal{T}$ -invariant, but it will be at least  $\mathcal{T}_S$ -  
27 symmetric.

### 28 2.3.2 Dynamical “quadrupole” and spin-quadrupole interaction

29 From the components of the standard rank-1 spherical tensor  $T^1(\mathcal{S})$

$$30 \quad T_0^1(\mathcal{S}) = S_1 \quad \text{and} \quad T_{\pm 1}^1(\mathcal{S}) = \mp S_\pm,$$

31 we construct the  $\mathcal{T}_S$ -invariant tensor of rank 2

$$32 \quad T^2(\mathcal{S}) = [T^1(\mathcal{S}) \times T^1(\mathcal{S})]^2$$

33 with components [Zare, 1988, Appendix 13, eqs.(8–10)]

$$34 \quad T_0^2(\mathcal{S}) = \frac{1}{\sqrt{6}}(3S_1^2 - \mathcal{S}^2), \quad T_{\pm 1}^2(\mathcal{S}) = \mp \frac{1}{2}[S_1, S_\pm]_+ \quad \text{and} \quad T_{\pm 2}^2(\mathcal{S}) = \frac{1}{2}S_\pm^2.$$

1 In the same fashion, we construct  $T^2(\mathbf{N})$  which models the electric quadrupole  $Q$ . In  
 2 terms of these tensors<sup>8</sup>, the closest degree-2 analog of (2.1) can be written as

$$3 \quad \hat{H} = \sqrt{5} \left[ T^2(\hat{\mathbf{S}}) \times T^2(\hat{\mathbf{N}}) \right]^0 = \left( (\hat{\mathbf{S}} \cdot \hat{\mathbf{N}})^2 - \frac{1}{3} \hat{\mathbf{S}}^2 \hat{\mathbf{N}}^2 \right). \quad (2.17)$$

4 Like (2.1), it is spherically symmetric. In the classical limit for  $\hat{\mathbf{N}}$  and spin- $\frac{3}{2}$  basis  
 5 (2.15), the corresponding semi-quantum spin Hamiltonian can be written as a quadratic  
 6 form (2.13) whose real symmetric traceless matrix  $Q(\mathbf{N})$  has elements<sup>9</sup>

$$7 \quad Q_{ii} = N_i^2 - \frac{1}{3} N^2 \quad \text{and} \quad Q_{ij} = N_i N_j.$$

8 In the same basis, quantum Hamiltonian (2.17) is represented as a  $4 \times 4$  matrix operator  
 9 whose matrix has quaternionic form (2.16) with

$$10 \quad g = \frac{1}{2} \left( N^2 - 3\hat{N}_1^2 \right) \quad (2.18a)$$

11 and the off-diagonal block

$$12 \quad \hat{M} = \frac{\sqrt{3}}{2} \begin{pmatrix} [\hat{N}_1, \hat{N}_+]_+ & \hat{N}_-^2 \\ \hat{N}_+^2 & -[\hat{N}_1, \hat{N}_-]_+ \end{pmatrix} \quad (2.18b)$$

13 which simplifies into classical expression

$$14 \quad M = \frac{\sqrt{3}}{2} \begin{pmatrix} 2N_1 N_+ & N_-^2 \\ N_+^2 & -2N_1 N_- \end{pmatrix}. \quad (2.18c)$$

So the parameters of the semi-quantum matrix (2.16) are (2.18a) with  $\hat{N}_1 \rightarrow N_1$  and

$$a = \frac{\sqrt{3}}{2} (N_2^2 - N_3^2), \quad b = -\sqrt{3} N_2 N_3, \quad c = -\sqrt{3} N_2 N_1, \quad d = \sqrt{3} N_3 N_1.$$

15 The system has, as expected, a pair of pseudo-symmetric semi-quantum eigenvalues

$$16 \quad \lambda_{\pm}(\mathbf{N}) = \pm N^2 \quad (2.19)$$

17 with multiplicity 2. The isotropy of (2.17) becomes the isotropy of (2.19) with respect  
 18 to arbitrary rotations of  $\mathbf{N}$ .

### 19 2.3.3 Spin-quadrupole and spin-orbit quantum spectra

20 We find out the structure of dynamical spin-quadrupole quantum bands that correspond  
 21 to the semi-quantum eigenvalues (2.19). It is instructive to do this in comparison to the  
 22 two bands of the spin- $\frac{1}{2}$  spin-orbit system with Hamiltonian (2.3) and semi-quantum  
 23 eigenvalues (2.4). The linear spin-orbit system with Hamiltonian (2.1) and the spin-  
 24 quadrupole system with Hamiltonian (2.17) are superintegrable. The integrals  $\mathbf{J} =$   
 25  $\mathbf{N} + \mathbf{S}$ ,  $J_1$ , and energy  $H$  are associated with the spherical isotropy group  $SO(3)$ ,  
 26 its axial subgroup  $SO(2)$ , and time-independence, respectively. For sufficiently large  
 27 amplitude of the slow (mechanical) angular momentum  $N > S$ , with  $N \in \mathbb{Z}_{\geq 0}$ , the  
 28 quantum spectrum consists of  $2S + 1$  multiplets labeled by half-integer  $J = N - S, N -$   
 29  $S + 1, \dots, N + S$ . The even number  $2J + 1$  of degenerate levels within each multiplet  
 30 can be further segregated into  $J + \frac{1}{2}$  Kramers doublets, each associated additionally

1 with  $|J_1| = \frac{1}{2}, \frac{3}{2}, \dots, J$ . Once the strict SO(3) isotropy is broken, this additional  
 2 classification becomes meaningful.

3 Both (2.1) and (2.17) are traceless and their spectra are centered at  $H = 0$ . For  
 4 spin  $\frac{1}{2}$  and  $\frac{3}{2}$ , respectively, these spectra split into two bands of positive ( $H > 0$ ) and  
 5 negative ( $H < 0$ ) energy. The difference is in the arrangement of  $J$ -multiplets with  
 6 respect to 0, and in the resulting composition of the bands. Being interested in  $N \gg S$ ,  
 7 we can use a small dimensionless parameter  $x$  to express

$$8 \quad J = N(1 + x) \quad \text{with } x \in [-\epsilon, \epsilon] \text{ and } \epsilon = \frac{S}{N} \ll 1.$$

9 Rewriting and renormalizing the linear spin-orbit coupling (2.1) as

$$10 \quad h(x) = \frac{\mathbf{S} \cdot \mathbf{N}}{N^2} = \frac{\mathbf{J}^2 - N^2 - \mathbf{S}^2}{2N^2} = \frac{x^2}{2} + x - \frac{\epsilon^2}{2},$$

11 we realize that it is a simple function, essentially linear across its domain,

$$12 \quad h(x) \approx x + O(\epsilon^2) \quad \text{for } |x| < \epsilon,$$

13 with single root

$$14 \quad x_0 = 0 + O(\epsilon^2) \in [-\epsilon, \epsilon].$$

15 Within the same approach, the spin-quadrupole term (2.17) equals

$$16 \quad h(x)^2 - \frac{1}{3}\epsilon^2 = x^2 - \frac{1}{3}\epsilon^2 + O(\epsilon^3).$$

17 It follows that the energies of  $J$ -multiplets in the spectrum of the spin-orbit term in-  
 18 crease linearly with  $J$ , and so, in particular, the  $J = N \pm \frac{1}{2}$  multiplets of the spin  
 19  $\frac{1}{2}$  system are opposite in energy  $\pm x N^2$ . On the other hand, the spectrum of the  
 20 spin-quadrupole term is quadratic in  $J$ , and furthermore, the energies are negative for  
 21  $|x| < \epsilon/\sqrt{3}$ . So in the particular case of spin  $\frac{3}{2}$ , the two multiplets with  $J = N \pm \frac{1}{2}$  and  
 22  $x = \pm\epsilon/3$  have negative energies, while those with  $J = N \pm \frac{3}{2}$  have positive energies.  
 23 To acknowledge their additional internal structure, we call the two bands of the spin- $\frac{3}{2}$   
 24 system *superbands*, implying that a superband is constituted by several subbands or  
 25 multiplets.

26 Knowing the values of  $J$  for the multiplets within each superband, we can easily  
 27 find the number of states with given  $|J_1|$  required to constitute these multiplets. So in  
 28 particular for  $S = \frac{3}{2}$ , we can see that typically, for small  $|J_1| \leq N - \frac{3}{2}$ , each band has  
 29 two such states, one per multiplet. For larger  $|J_1| = N - \frac{3}{2} + 1, \dots, N + \frac{3}{2}$ , i.e.,  $N - \frac{1}{2}$ ,  
 30  $N + \frac{1}{2}$ , and  $N + \frac{3}{2}$ , we have 3, 2, and one single doublet state, respectively. When the  
 31 number of doublets is even, i.e., for  $|J_1| = N + \frac{1}{2}$ , they split evenly between the bands.  
 32 Otherwise, the lower band has one extra doublet state with  $|J_1| = N + \frac{3}{2} - 2$  required  
 33 to complete the multiplet with  $J = N - \frac{1}{2}$ , and the upper band takes the sole doublet  
 34 with maximal  $|J_1| = N + \frac{3}{2}$ . We come to the following proposition.

35 **Proposition 2.1** (spectrum of (2.17)): *When  $N \gg S$ , the upper and lower superbands*  
 36 *(bands) of the spin- $\frac{3}{2}$  system with Hamiltonian (2.17) are formed by  $J = N \pm \frac{3}{2}$  and*  
 37  *$J = N \pm \frac{1}{2}$  multiplets, respectively. The superbands have an equal number  $2N + 1$  of*  
 38 *Kramers quantum level doublets labeled by the value of  $|J_1|$ . In each superband, the*  
 39 *number of doublets with  $|J_1|$  other than  $N + S$  and  $N + S - 2$  is the same. The lower*  
 40 *band has one extra doublet state with  $|J_1| = N + S - 2$ , while the upper band takes*  
 41 *the sole doublet with maximal  $|J_1| = N + S$  as part of its  $J = N + S$  multiplet.*

1 The exact quantum spectrum of (2.17) for concrete  $N$  and  $S$  can be, of course,  
 2 obtained if we use quantum expressions for the eigenvalues of all operators in  $h(x)$ .  
 3 Thus we should replace  $\mathbf{J}^2$  by  $N^2(1+x)^2 + N(1+x)$ . Alternatively, we can apply  
 4 the Wigner-Eckart theorem as detailed by eq. (5.71) of [Zare, 1988, chap. 5.4]

$$5 \quad \lambda(J) = (-1)^{S+N+J} \begin{Bmatrix} S & N & J \\ N & S & 2 \end{Bmatrix} \langle S \| \mathbf{T}^2(S) \| S \rangle \langle N \| \mathbf{T}^2(N) \| N \rangle \quad (2.20)$$

6 with reduced matrix elements of  $\mathbf{T}^2$  in eq. (35) of [Zare, 1988, Appendix 13]. Analyz-  
 7 ing the sign in (2.20), we confirm the statement of proposition 2.1 about the number of  
 8 states in the bands of the spin- $\frac{3}{2}$  system. It may also be instructive to see how (2.20)  
 9 converges to just two distinct values (2.19) when  $S = \frac{3}{2}$  and  $S/N \rightarrow 0$ .

10 The seeming triviality of the superbands of the spin- $\frac{3}{2}$  system does also merit a  
 11 comment. In fact, the individual subbands in these superbands are not trivial. The  
 12 corresponding eigenstate “superbundles”  $\Lambda^+$  and  $\Lambda^-$  representing upper and lower  
 13 superbands consist of two bundles representing the subbands and corresponding to the  
 14 individual semiquantum eigenstates. The bundles and the subbands are not trivial, but  
 15 indices for each superbundle sum up to 0. See more in sec. 5.3.

### 16 3 Original family without time-reversal symmetry

17 The system with the spin-orbit coupling Hamiltonian (2.1) has one essential shortcom-  
 18 ing: its degeneracy point  $\{N = 0\}$  happens to be the singularity of its slow dynamical  
 19 system, whose phase space  $\mathbb{S}_N^2$  contracts to one point. We need a different formal  
 20 control parameter  $\gamma$ , such that the topology of the phase space is not affected by its  
 21 variation, while  $N$  can simply be fixed.

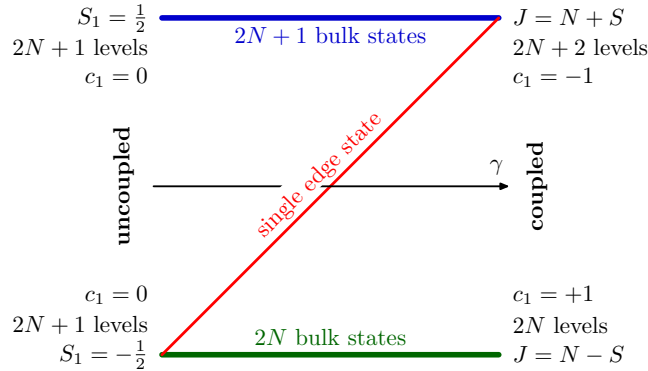


**Figure 2:** Correlation diagram of the deformed spin-orbit system with spin  $S = \frac{1}{2}$  and  $N \gg S$  as function of formal coupling control parameter  $\gamma$ . Bold solid lines represent the energies of the bulk states (blue and green) and the edge state (red). When the value of  $\gamma$  varies, one single state (edge) changes bands, while all other states (bulk) remain within the same band.

22 Additionally, we like to break the isotropy of (2.1) in order to have regular dynamics  
 23 on  $\mathbb{S}_N^2$  and a nondegenerate spectrum within the energy bands. As suggested by Pavlov-  
 24 Verevkin et al. [1988], this can be most trivially achieved by combining (2.1) with a  
 25 one parameter  $N$ -independent sub-family of (1.1). Without any loss of generality, we  
 26 can add  $\hat{S}_1$  times a  $\gamma$ -dependent factor  $B(\gamma)$ . It follows that we are bound to have

1 two limits, one of *coupled momenta* with dominating Hamiltonian (2.1a), the other of  
 2 *uncoupled momenta* with Hamiltonian (1.1) and  $\mathbf{B} = (1, 0, 0)$ . These limits and the  
 3 correlation diagram connecting them are represented in fig. 2.

4 The coupled limit has already been analyzed in sec. 2.1. The uncoupled system is  
 5 rather simple. The semi-quantum eigenstates with energies  $\lambda_{1,2} = \pm \frac{1}{2}$  are spin states  
 6  $|-\frac{1}{2}\rangle$  and  $|+\frac{1}{2}\rangle$  that remain unchanged over the parameter space  $\mathbb{S}_N^2$ , thus forming  
 7 two trivial line bundles over  $\mathbb{S}_N^2$  with  $c_1 = 0$ . The quantum system consists of two  
 8 multiplets (bands) with energies  $\lambda_{1,2}$ . Each multiplet has  $2N + 1$  degenerate levels,  
 9 the normal degeneracy of an isolated (uncoupled) quantum rotator with constant  $N$ .  
 10 We conclude that in the simplest case (fig. 2), going from one limit to the other should  
 11 involve a transfer of a single edge state. The Chern indices for the  $\Lambda_{1,2}$  bundles over  
 12  $\mathbb{S}_N^2$  for different values of  $\gamma$  can be defined and computed similarly to those in the  
 13 original geometric phase setup with (1.1) as discussed across secs. 1.1, 1.3, and 2.1 and  
 14 Appendix A.1. This allows to indicate  $c_1$  in fig. 2 without any special computations  
 15 which are relegated to Appendix A.5. The change  $\delta c_1$  corresponds to one state being  
 16 gained/lost by the respective bands.

### 17 3.1 Spin-orbit coupling in the presence of magnetic field

18 The parametric system with two coupled angular momenta  $\mathbf{N} = (N_1, N_2, N_3)$  and  
 19  $\mathbf{S} = (S_1, S_2, S_3)$  of constant respective lengths  $N := \|\mathbf{N}\|$  and  $S := \|\mathbf{S}\|$  (footnote 3)  
 20 exhibiting the redistribution phenomenon in fig. 2 was suggested in [Pavlov-Verevkin  
 21 et al., 1988] and was further analyzed in [Sadovskii and Zhilinskiĭ, 1999, Iwai and  
 22 Zhilinskiĭ, 2011]. We associate  $\mathbf{N}$  and  $\mathbf{S}$  with “slow” mechanical angular momentum  
 23 and “fast” spin subsystem, respectively. The Hamiltonian

$$24 \quad \hat{H}_\gamma = (1 - \gamma) \frac{\hat{S}_1}{\|\mathbf{S}\|} + \gamma \frac{\mathbf{N} \cdot \hat{\mathbf{S}}}{\|\mathbf{N}\| \|\mathbf{S}\|}, \quad \text{for } S = \frac{1}{2} \text{ and } \gamma \in [0, 1]. \quad (3.1)$$

25 can represent two coupled angular momenta in the presence of magnetic field. Both the  
 26 spin-orbit coupling constant  $\alpha$  and the norm  $B$  of the magnetic field  $\mathbf{B} = B(1, 0, 0)$   
 27 depend on the formal control parameter  $\gamma$  so that at the boundaries of the parameter  
 28 domain, we reach the limits of uncoupled ( $\gamma = 0$ ) and coupled ( $\gamma = 1$ ) momenta  
 29 occurring in fig. 2. Exploiting conservation of  $N > 0$  and  $S > 0$ , we scale the terms in  
 30 (3.1) to make the results dimensionless and concise. Using quantum numbers  $N > 0$   
 31 and  $S > 0$  as scaling constants (footnote 3) simplifies expressions further as some  
 32 factors cancel out.

33 The Hamiltonian (3.1) has nontrivial Lie isotropy group  $\mathbb{S}^1$  constituted by simul-  
 34 taneous rotations of  $\mathbf{N}$  and  $\mathbf{S}$  about axis 1 (also called axis  $z$  elsewhere). The corre-  
 35 sponding conserved quantity is the combined projection

$$36 \quad J_1 = N_1 + S_1 \quad (3.2)$$

37 of  $\mathbf{N}$  and  $\mathbf{S}$  on the axis of symmetry. One of the consequences of this symmetry is that  
 38 the classical analog system is integrable, another consequence is the factorization of  
 39 the matrix of the quantum Hamiltonian  $\hat{H}$  into one- and two-dimensional blocks. This  
 40 all is very similar to the Dirac oscillator symmetry with generator  $\hat{n} + \hat{S}_1$  (sec. 2.2).



### 3.1.1 Semiquantum energies

The semi-quantum (spinor) matrix representation of Hamiltonian (3.1)

$$\hat{H}_\gamma = (1 - \gamma) \begin{pmatrix} -1 & 0 \\ 0 & 1 \end{pmatrix} + \frac{\gamma}{N} \begin{pmatrix} -N_1 & 0 \\ 0 & N_1 \end{pmatrix} + \frac{\gamma}{N} \begin{pmatrix} 0 & N_+ \\ N_- & 0 \end{pmatrix} \quad (3.3)$$

is obtained similarly to (2.3). It commutes with

$$\hat{J}_1 = \begin{pmatrix} N_1 - \frac{1}{2} & 0 \\ 0 & N_1 + \frac{1}{2} \end{pmatrix} \quad (3.4)$$

and its eigenvalues

$$\lambda_{1,2} = \pm \sqrt{1 - 2\gamma(1 - \gamma)(N - N_1)N^{-1}} \in [\pm|1 - 2\gamma|, \pm 1] \quad (3.5)$$

are axially symmetric simplest Morse functions on  $\mathbb{S}_N^2$  with just one mandatory pair of stationary points, a maximum and a minimum. The action of axial symmetry on  $\mathbb{S}_N^2$  (rotation about axis  $N_1$ ) has two isolated critical points with extremal values ( $\pm N$ ) of  $N_1$  (poles) at which semi-quantum energies (3.5) reach their critical values. These energies become degenerate at the south pole  $(N_1, N_2, N_3) = (-N, 0, 0)$  when  $\gamma = 1/2$ . The degeneracy of  $\lambda_{1,2}$  has the generic local form of a conical intersection of two 2-surfaces. The eigenfunctions corresponding to  $\lambda_{1,2}$  form two nontrivial bundles  $\Delta_{1,2}$  over a 2-sphere surrounding the isolated degeneracy point in the parameter space  $(\gamma, N_2, N_3)$ . These bundles have indices<sup>10</sup>  $c_1 = \pm 1$ , see Appendix A.5. We can also consider bundles  $\Lambda_{1,2}(\gamma)$  with  $\gamma \neq \frac{1}{2}$  of the same eigenvectors over the base  $\mathbb{S}_N^2$ . In this case, the bundles are trivial ( $c_1 = 0$ ) when  $\gamma \in [0, \frac{1}{2})$  and nontrivial ( $c_1 = \pm 1$ ) when  $\gamma \in (\frac{1}{2}, 1]$ . Such bundles represent the energy bands of the quantum system (fig. 3) and the index change reflects the redistribution of one energy level between the bands (fig. 2).

On the slow phase space  $\mathbb{S}_N^2$ , the classical motion goes along the orbits of the axial symmetry which are constant level sets of  $N_1$ . In sec. 3.2 we relate these sets to the orbits of the Dirac oscillator (sec. 2.2). The system has two elliptic equilibria at the poles  $\{|N_1| = N\}$ . All other orbits are generic  $\mathbb{S}_{|N_1|}^1$  circles

$$\{N_2^2 + N_3^2 = N^2 - N_1^2, |N_1| < N\} \subset \mathbb{S}_N^2.$$

The slow dynamics under (3.3) can be described using variables  $(N_2, N_3)$  if we distinguish additionally the south ( $N_1 < 0$ ) and the north ( $N_1 > 0$ ) hemispheres (charts). The  $\mathbb{S}_{|N_1|}^1$  orbits lie in the base of both the  $\Lambda_{1,2}$  and the  $\Delta_{1,2}$  bundles. In either case, they are associated with a nonzero geometric phase (cf sec. 2.1). The latter can be, in particular, seen as the origin of a specific additional contribution in the semi-classical quantization of slow dynamics (sec. 3.1.2).

### 3.1.2 Edge and bulk states of the quantum spectrum

The full quantum system is solvable on finite Hilbert subspaces  $\mathcal{H}_j$  spanned by eigenfunctions  $\psi_j$  of operator  $\hat{J}_1$  with the same eigenvalue  $j$ . Using spin functions  $|\frac{1}{2}, \pm\frac{1}{2}\rangle$  and spherical functions  $|N, k\rangle = Y_{N,k}$  with  $|k| = 0, 1, \dots, N$ , we construct uncoupled basis spinor functions

$$\psi_j = a|\frac{1}{2}, -\frac{1}{2}\rangle|N, k\rangle + b|\frac{1}{2}, +\frac{1}{2}\rangle|N, k-1\rangle =: \begin{bmatrix} a \\ b \end{bmatrix}_j \quad \text{with } \bar{a}a + \bar{b}b = 1$$

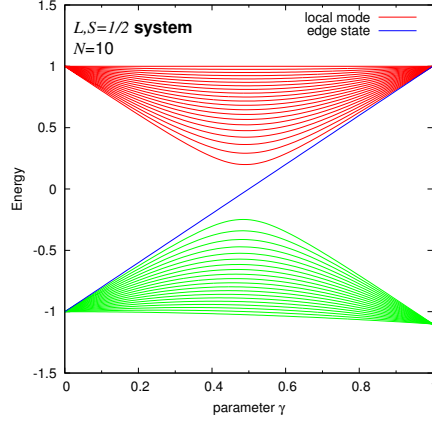


**Figure 3:** Spectrum of the  $N, S = \frac{1}{2}$  system (two coupled angular momenta of conserved lengths) with Hamiltonian  $\hat{H}_\gamma$  (3.1) as function of parameter  $\gamma$  (scaled magnetic field strength). Green and red solid lines represent the “bulk” states of the lower and upper band (multiplet); blue solid line marks the energy of the single “edge” state redistributed at  $\gamma = \frac{1}{2}$ .

1 for all values of  $k \in \mathbb{Z}$  and  $j = k - \frac{1}{2}$  such that  $|j| < N + \frac{1}{2}$ , while for the exceptional  
 2 extremal values  $j = \pm(N + \frac{1}{2})$  we have two single functions

$$3 \quad \psi_{-N-\frac{1}{2}} = |\frac{1}{2}, -\frac{1}{2}\rangle|N, -N\rangle \text{ and } \psi_{N+\frac{1}{2}} = |\frac{1}{2}, \frac{1}{2}\rangle|N, N\rangle.$$

4 The eigenvalues of the action of quantum Hamiltonian  $\hat{H}_\gamma$  (3.1) on  $\mathcal{H}_j$  with regular  $j$

$$5 \quad \lambda_j = \pm \sqrt{1 + 2\gamma(1-\gamma) \frac{j-N}{N} + \gamma^2 \frac{4N+1}{4N^2}} - \frac{\gamma}{2N}, \quad \text{where } |j| < N + \frac{1}{2}, \quad (3.6)$$

6 represent bulk eigenstates belonging to different bands. The exceptional functions  
 7  $\psi_{\pm(N+1/2)}$  are eigenfunctions of  $\hat{H}_\gamma$  with eigenvalues

$$8 \quad \lambda_\pm := \lambda_{\pm(N+1/2)} = \pm(1-\gamma) + \gamma.$$

9 So  $\lambda_+ \equiv 1$  remains constant, while  $\lambda_- = 2\gamma - 1$  increases linearly from  $-1$  to  $1$  as  $\gamma$   
 10 sweeps through the interval  $[0, 1]$ .

11 Figure 3 shows the spectrum of the system. Considering the localization patterns  
 12 of the exceptional states, their energies  $\lambda_\pm$  can be easily understood<sup>11</sup>. The states  
 13  $|N, \pm N\rangle$  correspond to coherent states localized maximally around the poles  $N_1 =$   
 14  $\pm N$  of the slow phase space  $\mathbb{S}_N^2$ , i.e., near the equilibria of the slow system. Their  
 15 Wigner distribution has a small “round shape” with a maximum at the respective pole  
 16 and a near Gaussian profile similar to that of the harmonic oscillator ground state. The  
 17 eigenfunction  $\psi_+$  is localized near the  $N_1 = N$  pole, opposite to the one where the  
 18 degeneracy occurs. It is the state which is most distant from the conical intersection  
 19 point and its energy is not affected by the interaction between (coupling of) the bands.  
 20 On the other hand, the eigenfunction  $\psi_-$  is localized right where bad things happen.  
 21 It represents the edge state. This state is critically affected by slow-fast separation  
 22 breakdown which occurs when  $\gamma \approx \frac{1}{2}$ .

### 3.2 Linearization at the degeneracy point

The conical intersection of the semi-quantum energy surfaces  $\lambda_{1,2}(N; \gamma)$  of the original system with Hamiltonian (3.1) occurs at the  $N_1 = -N$  pole on the slow phase space  $\mathbb{S}_N^2$ . Near this pole, when  $\gamma$  approaches its critical value  $\frac{1}{2}$ , the dynamics accelerates, the slow-fast separation breaks down locally, and the exceptional highly localized (see footnote 11) quantum state  $\psi_-$  gets redistributed. We linearize our system near this point following the outline in sec. 2.1.4, and move to the tangent plane  $\mathbb{R}_{q,p}^2 = T_{N_1=-N}\mathbb{S}_N^2$  which serves as a symplectic chart of  $\mathbb{S}_N^2$  with local symplectic coordinates  $(q, p)$ .

In the basic approximation of eq. (2.7), the Hamiltonian (3.3) becomes

$$\hat{H}_\gamma|_{N_1 \approx -N} = (1 - 2\gamma) \begin{pmatrix} -1 & 0 \\ 0 & 1 \end{pmatrix} + \gamma \frac{\sqrt{2}}{\sqrt{N}} \begin{pmatrix} 0 & ia^+ \\ -ia^- & 0 \end{pmatrix}. \quad (3.7)$$

Rescaling the energy, reparameterizing with new formal control parameter

$$\mu = \frac{1 - 2\gamma}{\gamma} \frac{\sqrt{N}}{\sqrt{2}},$$

and adjusting the phase of one of the basis functions turn it into the standard Hamiltonian (2.10) of the one-dimensional (1D) Dirac oscillator [Moshinsky and Szczepaniak, 1989], see sec. 2.2. The two semi-quantum eigenvalues of (2.10) and (3.7) are functions on the flat noncompact slow phase space  $\mathbb{R}_{q,p}^2$ . It follows that  $\mu \rightarrow \infty$  makes the two bands of the Dirac oscillator completely uncoupled. While the uncoupled limit is unreachable for finite values of formal control parameter  $\mu$ , near  $\mu = 0$  and  $\gamma = \frac{1}{2}$ , the two respective systems exhibit the same redistribution phenomenon and their local eigenstate bundles  $\Delta_{1,2}$  (cf. footnote 10) over a sphere  $\mu^2 + n = \text{const}$  are isomorphic.

Linearization (3.7) allows making the correspondence of the systems with Hamiltonians (3.3) and (2.10) explicit and complete. The 1:1 correspondence of the harmonic oscillator wavefunctions  $|n\rangle$  of the noncompact slow system and the angular momentum wavefunctions  $|N, k\rangle$  with  $k = j + \frac{1}{2}$  can be readily established after noting that the oscillator ground state  $|0\rangle$  corresponds to the coherent state  $|N, -N\rangle$  localized at the south pole, and that the number of nodes of the excited states  $|n\rangle$  equals the number of nodes in the radial direction (footnote 11)). This suggests  $n = -N + k$ . Expanding  $N_1$  near  $-N$  to order  $O((q, p)^4)$  gives the same result, see (2.7). Furthermore, through the equivalence of the two first integrals,  $J_1$  with value  $j$  and  $n + S_1$  with value  $k'$ , we come to the correspondence of the respective Hilbert subspaces  $\mathcal{H}_j$  and  $\mathcal{H}_{k'}$ , and subsequently—to the equivalence of the edge states and the first  $N$  bulk states of the two systems. For  $k' > N$  we lose nodal correspondence, and of course, beyond  $k' = 2N$ , the states of the Dirac oscillator find no analogue in the spin-orbit system. The correspondence can be followed as well at the semiclassical level where the circular orbits  $\mathbb{S}_{N_1}^1 \subset \mathbb{S}_N^2$  with  $N_1 < 0$  map to harmonic oscillator trajectories in  $\mathbb{R}_{q,p}^2$  with sufficiently small  $n$ . In other words, the orbits of the Lie symmetries of the two slow classical systems, the axial symmetry and the oscillator symmetry, respectively, are diffeomorphic for  $n \leq N$ . And finally, at the classical level, both systems exhibit the same kind of nontrivial Hamiltonian monodromy [Sadovskii and Zhilinskiĭ, 1999].

## 4 Spin-orbit systems with time-reversal symmetry

Unless in the presence of an external magnetic field, molecular and atomic systems are invariant with respect to time reversal (2.5), see footnote 5. The system with Hamil-

1 tonian (3.1) is not  $\mathcal{T}$ -invariant for  $\gamma < 1$ . We like to find a  $\mathcal{T}$ -invariant system which  
 2 exhibits similar qualitative behaviour with respect to the variation of a single control  
 3 parameter. Specifically, we want this system to have two bands of approximately  $2N$   
 4 states each for all typical values of parameter  $\alpha \in [-1, 1]$ , and we like a redistribution  
 5 of (few) levels between the bands to occur at the isolated critical value  $\alpha = 0$ .

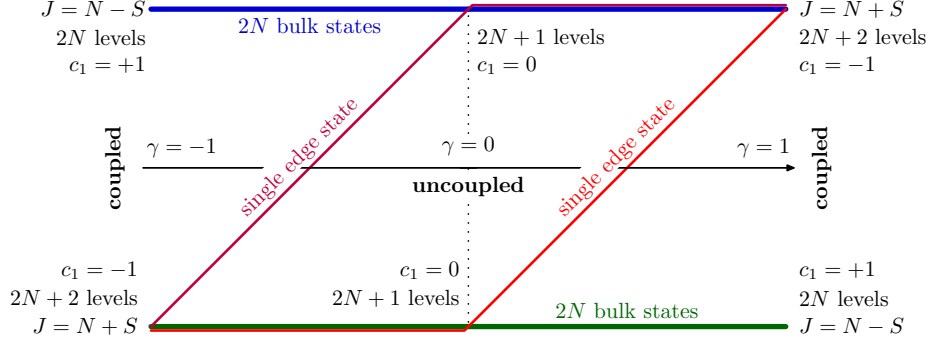


**Figure 4:** Correlation diagram of the deformed spin-orbit system with Hamiltonian (3.1\*), spin  $S = \frac{1}{2}$ , and  $N \gg S$  as function of formal coupling control parameter  $\gamma$ . In comparison to the diagram in fig. 2, the domain of  $\gamma$  is extended from  $[0, 1]$  to  $[-1, 1]$ ; the  $\gamma > 0$  parts of both diagrams are identical. The value 0 of  $\gamma$  corresponds to the uncoupled system (two bands of equal number of states), while the values  $-1$  and  $+1$  correspond to the coupled spin-orbit system with negative and positive coupling Hamiltonian (2.1). Bold solid lines represent the energies of the bulk states (blue and green) and the edge states (red). When the value of  $\gamma$  varies, two single states (edge) change bands, while all other states (bulk) remain within the same bands.

6 Hamiltonian (3.1) becomes  $\mathcal{T}$ -invariant in the limit  $\gamma \rightarrow 1$  which is discussed in  
 7 detail in sec. 2.1. Its upper and lower  $2(J + 1)$ -degenerate bands with  $J = N + \frac{1}{2}$   
 8 and  $J = N - \frac{1}{2}$ , respectively, include  $2N + 2$  and  $2N - 2$  levels (see fig. 2). If we  
 9 reparameterize (3.1) so that the new Hamiltonian

$$10 \quad \hat{H}_\gamma^* = (1 - |\gamma|) \frac{S_1}{\|S\|} + \gamma \frac{N \cdot S}{\|N\| \|S\|}, \quad \text{with } S = \frac{1}{2} \text{ and } |\gamma| \leq 1, \quad (3.1^*)$$

11 is identical to (3.1) for  $\gamma > 0$  and has the extended parameter domain  $[-1, 1]$ , we  
 12 get another  $\mathcal{T}$ -invariant limit with  $\gamma = -1$ . In comparison to  $\gamma = 1$ , the upper band  
 13 corresponds now to  $J = N - \frac{1}{2}$  and has fewer levels. In the spectrum of (3.1\*),  
 14 when  $\gamma$  decreases on the interval  $\gamma \in [0, 1]$ , i.e., as we follow fig. 2 and 3 right to  
 15 left, one state is redistributed top down at  $\gamma = +\frac{1}{2}$ . For  $|\gamma| < \frac{1}{2}$ , both bands have  
 16  $2N + 1$  states. Subsequently, when  $\gamma$  decreases further on the interval  $\gamma \in [0, -1]$ , one  
 17 additional state is redistributed top down at  $\gamma = -\frac{1}{2}$ . This process is represented by  
 18 the correlation diagram in fig. 4. The combination of the two one-state redistributions  
 19 connects one  $\mathcal{T}$ -limit to another by passing through a family systems with Hamiltonian  
 20 (3.1\*) which are not  $\mathcal{T}$ -invariant.

21 It can be conjectured that another passage exists entirely within the class of  $\mathcal{T}$ -  
 22 invariants. In such a case, since all quantum states form Kramers degenerate doublets  
 23 when the norm of the total angular momentum  $J$  is half-integer, specifically, when  
 24  $S = \frac{1}{2}$  and  $N \in \mathbb{Z}_{>0}$ , the two edge states in fig. 4 must become one doublet state. As  
 25 illustrated in fig. 5, this single doublet state is redistributed, while all other states (bulk)  
 26 remain within their bands. Mapped between themselves by the  $\mathcal{T}$  symmetry operation,  
 27 the two states in the edge doublet are localized at the opposite points on the slow phase

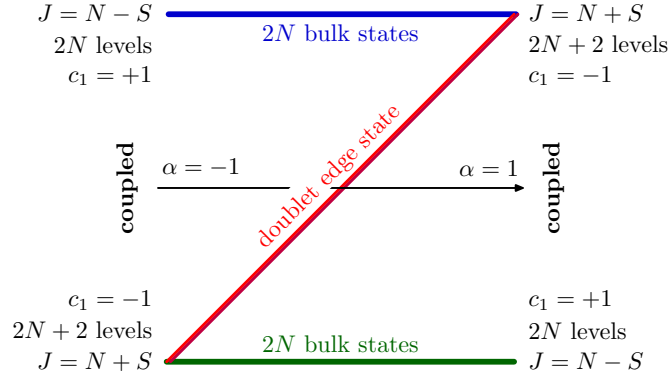


**Figure 5:** Correlation diagram of the spin-orbit system with the conjectured  $\mathcal{T}$ -equivariant deformation, spin  $S = \frac{1}{2}$ , and  $N \gg S$  as function of formal coupling control parameter  $\alpha$ . In comparison to the diagram in fig. 4, the  $[-\frac{1}{2}, \frac{1}{2}]$  part of the domain of  $\gamma$  is shrunk to 0, while the endpoints of the two diagrams are identical. There is no uncoupled system, the values  $-1$  and  $+1$  of  $\alpha$  correspond to the coupled spin-orbit system with isotropic negative and positive coupling Hamiltonian (2.1). Bold solid lines represent the energies of the bulk states (blue and green) and one Kramers doublet edge state (red).

1 space  $\mathbb{S}_N^2$ . So, if the axial symmetry is preserved, they will be pole-localized coherent  
 2 states  $\psi_{\pm J_1}$  with  $|J_1| = N + S$  which we have already encountered in sec. 3.1.2.

### 3 4.1 The family of $\mathcal{T}$ -invariant Hamiltonians

4 We construct explicitly the conjectured  $\mathcal{T}$ -equivariant connection of the  $\alpha = \gamma = \pm 1$   
 5 limits of Hamiltonian (3.1\*) as a one parameter family. The reparameterized spheri-  
 6 cally symmetric spin-orbital coupling term (2.1)

$$7 \quad \alpha \frac{\mathbf{N} \cdot \mathbf{S}}{\|\mathbf{N}\| \|\mathbf{S}\|}, \quad \text{with } S = \frac{1}{2} \text{ and } \alpha \in [-1, 1],$$

8 defines the two limits with  $\alpha = \pm 1$  and is the principal term of the family. However,  
 9 with only this term, the two bands collapse for  $\alpha = 0$  and then change places for  $\alpha \neq 0$ .  
 10 We must introduce another  $\mathcal{T}$ -invariant term with a fixed parameter  $0 < \varepsilon < 1$  in order  
 11 to recover most of the band structure (bulk states) for all values of  $\alpha$ . This additional  
 12  $\varepsilon$ -term breaks the spherical symmetry of (2.1).

13 Similarly to the systems with Hamiltonians (3.1) and (3.1\*), our  $\mathcal{T}$ -invariant family  
 14 of systems can retain the global axial symmetry with first integral  $J_1$ . It can be argued  
 15 that an approximate  $\mathbb{S}^1$  symmetry action on the slow (classical) space can always be  
 16 introduced and exploited near an isolated degeneracy point of the two semi-quantum  
 17 eigenvalues. In the presence of this symmetry, the redistributed edge states are strongly  
 18 localized (footnote 11) near the symmetry axis. In our  $\mathcal{T}$ -invariant spin- $\frac{1}{2}$  system with  
 19 integer  $N$ , the edge states correspond to the states  $\psi_{\pm |J_1|}$  with maximal  $|J_1| = N + \frac{1}{2}$   
 20 (see sec. 3.1.2) now forming one Kramers doublet. The presence of the global  $\mathbb{S}^1$   
 21 symmetry, if possible, will greatly simplify the analysis without any loss of generality.

22 Since any additional terms should not affect the redistribution of the edge state  
 23 doublet (fig. 5), we may require these terms to be function of  $\mathbf{S}$  and  $N_2, N_3$  (or  $N_{\pm}$ )  
 24 only. Such terms can be called “equatorial” because they vanish, or become maximal  
 25 when  $\mathbf{N}$  is aligned with, or is orthogonal to axis 1, respectively, i.e., when  $\mathbf{N} \cdot \mathbf{e}_1 = N$   
 26 or  $\mathbf{N} \cdot \mathbf{e}_1 = 0$ .

Under the action of  $\mathcal{T}$ , the equator becomes the critical set on the slow (classical) space  $\mathbb{S}_N^2$ . The ‘‘equatorial’’ states with  $N_1 \approx 0$  are the most distant from the edge states  $\psi_{\pm}$ , and we can expect the critical value  $\lambda_{\text{crit}}$  of the semi-quantum eigenvalue  $\lambda(\mathbf{N}, \alpha)$  on the equator to mark the absolute maximum and minimum energy of the ‘‘bulk’’ states in the upper and lower bands (multiplets) with large  $|\alpha| \approx 1$ . As a consequence, in order to remain the absolute maximum and minimum in the transition region,  $\lambda_{\text{crit}}$  should be essentially quadratic in  $\alpha$  for small  $|\alpha/\varepsilon| \ll 1$ .

In summary, the requirements on the potential  $\varepsilon$ -term(s) are: (i) to preserve, if possible, the  $\text{SO}(2)$  symmetry, (ii) to have the equatorial behaviour (on the slow space), and (iii) to provide the essential quadratic dependence of the critical equatorial energy on  $\alpha$ . These requirements can be reformulated somewhat differently and more stringently by demanding the quantum spectrum of the  $\varepsilon$ -term alone (i.e., for  $\alpha = 0$ ) to be pseudo-symmetric with two edge states remaining at zero energy and with equal numbers of bulk states of positive and negative energy. This means that the two eigenvalues of the corresponding semiquantum system with spin  $\frac{1}{2}$  are also pseudo-symmetric and have degeneracy points at the poles.

Considering all bilinear (and so necessarily  $\mathcal{T}$ -invariant) forms in  $\mathbf{N}$  and  $\mathbf{S}$ , we come up with two Hermitian axially symmetric terms other than (2.1)

$$\frac{1}{2}(N_+S_- + N_-S_+) = \mathbf{N} \cdot \mathbf{S} - N_1S_1 \quad \text{and} \quad (4.1a)$$

$$\frac{i}{2}(N_-S_+ - N_+S_-) = (\mathbf{N} \wedge \mathbf{S}) \cdot \mathbf{e}_1. \quad (4.1b)$$

Of these, only (4.1b) satisfies the above conditions, while the trivial choice (4.1a) does not conform to requirement (iii). On the same Hilbert space as in (2.3), the Hamiltonian

$$\hat{H}_\alpha^1 = \alpha \frac{\mathbf{N} \cdot \mathbf{S}}{\|\mathbf{N}\| \|\mathbf{S}\|} - i\varepsilon \frac{N_+S_- - N_-S_+}{2\|\mathbf{N}\| \|\mathbf{S}\|}, \quad (4.2)$$

with  $\|\mathbf{S}\| = S = \frac{1}{2}$ ,  $\alpha \in [-1, 1]$ , and small  $\varepsilon \neq 0$ , has spinor representation

$$\hat{H}_\alpha^1 = \frac{\alpha}{N} \begin{pmatrix} -N_1 & 0 \\ 0 & N_1 \end{pmatrix} + \frac{\alpha}{N} \begin{pmatrix} 0 & N_+ \\ N_- & 0 \end{pmatrix} - i \frac{\varepsilon}{N} \begin{pmatrix} 0 & N_+ \\ -N_- & 0 \end{pmatrix}. \quad (4.3)$$

Its semi-quantum eigenvalues

$$\pm \sqrt{\varepsilon^2 \sin^2 \theta + \alpha^2} \quad (4.4)$$

have critical points at the poles with latitudinal angle  $\theta = 0, \pi$  and the equatorial critical set  $\mathbb{S}^1 = \{\theta = \pi/2\}$ . The corresponding critical values of semi-quantum energies  $\lambda_{1,2}(\mathbf{N}, \alpha)$  with  $\theta = 0, \pi$  and  $\theta = \pi/2$  are shown by dotted lines in fig. 6. The poles belong to the same critical 2-point orbit of the  $\text{SO}(2) \wedge \mathcal{T}$ -group action on  $\mathbb{S}_N^2$  and the energy at both poles has the same critical value  $\pm|\alpha|$ . This value describes the behaviour of the edge states localized (footnote 11) near the poles. The equatorial energy  $\pm\sqrt{\varepsilon^2 + \alpha^2}$  has the desired property (iii). This confirms the family (4.2–4.3).

#### 4.1.1 Quantum spectrum of the $\mathcal{T}$ -invariant family

We analyze the spectrum of (4.2) using its spinor representation (4.3). Following the approach in sec. 3.1.2, specifically see (3.3), we compute the action of (4.3) on each

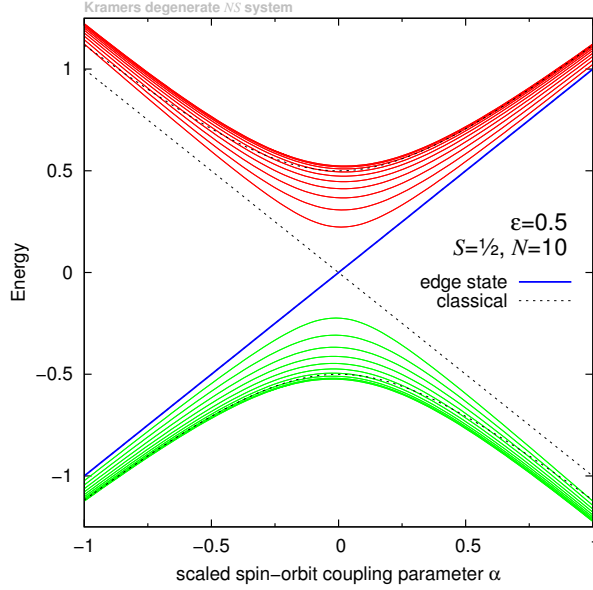


**Figure 6:** Spectrum of the  $N, S = \frac{1}{2}$  system (two coupled angular momenta of conserved lengths) with  $\mathcal{T}$ -invariant Hamiltonian (4.2) as function of scaled spin-orbit coupling parameter  $\alpha$ . Each solid line represents a Kramers doublet quantum state. Energies of the bulk states (red and green solid lines) are given by (4.5), while the solid blue line represents the edge state. Dotted lines indicate critical values of the semi-quantum energies (4.4).

1 Hilbert subspace  $\mathcal{H}_j$  with  $|j| < N + \frac{1}{2}$  and  $k = j + \frac{1}{2} \in \mathbb{Z} \cap (-N, N + 1)$ . This gives  
2 the energies

$$3 \quad \lambda_j = -\frac{\alpha}{2N} \pm \frac{1}{N} \sqrt{\alpha^2 j^2 + R_j^2 (\alpha^2 + \varepsilon^2)} \quad (4.5)$$

4 of the bulk states with

$$5 \quad R_j := \sqrt{(N+k)(N-k+1)} = \sqrt{(N+j+\frac{1}{2})(N-j+\frac{1}{2})} > 0. \quad (4.6)$$

6 Since  $R_j$  is invariant with respect to sign flipping  $j \mapsto -j$ , we observe that each  $\lambda_{\pm j}$   
7 constitute a pair of Kramers degenerate doublets with energies (4.5). For nonzero  $\varepsilon$ ,  
8 the splitting between the doublets never vanishes. If we consider  $N \gg 1 \geq |\alpha|$ , i.e.,  
9 being reasonably close to the classical limit for the slow subsystem, the energies of  
10 these doublets are nearly opposite, and consequently, the  $\pm$  signs in (4.5) correspond  
11 to the “bulk” states belonging permanently to the upper and lower bands<sup>12</sup>, see fig. 6.

12 It remains to find out what happens to the edge states. As before in sec. 3.1.2,  
13 they are readily constructed as single states  $\psi_{\pm(N+S)}$  which are not affected by the  
14 nondiagonal terms in (4.3). Engaging only the diagonal part of the first (principal)  
15 term of (4.2), we obtain

$$16 \quad \hat{H}_\alpha^1 \psi_\pm = \frac{\alpha}{NS} N_1 S_1 \psi_\pm = \frac{\alpha}{NS} (\pm N) (\pm \frac{1}{2}) \psi_\pm = \alpha \psi_\pm.$$

17 So the two “edge” states form an exceptional Kramers doublet with energy  $\alpha$  which is  
18 redistributed between the two bands top down as  $\alpha$  decreases from 1 to  $-1$ , see fig. 6.

## 4.2 Linearization of Kramers-degenerate systems

Linearization near the sole degeneracy point of the original spin-orbit system in sec. 3 lead to the Dirac oscillator. Applying the same approach to the  $\mathcal{T}$ -invariant Kramers-degenerate system with Hamiltonian (4.2–4.3), requires *two independent linearizations* at poles  $N_1/N = \pm 1$  of the slow space  $\mathbb{S}_N^2$ . These linearizations differ in the definition of local symplectic coordinates  $(q, p)$  which are summarized in (2.7).

Replacing  $N_1$  and  $N_{\pm}$  in (4.3) according to (2.7) gives the spinor forms of the Hamiltonian (4.3) linearized near each pole

$$\hat{H}_\alpha^1|_{N_1=+N} = \alpha \begin{pmatrix} -1 & 0 \\ 0 & 1 \end{pmatrix} + \frac{2\alpha}{\sqrt{2N}} \begin{pmatrix} 0 & a^- \\ a^+ & 0 \end{pmatrix} - \frac{2\varepsilon i}{\sqrt{2N}} \begin{pmatrix} 0 & a^- \\ -a^+ & 0 \end{pmatrix}, \quad (4.7a)$$

$$\hat{H}_\alpha^1|_{N_1=-N} = \alpha \begin{pmatrix} 1 & 0 \\ 0 & -1 \end{pmatrix} + \frac{2\alpha i}{\sqrt{2N}} \begin{pmatrix} 0 & a^+ \\ -a^- & 0 \end{pmatrix} + \frac{2\varepsilon}{\sqrt{2N}} \begin{pmatrix} 0 & a^+ \\ a^- & 0 \end{pmatrix}. \quad (4.7b)$$

Their respective operator forms are obtained from (4.1a), (4.2), and (2.7)

$$\hat{H}_\alpha^1|_{N_1=+N} = \alpha \frac{S_1}{S} + \alpha \frac{a^- S_- + a^+ S_+}{\sqrt{2N}S} - i\varepsilon \frac{a^- S_- - a^+ S_+}{\sqrt{2N}S}, \quad (4.8a)$$

$$\hat{H}_\alpha^1|_{N_1=-N} = -\alpha \frac{S_1}{S} + i\alpha \frac{a^+ S_- - a^- S_+}{\sqrt{2N}S} + \varepsilon \frac{a^+ S_- + a^- S_+}{\sqrt{2N}S}. \quad (4.8b)$$

Similarly to (3.7), Hamiltonians (4.7a) and (4.7b) have first integrals  $\hat{n} - \hat{S}_1$  and  $\hat{n} + \hat{S}_1$ , respectively, with spinor forms

$$\hat{n} \pm \hat{S}_1 = \begin{pmatrix} n \mp \frac{1}{2} & 0 \\ 0 & n \pm \frac{1}{2} \end{pmatrix}. \quad (4.9)$$

This follows from direct computation of commutators of (4.9) and (4.7). At the same time, it is instructive to see integrals (4.9) as linearizations of  $\hat{J}_1$  in (3.4). To this end recall that in the Holstein–Primakoff approximation [Holstein and Primakoff, 1940] near each pole (2.7) of the slow phase space  $\mathbb{S}_N^2$ , the angular momentum  $N_1$  equals<sup>13</sup>  $\mp N \pm n$ , where  $n$  is the number of quanta in the local harmonic oscillations about the poles. Consequently, the spinor form (3.4) of  $J_1$  becomes

$$\hat{J}_1|_{N_1=\pm N} = \begin{pmatrix} \pm N \mp n - \frac{1}{2} & 0 \\ 0 & \pm N \mp n + \frac{1}{2} \end{pmatrix} = \pm \hat{1}N \mp \hat{n} + \hat{S}_1$$

which is, to a sign and a constant scalar term  $\hat{1}N$ , equivalent to (4.9). We also recognize the first integral of the Dirac oscillator (sec. 2.2).

We further notice that systems with Hamiltonians (4.7) and respective first integrals (4.9) are related by time-reversal symmetry  $\mathcal{T}$  in (2.5). While this operation maps the polar regions of  $\mathbb{S}_N^2$  into each other, it interchanges the symplectic coordinates  $(q, p)$  in these regions as well as changes their sign. We have

$$\mathcal{T} : (S, q, p) \mapsto -(S, p, q) \quad \text{and} \quad \mathcal{T} : a^\pm \rightarrow \pm i a^\mp.$$

It can be seen that Hamiltonians (4.8) are related by this operation and that so are the respective semi-quantum spinor matrices (4.7), cf. footnote 5. As a result, Hamiltonians (4.7) are *isospectral*. Furthermore, to a reparameterization, their spectra are equivalent to that of the Dirac oscillator in sec. 2.2. The eigenstates of either (4.7a) or (4.7b) have



1 nondegenerate eigenvalues, with a single “edge” state of energy  $\alpha$  and the “bulk” states  
 2 forming two bands with a pseudo-symmetric spectrum.

3 We compute the spectrum. Since both (2.10) and (4.7b) commute with  $\hat{n} + \hat{S}_1$ ,  
 4 we can work on the Hilbert subspaces  $\mathcal{H}_k$  with  $k - \frac{1}{2} = n \in \mathbb{Z}_{>0}$  of functions  $\psi_k$   
 5 already defined in sec. 2.2. On these subspaces, we find the corresponding bulk state  
 6 eigenvalues

$$7 \quad \lambda_n = \pm \sqrt{\frac{2n}{N}(\varepsilon^2 + \alpha^2) + \alpha^2} \quad (4.10)$$

8 while the single edge state  $\psi_0$  of (4.7b) has energy  $\alpha$ , see fig. 7. The bands are sepa-  
 9 rated at least by  $\pm\varepsilon\sqrt{2/N}$ . Scaling these energies by  $\sqrt{2(\varepsilon^2 + \alpha^2)}/N > 0$  gives the  
 10 spectrum of the Dirac oscillator in fig. 1 with

$$11 \quad \mu = -\alpha \sqrt{\frac{N}{2(\varepsilon^2 + \alpha^2)}}.$$

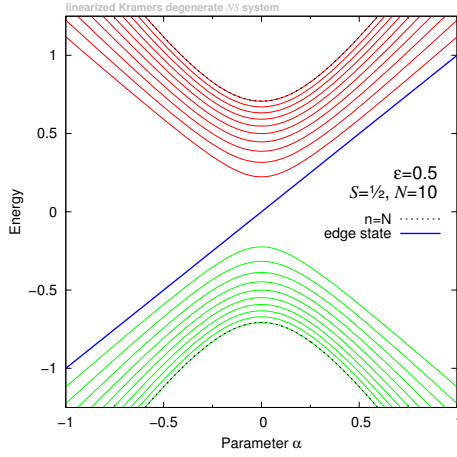


**Figure 7:** Spectrum of the system with Hamiltonian (4.7b) obtained as linearization of  $\mathcal{T}$ -reversal  $NS$ ,  $S = \frac{1}{2}$  Hamiltonian (4.3) for coupling parameter  $\alpha \in [-1, 1]$ . Compare to fig. 1 and 6. The bulk state energies (red and green lines) are given by (4.10).

12 In order to finalize the description of the spectrum, we turn to the spinor Hamilto-  
 13 nian (4.7a) (linearization at  $N_1/N = 1$ ). This operator commutes with  $\hat{n} - \hat{S}_1$ . We  
 14 should, therefore, work on the Hilbert subspaces of eigenfunctions of  $\hat{n} - \hat{S}_1$

$$15 \quad \mathcal{H}_k^* \ni \psi_k^* = \sum_{\sigma} c_{\sigma,k} |\frac{1}{2}, \sigma\rangle |k + \sigma\rangle, \quad \text{where } k + \frac{1}{2} = n \in \mathbb{Z}_{>0},$$

16 with eigenvalue  $k$ . These subspaces contain the bulk states. The action of (4.7a) on  $\psi_n^*$   
 17 has the bulk eigenvalues identical to (4.10). The sole edge function

$$18 \quad \psi_{-\frac{1}{2}}^* = |\frac{1}{2}, \frac{1}{2}\rangle |0\rangle$$

19 is the eigenfunction of  $\hat{n} - \hat{S}_1$  with eigenvalue  $-\frac{1}{2}$ . The energy of this edge state  
 20 equals  $\alpha$ . We conclude that the entire spectrum of the original system with Hamiltonian  
 21 (3.1\*) is reproduced as a sum of two identical spectra (4.10). Each of these spectra  
 22 corresponds to a Dirac oscillator, a system without  $\mathcal{T}$ -invariance. Their sum reproduces  
 23 Kramers degeneracy of the  $\mathcal{T}$ -invariant system (footnote 5).

### 4.3 Combining Dirac oscillators and Chern indices

Our results in sec. 3.2 suggest that the redistribution phenomenon in the  $\mathcal{T}$ -invariant system can be analyzed entirely by exploiting what we know already for simpler systems in sec. 2.1, 2.2, and 3. The eigenstate bundles  $\Lambda_{1,2}$  over  $\mathbb{S}_N^2$  have Chern indices  $c_1 = \pm 1$ . More specifically, denoting these bundles as  $\Lambda_{\pm}$  for positive/negative semi-quantum energies (4.4) respectively, we find (Appendix A.6 and A.7)  $c_1 = \mp 1$  for  $\alpha > 0$  and  $\pm 1$  for  $\alpha < 0$ , cf. fig. 5. The *index change*  $|\delta c_1|$  of 2 corresponds to the two edge states (forming one Kramers doublet) exchanged at  $\alpha = 0$ . Alternatively, within the standard geometric phase framework, the eigenbundles are constructed *locally*, near each degeneracy point, after the total degeneracy at  $\alpha = 0$  is removed by the  $\varepsilon$ -term. The computations are equivalent to those for the original system with Hamiltonian (3.1) near its sole degeneracy with  $N_1 = -N$  and  $\gamma = \frac{1}{2}$  and for the Dirac oscillator in sec. 2.2. Two linearizations  $\lambda(\alpha, N_2, N_3)|_{N_1=\pm N}$  are required, leading to the analysis of the eigenbundles  $\Delta_{1,2}|_{N_1=\pm N}$ . In this way, choosing an appropriate sign convention, we obtain  $c_1 = 1$  for  $\Delta_1$  defined near either of the poles, giving the total of +2, while for  $\Delta_2$ , the indices have opposite signs totalling up to -2, see Appendix A.7. This sum of indices computed locally near each pole corresponds to the total number of gained/lost levels by the corresponding energy band.

## 5 Quadratic spin-orbit coupling

As we explain in sec. 2.3, the  $\mathcal{T}$ -invariant system in sec. 4 cannot provide a dynamical analogy of the spin-quadrupole systems in [Mead, 1987, Avron et al., 1988] because the spin-orbit Hamiltonian (4.2) has no  $\mathcal{T}_S$  symmetry. At the same time, for lack of a better idea and because it seems quite a reasonable thing to begin with when moving into unknown territory, we like to recycle the approach of sec. 4. Recall that in order to construct a two-band system with elementary  $\mathcal{T}$ -equivariant energy level redistribution, we retained the spherically symmetric spin-orbit term (2.1) and we used its coefficient  $\alpha$  as the principal (sole) parameter of the system. In order to lift the complete collapse of the bands at  $\alpha = 0$ , we added an  $\varepsilon$ -term (4.1b) with specific properties making the sign and the concrete value of  $\varepsilon$  unimportant as long as  $\varepsilon \neq 0$ .

The isotropic Hamiltonian (2.17) introduced in sec. 2.3.2 seems to be a most natural choice for the quadratic  $\alpha$ -term. However, before we attempt constructing the  $\mathcal{T}_S$ -invariant and, possibly, axially symmetric quadratic  $\varepsilon$ -term (sec. 5.1), we should pay attention to one important difference between (2.17) and plain linear spin-orbit Hamiltonian (2.1). As we show in sec. 2.3.3, the spectrum of the spin- $\frac{3}{2}$  system with Hamiltonian (2.17) and the spectrum of the spin- $\frac{1}{2}$  system with plain spin-orbit Hamiltonian (2.1b) have both two bands. However, while the latter system has bands with different number of states, the bands of the former system have equal number of levels (proposition 2.1).

More specifically, the bands of the spin- $\frac{3}{2}$  system with Hamiltonian (2.17) can be seen as two “super-bands”, each having two complete multiplets of  $2J + 1$  states with a fixed value of  $J = N - S, \dots, N + S$  as two “sub-bands”. These “sub-bands” appear naturally for large  $|\alpha|$  after adding small perturbation term  $\mathcal{S} \cdot N$  preserving the time reversal symmetry (2.5) and the SO(3) isotropy but breaking the  $\mathcal{T}_S$  symmetry. Sub-bands have different  $J$  and differ in the number of levels, but each super-band has the same total number of levels. Nevertheless, the super-bands are qualitatively different because the values of  $J$  are unique. This makes the limits of  $\alpha = -1$  and

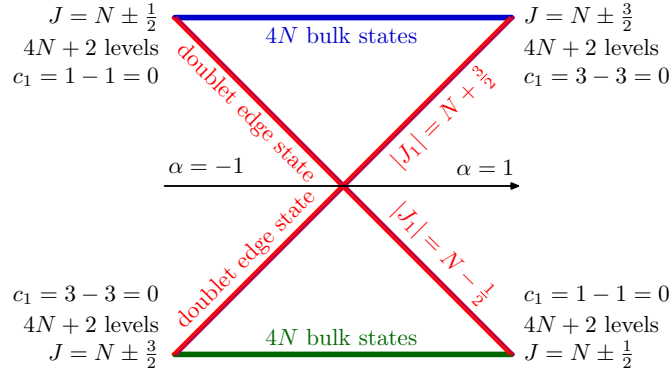


**Figure 8:** Correlation diagram for the quadratic dynamical spin-quadrupole system in sec. 2.3.2 with the conjectured  $\mathcal{T}_S \times \mathcal{T}_N$ -equivariant deformation in sec. 5, spin  $S = \frac{3}{2}$ , and  $N \gg S$  as function of formal control parameter  $\alpha$  of the isotropic quadrupolar coupling term (2.17). The values  $\pm 1$  of  $\alpha$  correspond to the coupled system with Hamiltonian (2.17) times  $\pm 1$ . Bold solid lines represent the energies of the bulk states (blue and green) and of the two Kramers doublet edge states (red) exchanged in opposite directions. Unlike the indices  $c_1$  in fig. 2 and 4 which can be computed in the standard way for the  $\Lambda_{1,2}$  bundles on  $\mathbb{S}_N^2$  (see sec. 1.2 and 2.1), the values of  $c_1$  in this diagram are conjectured so that they agree with the number of states in each band. See text for more detail.

1  $\alpha = +1$  qualitatively different and when  $\alpha$  changes sign, a number of states must  
2 be redistributed to rebuild the two super-bands. However, since the total number of  
3 states remains unchanged, the redistribution should go *both* ways. From the detailed  
4 classification of states in each band given in proposition 2.1, we can conjecture that  
5 the two Kramers doublets with  $|J_1| = N + S$  and  $|J_1| = N + S - 2$  have to be  
6 exchanged. Assuming that both  $\mathcal{T}_S$  and  $\mathcal{T}_N$  symmetries (sec. 2.3.1) are preserved by the  
7  $\varepsilon$ -deformation, i.e., that the  $\mathcal{T}$  symmetry is also present and Kramers doublets remain  
8 intact, the entire redistribution is given by the correlation diagram in fig. 8.

9 In this diagram, the hypothetical values of the super-bands indices  $c_1$  and their de-  
10 composition into a sum of two sub-band indices are deduced from the total number of  
11 states in each super-band and sub-band. Compared to the previous sections, the actual  
12 calculation of these indices is now hampered by the degeneracy of the semi-quantum  
13 eigenvalues. The four eigenstates of the  $\mathcal{T}_S$ -symmetric spin- $\frac{3}{2}$  semi-quantum system  
14 form two Kramers doublets which correspond to the super-bands. The  $\Lambda$ -bundle for  
15 each super-band is, therefore, formed by two semi-quantum eigenstates with degener-  
16 ate eigenvalue  $\lambda : \mathbb{S}_N^2 \rightarrow \mathbb{R}$ . Assuming that this  $\Lambda$ -bundle can be decomposed contin-  
17 uously over  $\mathbb{S}_N^2$  into two respective sub-bundles, these indices can be computed. The  
18 linearization in sec. 5.2 may suggest that such decomposition is indeed possible. At  
19 the same time, the difference of the indices, or delta-Chern  $\delta c_1 = 0$ , can be confirmed  
20 as previously (sec. 2.2) using the linearization in sec. 5.2. The calculation of Chern  
21 indices for superbands, i.e., for the rank-2 bundles, is discussed in appendix A.8.

## 5.1 The family of quadrupolar spin-orbit Hamiltonians

Using tensors  $T^2$  introduced in sec. 2.3.2 and incorporating spherically symmetric  $\alpha$ -term (2.17), the closest degree-2 analog of (4.2) can be written as

$$\hat{H}_{\alpha_0} = \alpha_0 \sqrt{5} \left[ T^2(\hat{S}) \times T^2(\hat{N}) \right]^0 + i\varepsilon \sqrt{5} \frac{\sqrt{2}}{\sqrt{3}} \left[ T^2(\hat{S}) \times T^2(\hat{N}) \right]^1, \quad (5.1a)$$

$$= \alpha_0 \left( (\hat{S} \cdot \hat{N})^2 - \frac{1}{3} \hat{S}^2 \hat{N}^2 \right) + \varepsilon \frac{1}{\sqrt{3}} \left[ \hat{S} \cdot \hat{N}, (\hat{S} \wedge \hat{N}) \cdot e_1 \right]_+. \quad (5.1b)$$

This Hamiltonian is axially symmetric and is invariant under both  $\mathcal{T}_S$  and  $\mathcal{T}_N$  reversal symmetries in sec. 2.3.1. Similarly to its predecessor (4.1b), the axially-symmetric  $\varepsilon$ -term in (5.1) incorporates the exterior product of  $S$  and  $N$  (of rank 1). In the basis (2.15), this term contributes solely to the off-diagonal block

$$\hat{M} = \frac{1}{2} \begin{pmatrix} (\alpha_0 \sqrt{3} + i\varepsilon)[N_1, N_+]_+ & (\alpha_0 \sqrt{3} - 2i\varepsilon)N_-^2 \\ (\alpha_0 \sqrt{3} + 2i\varepsilon)N_+^2 & -(\alpha_0 \sqrt{3} - i\varepsilon)[N_1, N_-]_+ \end{pmatrix}. \quad (5.2)$$

of the quaternion-form matrix (2.16) of (5.1).

### 5.1.1 Semi-quantum energies

The system has, as expected, a pair of pseudo-symmetric semi-quantum eigenvalues

$$\lambda_{\pm}(\alpha_0, N) = \pm N \sqrt{(\alpha_0^2 + \varepsilon^2)N^2 - \varepsilon^2 N_1^2} = \pm N^2 \sqrt{\alpha_0^2 + \varepsilon^2 \sin^2 \theta}, \quad (5.3)$$

the same as (4.4) but with multiplicity 2. Figuratively, multiplicity doubles all features of the semi-quantum system in sec. 4.

Thus, critical semiquantum energies in fig. 9 and fig. 6 are the same. In particular, for all  $\alpha_0 \neq 0$ , the eigenvalue  $\lambda_+(\alpha_0, N)$  has a double minimum at the poles, and a degenerated maximal circle on the equator. Degeneracy occurs only at energy 0 and only when  $\alpha_0 = 0$  and only as conical intersections at the poles  $\{N_1 = \pm N\}$ .

### 5.1.2 Quantum spectrum

The quantum spectrum of (5.1) with nonzero  $\varepsilon$  requires numerical diagonalization (typically of  $4 \times 4$  matrices). As can be clearly seen in fig. 9, for large  $|\alpha_0| \gg \varepsilon > 0$ , this spectrum tends to the SO(3) isotropic limit which is analyzed in detail in sec. 2.3.3. Specifically, we can see how the states in this limit regroup into subbands with given total angular momentum  $J$ .

It is instructive to consider the spectrum for  $\alpha_0 = 0$ , i.e., the eigenstates of the  $\varepsilon$ -term of (5.1). These eigenstates, labelled by the absolute value  $|J_1|$  of momentum  $J_1$ , are represented in fig. 10 in the form of an energy-momentum diagram. We notice that, similarly to that of (4.1b), the spectrum of the  $\varepsilon$ -term in (5.1) is pseudo-symmetric (the eigenvalues come either in  $\pm$  pairs or equal 0), and is nondegenerate on each Hilbert space  $\mathcal{H}_{J_1}$  spanned by eigenfunctions of  $\hat{J}_1$  with given fixed eigenvalue  $J_1$ . This follows from the fact that both these  $\varepsilon$ -terms have imaginary skew-symmetric matrices which are not block-diagonal unless  $\dim \mathcal{H}_{J_1}$  is odd, in which case there is one zero eigenvalue. As fig. 10 illustrates, and in accordance with proposition 2.1, the two edge state doublets in the spin- $\frac{3}{2}$  spectrum of the  $\varepsilon$ -term of (5.1) have unambiguous superband destination in the isotropic limits with  $|\alpha_0| \gg \varepsilon$ . The destination is predefined

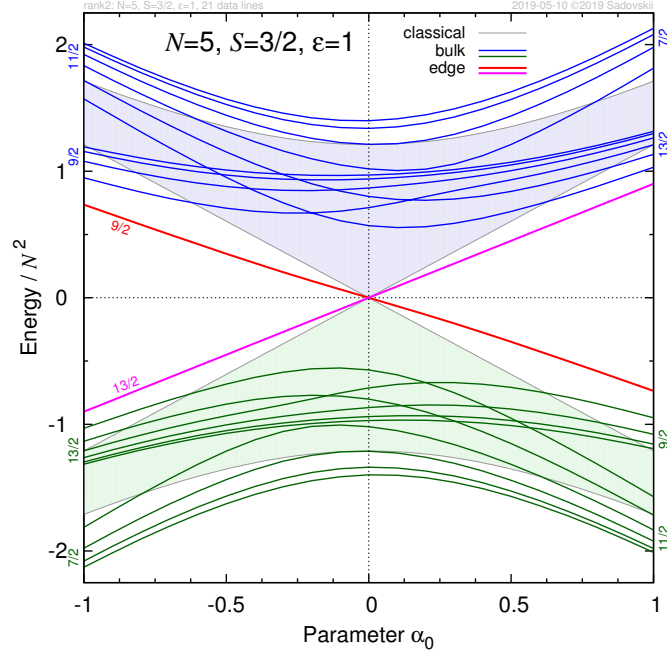


**Figure 9:** Spectrum of the Kramers degenerate  $\mathcal{T}_N \times \mathcal{T}_S$ -invariant axially symmetric system of coupled angular momenta  $\mathcal{S}$  (fast) and  $\mathcal{N}$  (slow) of conserved lengths  $S = \frac{3}{2}$  and  $N = 5$  with Hamiltonian (5.1) as function of the “quaternionic” spin-orbit coupling parameter  $\alpha_0$ . Solid color lines represent quantum Kramers doublet states. Specifically, the bulk state energies are depicted in blue and green, while red and purple correspond to the two edge state doublets. For the end values  $\pm 1$  of  $\alpha_0$ , the levels within each band reassemble visibly into multiplets with conserved length  $J$  of the total angular momentum  $N + \mathcal{S}$  and the respective values of  $J$  are marked along the left and right vertical axes, cf. sec. 2.3.3. The edge states are distinguished by the conserved value of  $J_1$  displayed near the  $\alpha_0 = -1$  end of the plot. The boundaries of the lightly shaded semi-quantum energy domains (gray lines) are given by (5.3) where  $N_1$  takes one of the critical values  $\{N, 0\}$  and with  $N$  replaced by  $N_{\text{classical}} = N + \frac{1}{2}$ .

- 1 by the conserved value of  $|J_1|$ . For example, the doublet with the maximal  $|J_1| =$
- 2  $N + \frac{3}{2}$  joins necessarily the multiplet with the maximal  $J = N + \frac{3}{2}$  of the  $J = N \pm \frac{3}{2}$
- 3 superband.

## 4 5.2 Linearization at the degeneracy points

- 5 The  $\text{SO}(2) \wedge (\mathcal{T}_S \times \mathcal{T}_N)$ -invariant Hamiltonian (5.1) in sec. 5.1 can be linearized
- 6 straightforwardly tracing the outline in the beginning of sec. 4.2. Linearizing at both
- 7 poles of the classical slow phase space  $\mathbb{S}^2$  and using (2.7) produce two *isospectral* sys-
- 8 tems with  $\mathcal{T}_S$ -invariant (but *not*  $\mathcal{T}$ -invariant) Hamiltonians

$$9 \quad \hat{H}_{\alpha_0}|_{N_1=\pm N} = N^2 \hat{S} \tilde{Q} \hat{S} \quad \text{with} \quad \tilde{Q} = N^{-2} \mathcal{Q}|_{N_1=\pm N}. \quad (5.4)$$

The elements (see footnote 9) of the linearized matrices  $\tilde{Q}$  in (5.4) are given by

$$\tilde{Q}_{xx} = \tilde{Q}_{yy} = -\frac{1}{3} \alpha_0, \quad \tilde{Q}_{zz} = \frac{2}{3} \alpha_0, \quad \tilde{Q}_{xy} = 0, \quad \text{for } N_1 = \pm N$$

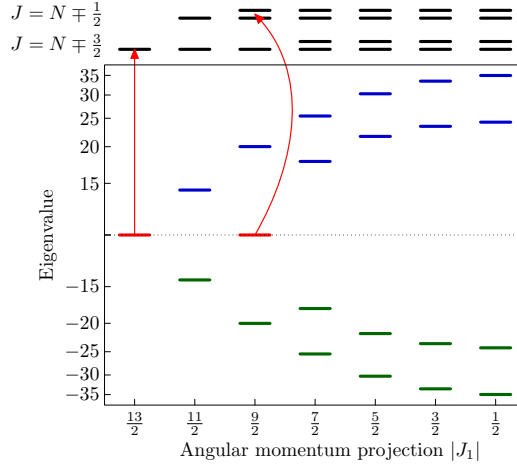


**Figure 10:** Joint spectrum of the  $\varepsilon$ -term of the quadratic spin-orbit Hamiltonian (5.1) and  $\hat{J}_1$ . The values of spin  $S = \frac{3}{2}$  and slow angular momentum  $N = 5$  correspond to fig. 9. Bold solid bars represent the bulk states (blue and green) and two Kramers doublet edge states (red). Above the energy-momentum diagram, we show the composition of the two multiplets in each superband of the spectrum of the isotropic term in sec. 2.3.3. Red arrows indicate which of the subbands takes in the particular edge states, see proposition 2.1.

and

$$\begin{aligned} \tilde{Q}_{xz} &= +\frac{1}{\sqrt{N}}\left(\alpha_0 q - \frac{\varepsilon}{\sqrt{3}} p\right), & \tilde{Q}_{yz} &= +\frac{1}{\sqrt{N}}\left(\alpha_0 p + \frac{\varepsilon}{\sqrt{3}} q\right), & \text{for } N_1 = +N, \\ \tilde{Q}_{xz} &= -\frac{1}{\sqrt{N}}\left(\alpha_0 p - \frac{\varepsilon}{\sqrt{3}} q\right), & \tilde{Q}_{yz} &= -\frac{1}{\sqrt{N}}\left(\alpha_0 q + \frac{\varepsilon}{\sqrt{3}} p\right), & \text{for } N_1 = -N. \end{aligned}$$

1 In the spinor basis (2.15), Hamiltonian (5.4) becomes a matrix operator with quaternionic matrix of the form (2.16). It has diagonal parameter

$$2 \quad g|_{N_1=\pm N} = -\alpha_0 N^2 \quad (5.5a)$$

and the off-diagonal block

$$\hat{M}|_{N_1=+N} = +\begin{pmatrix} \beta a^- & 0 \\ 0 & -\beta a^+ \end{pmatrix}, \quad (5.5b)$$

$$\hat{M}|_{N_1=-N} = -i\begin{pmatrix} \beta a^+ & 0 \\ 0 & \beta a^- \end{pmatrix}, \quad \text{with } \beta = (\alpha_0\sqrt{3} + i\varepsilon)N\sqrt{2N}. \quad (5.5c)$$

4 In the basis  $\{|\frac{3}{2}, -\frac{1}{2}\rangle, |\frac{3}{2}, -\frac{3}{2}\rangle\} \oplus \{|\frac{3}{2}, \frac{3}{2}\rangle, |\frac{3}{2}, \frac{1}{2}\rangle\}$ , this matrix becomes block-diagonal

$$5 \quad \text{diag}(\hat{H}, -\hat{H}) \quad \text{with } \hat{H} = \begin{pmatrix} g & h \\ h^\dagger & -g \end{pmatrix} \quad (5.6a)$$

7 where

$$8 \quad h = \beta a^- \text{ for } N_1 = N \quad \text{and} \quad h = -i\beta a^+ \text{ for } N_1 = -N. \quad (5.6b)$$

9 To a sign and a scalar factor,  $\hat{H}$  is isospectral to one of Hamiltonians (4.7). They all are, essentially, Dirac oscillators (2.10). The sign is important as it defines the transfer direction of the sole edge state in each block (see fig. 7). Linearizations for  $N_1 = +N$  or  $-N$  are isospectral,  $\mathcal{T}_N$  invariance obliging. Superposition of the spectra of the  $\pm\hat{H}$  blocks for either linearization gives two edge states transferred in opposite directions.

### 5.3 Redistribution, Chern indices, and the number of states

Linearization in sec. 5.2 elucidates the point that we have already made when discussing semiquantum energies (5.3): our system is a double cover of the one in sec. 4.1 with the two copies having opposite redistribution directions. Due to the multiplicity of (5.3), the semi-quantum system has *four* degeneracy points, each point corresponding to one of the four quantum edge states exchanged as suggested by the correlation diagram in fig. 8 and confirmed by the concrete computation represented in fig. 9. The four quantum edge states are grouped into two Kramers doublets, while the respective four degeneracy points form two pairs with the points in each pair related by the  $\mathcal{T}_N$  symmetry operation. Comparing to the redistribution phenomenon in fig. 5 of sec. 4, we have now twice as many degeneracy points and edge state doublets. For each doublet (and respective pair of  $\mathcal{T}_N$ -equivalent points at the poles), the phenomenon is the same as in sec. 4.

In general, on the entire interval of the tuning control parameter  $\alpha_0$ , the four individual semiquantum eigenvalues (5.3) form two bundles  $\Lambda^\pm$  of rank two, their superscripts  $\pm$  replicating the sign of (5.3) and so referring to the upper and lower superbands. There is no further natural decomposition of the  $\pm$  eigenspaces into a direct sum of one-dimensional subspaces. In fact, as we can see in fig. 9, there is no continuous uniform way to represent the bulk spectrum of (5.1) as a sum of Dirac oscillator spectra similarly to the way it was possible previously in sec. 3 and 4. On the other hand, the linearization in sec. 5.2 and the SO(3)-isotropic limit in sec. 2.3.2 and 2.3.3 provide certain grounds for the conjecture that  $\Lambda^\pm$  at large  $|\alpha_0|$  split into bundles  $\Lambda_{1,2}^\pm$  where the subscripts (1, 2) account for multiplicity 2 of (5.3). Then in the limit of large  $|\alpha_0|$ , as indicated in fig. 8, we should find  $c_1 = \pm 3$  for one pair of  $\Lambda_{1,2}$  and  $c_1 \pm 1$  for the other. These indices correspond to the number of states in the multiplets of the isotropic system, see proposition 2.1. In both cases, the sum of Chern indices gives index 0 for the rank-2 bundles  $\Lambda^\pm$ . Continuing from the large  $|\alpha_0|$  limits towards the degeneracy point  $\alpha_0 = 0$ , we can assume that  $c_1$  indices of  $\Lambda^\pm$  remain zero. For the quantum system, such combined zero index means that the total number of states in each superband equals  $2(2N + 1)$ , including  $2N$  bulk state doublets plus one edge state doublet, see fig. 8. This number is given by twice the phase space volume of  $\mathbb{S}_N^2$  without any corrections.

On the other hand, within the geometric phase framework, we should consider four local bundles  $\Delta_{1,2}^\pm$  over spheres  $\mathbb{S}^2$  enclosing one of the two degeneracies. This can be combined with one of the linearizations in sec. 5.2 which have formal control parameter  $\alpha_0$  and dynamical parameters  $(q, p)$ . For each linearization, we study the bundles  $\Delta$  over the base  $\mathbb{S}^2 \subset \mathbb{R}_{\alpha_0, q, p}$  enclosing the origin. Like in sec. 4.2, Kramers degeneracy ensures that the analysis for linearization at the poles  $\{N_1 = N\}$  and  $\{N_1 = -N\}$  gives the same result. For example, if  $\Delta|_{N_1=N}$  has index  $c_1 = 1$ , then so does  $\Delta|_{N_1=-N}$ . Block-diagonal form (5.6) means that for either linearization, we can construct unambiguously four bundles  $\Delta_1^\pm$  and  $\Delta_2^\pm$ , where (1, 2) label Dirac oscillator factor-blocks in (5.6) and  $\pm$  refer to the upper and lower superbands. Since the oscillator blocks are of opposite signs,  $\Delta_1^\pm$  and  $\Delta_2^\pm$  have indices  $c_1 = \mp 1$  and  $c_1 = \pm 1$ , respectively. So, for example, for  $\Delta_1^+$  and  $\Delta_2^+$  with indices  $c_1 = -1$  and  $c_1 = +1$  this means that one subband of the upper superband loses a state (to the lower superband) while the other subband of the same superband gains a state (from the lower superband). Adding up for two linearizations, we reconstruct lost/gained Kramers doublets. At the same time, the sum of indices for either  $\Delta_{1,2}^+$  or  $\Delta_{1,2}^-$  gives zero, reflecting that the number of states in the superbands remains unchanged.

## 6 Discussion

The simple Hamiltonian (1.1) has been widely recognized as relevant in many different physical problems [Wilczek and Shapere, 1989]. The geometric phase phenomenon in the parametric family of model systems with this Hamiltonian is directly related to the fundamental mathematical construction of vector bundles, realized as eigenstate bundles over the parameter space, and to the naturally defined connections on these bundles and topological invariants [Simon, 1983]. The parallel discovery of the quantum Hall effect [Thouless et al., 1982, Kohmoto, 1985], topological insulators, and more generally, topological phase transitions and topological phases of matter [Thouless, 1998] have arisen considerable interest in topological effects mainly in solid state and high-energy physics. On the other hand, despite being suggested very early, the same year as the paper by Haldane [1988] on the Hall effect, the dynamical modification of the geometrical phase setup [Pavlov-Verevkin et al., 1988] in finite particle systems with compact phase spaces and its relation to the separation of slow and fast variables and associated rearrangement of energy bands met with little enthusiasm in molecular and atomic physics. One possible reason may be that there are still many important discrete quantum states of these systems that can be studied individually, repeatedly, and with ever increasing accuracy, while large groups of levels, such as polyads, multiplets, shells, and generally—bands require higher excitations, special conditions, and are difficult to reach experimentally, to interpret, and to investigate theoretically. Yet energy bands and their rearrangements are common features of excited molecular systems and their thorough investigation is impending.

Our work reviewed and summarized the universal properties of slow-fast parametric semi-quantum systems with one slow degree of freedom and paws the way for the study of systems with two slow degrees of freedom (four dynamical parameters), specifically the 4-level quaternionic semiquantum systems and their full quantum analogues, and more concretely, the model quadratic spin systems with time-reversal symmetry and spin  $\frac{3}{2}$ , which are direct dynamical analogues of [Mead, 1987, Avron et al., 1989]. These systems have a slow phase space  $P$  of dimension four supplemented by one formal control parameter. The local semi-quantum eigenstate bundles  $\Delta$  and the semi-quantum eigenstate bundles  $\Lambda$  over  $P$  are now characterized by the second index  $c_2$  (cf [Faure and Zhilinskiĭ, 2002a,b]). This brings up the fundamental question of how the value of  $c_2$  and its change are reflected by the numbers of quantum states in the corresponding energy bands and by the redistribution phenomenon, respectively. This question remains yet to be fully addressed. Several compact and non-compact possibilities for  $P$  can be envisaged and their analysis promises to be of great interest and importance to mathematical theory and physical applications.

## A Chern number calculations

This appendix presents explicit calculations of Chern numbers for eigenstate bundles of several semi-quantum systems analyzed in the main body of the article. The relation between Berry setup [Berry, 1984] and topological Chern numbers was immediately recognized by Simon [1983] and concrete calculations of Chern numbers for the model Hamiltonian (1.1) were described about 30 years ago by Avron et al. [Avron et al., 1989] along with more difficult calculations for the quadratic spin Hamiltonian (cf. sec. 2.3). We reproduce these calculations for concrete Hamiltonians following the outline in [Iwai and Zhilinskiĭ, 2011].



## A.1 Chern numbers for a spin-orbital coupling system

Let us consider the semi-quantum angular momentum coupling Hamiltonian (2.1a) for  $S = \frac{1}{2}$ , which is expressed in the basis  $\{|\frac{1}{2}, \frac{1}{2}\rangle, |\frac{1}{2}, -\frac{1}{2}\rangle\}$  as

$$H = \frac{1}{2} \begin{pmatrix} N_1 & N_- \\ N_+ & -N_1 \end{pmatrix}, \quad N_{\pm} = N_2 \pm iN_3, \quad (\text{A.1})$$

cf. (2.3) and recall that in the semi-quantum setting, we view the ‘‘slow’’ angular momentum operator  $\hat{N}$  as a classical vector variable  $\mathbf{N}$ . This brings us within the geometric phase setup [Simon, 1983]. The eigenvalues of the semi-quantum Hamiltonian

$$\lambda_{\pm}(\mathbf{N}) = \pm \frac{1}{2} N, \quad N = \|\mathbf{N}\| \quad (\text{A.2})$$

are obtained straightforwardly. The eigenvector associated with  $\lambda_+(\mathbf{N})$  can be expressed in two ways

$$|u_{\text{up}}^+\rangle = \frac{1}{N_{\text{up}}^+} \begin{pmatrix} N_2 - iN_3 \\ N - N_1 \end{pmatrix}, \quad N_{\text{up}}^+ = \sqrt{2N(N - N_1)}, \quad \text{and} \quad (\text{A.3a})$$

$$|u_{\text{down}}^+\rangle = \frac{1}{N_{\text{down}}^+} \begin{pmatrix} N + N_1 \\ N_2 + iN_3 \end{pmatrix}, \quad N_{\text{down}}^+ = \sqrt{2N(N + N_1)}. \quad (\text{A.3b})$$

It should be pointed out that  $|u_{\text{up}}^+\rangle$  and  $|u_{\text{down}}^+\rangle$  cannot be defined at the north (N) and the south (S) poles of the two-sphere  $\mathbb{S}_N^2$  of radius  $N$ , respectively. In other words, their respective domains are

$$U_{\text{up}}^+ = \mathbb{S}_N^2 \setminus \text{N} \quad \text{and} \quad U_{\text{down}}^+ = \mathbb{S}_N^2 \setminus \text{S}. \quad (\text{A.4})$$

We call the points where the eigenvectors cannot be defined *exceptional*. On the intersection  $U_{\text{up}}^+ \cap U_{\text{down}}^+$ , the eigenvectors  $|u_{\text{up}}^+\rangle$  and  $|u_{\text{down}}^+\rangle$  are related by

$$|u_{\text{up}}^+\rangle = \eta |u_{\text{down}}^+\rangle \quad \text{with} \quad \eta = \frac{N_2 - iN_3}{\sqrt{N_2^2 + N_3^2}} = \exp(-i\phi). \quad (\text{A.5})$$

This relation and (A.3) determine the eigenvector bundle  $\Lambda_+$  over  $\mathbb{S}_N^2$  associated with eigenvalue  $\lambda_+(\mathbf{N})$ . The local connection forms are defined, respectively, as

$$A_{\text{up/down}}^+ = \langle u_{\text{up/down}}^+ | d | u_{\text{up/down}}^+ \rangle, \quad (\text{A.6})$$

and are related on  $U_{\text{up}} \cap U_{\text{down}}$  by

$$A_{\text{up}}^+ = A_{\text{down}}^+ + \eta^{-1} d\eta. \quad (\text{A.7})$$

The local curvature forms are defined, respectively, as

$$F_{\text{up/down}}^+ = dA_{\text{up/down}}^+. \quad (\text{A.8})$$

Since  $F^+ := F_{\text{up}}^+ = F_{\text{down}}^+$  on  $U_{\text{up}} \cap U_{\text{down}}$ , the curvature form  $F^+$  is defined globally on  $\mathbb{S}_N^2$ .

In order to evaluate the first Chern number  $c_1$  of  $\Lambda_+$ , we integrate the curvature form  $F^+$  over  $\mathbb{S}_N^2$  with spherical coordinates  $(\theta, \phi)$ . Let  $\mathbb{S}_{N+}^2$ ,  $\mathbb{S}_{N-}^2$ , and  $\mathbb{S}_N^1$  denote

the northern and southern hemispheres, and of the equator of  $\mathbb{S}_N^2$ . Then, the integral of  $F^+$  over  $\mathbb{S}_N^2$  is calculated using the Stokes theorem, (A.5), and (A.7)

$$\begin{aligned} \int_{\mathbb{S}_N^2} F^+ &= \int_{\mathbb{S}_{N+}^2} F_{\text{down}}^+ + \int_{\mathbb{S}_{N-}^2} F_{\text{up}}^+ = \int_{\mathbb{S}_N^1} (A_{\text{down}}^+ - A_{\text{up}}^+) \\ &= - \int_{\mathbb{S}_N^1} \eta^{-1} d\eta = i \int_0^{2\pi} d\phi = 2\pi i. \end{aligned} \quad (\text{A.9})$$

1 It follows that the first Chern number for the bundle  $\Lambda_+$  is defined and evaluated as

$$2 \quad c_1 = \frac{i}{2\pi} \int_{\mathbb{S}_N^2} F^+ = -1. \quad (\text{A.10})$$

3 In the same manner, we find that the first Chern number  $c_1$  for the eigenspace bundle  
4  $\Lambda_-$  associated with  $\lambda_-(N)$  equals 1.

## 5 A.2 Index for a vector field

6 The Chern number can be equally calculated locally through the index of the vector  
7 field. This is important for further applications to linearized problems.

Manipulation (A.9) is valid also when the equator  $\mathbb{S}_N^1$  is deformed into a small circle  $\Gamma(\theta_0)$  around the north pole with small constant latitude  $\theta_0$ . In the limit  $\theta_0 \rightarrow 0$ , the integral of  $\eta^{-1}d\eta$  along  $\Gamma(\theta_0)$  gives the index of a vector field locally defined in the neighbourhood of the north pole [Iwai and Zhilinskiĭ, 2011]. To see this, we take  $(x, y) = (N_2, N_3)$  as local coordinates on the northern hemisphere. Then, we can view twice the upper right component  $N_-$  of  $H$  as a vector field  $\mathbf{W} = (X, Y) = (N_2, -N_3)$  on the vicinity of the north pole, where  $\mathbf{W}$  has a singular point (or vanishes) at the north pole. In terms of  $(X, Y)$ , we rewrite  $\eta$  as

$$\eta = \frac{X + iY}{\sqrt{X^2 + Y^2}},$$

and further obtain

$$\eta^{-1}d\eta = i \frac{XdY - YdX}{X^2 + Y^2}.$$

Outside of the north pole, we denote the normalized  $\mathbf{W}$  by  $\mathbf{w}$  and define  $\mathbf{v}$  to be the vector field  $\mathbf{w}$  rotated counterclockwise by  $\pi/2$ ,

$$\mathbf{w} = \frac{1}{\sqrt{X^2 + Y^2}} \begin{pmatrix} X \\ Y \end{pmatrix}, \quad \mathbf{v} = \frac{1}{\sqrt{X^2 + Y^2}} \begin{pmatrix} -Y \\ X \end{pmatrix}.$$

Then, the  $\eta^{-1}d\eta$  is rewritten as

$$\eta^{-1}d\eta = i\mathbf{v} \cdot d\mathbf{w},$$

so that one obtains

$$\frac{1}{2\pi i} \int_{\Gamma(\theta_0)} \eta^{-1}d\eta = \frac{1}{2\pi} \int_{\Gamma(\theta_0)} \mathbf{v} \cdot d\mathbf{w}.$$

If we make  $\theta_0$  tend to zero, then the right-hand side of the above equation becomes the definition of the index of the vector field  $\mathbf{W}$  at the singular point;

$$\text{ind}(\mathbf{W}) = \lim_{\theta_0 \rightarrow 0} \frac{1}{2\pi} \int_{\Gamma(\theta_0)} \mathbf{v} \cdot d\mathbf{w}.$$

1 In calculating the index, the linear approximation of  $\mathbf{W}$  works well. In fact, we see  
2 that

$$3 \quad \text{Ind}(\mathbf{W}) = \begin{cases} 1 & \text{if } \det A > 0, \\ -1 & \text{if } \det A < 0, \end{cases} \quad A = \begin{pmatrix} \frac{\partial X}{\partial x} & \frac{\partial X}{\partial y} \\ \frac{\partial Y}{\partial x} & \frac{\partial Y}{\partial y} \end{pmatrix}, \quad (\text{A.11})$$

where  $A$  is the Jacobi matrix evaluated at the origin  $(x, y) = (0, 0)$ . For the vector field  $\mathbf{W} = (N_2, -N_3)$ , one has

$$A = \begin{pmatrix} 1 & 0 \\ 0 & -1 \end{pmatrix},$$

4 so that  $\text{ind}(\mathbf{W}) = -1$ . It then turns out that

$$5 \quad c_1 = \frac{i}{2\pi} \int_{\mathbb{S}_N^2} F^+ = \text{Ind}(\mathbf{W}) = -1. \quad (\text{A.12})$$

6 Eqs. (A.11) and (A.12) are put together to show that the Chern number  $c_1$  is determined  
7 through the linearization of the Hamiltonian at the exceptional point for the eigenvector.

So far we have taken a small circle around the north pole. We may equally take a small circle around the south pole. In the southern hemisphere, we have to take  $(x, y) = (N_3, N_2)$  as local coordinates on account of the orientation of the sphere. In this setting, the locally defined vector field determined by twice the upper-right component  $N_-$  is given by  $\mathbf{W}' = (X', Y') = (-N_3, N_2)$ , where  $X'$  and  $Y'$  are the imaginary and the real parts of  $N_-$ . Then, the Jacobi matrix evaluated at the south pole is

$$\begin{pmatrix} \frac{\partial X'}{\partial x} & \frac{\partial X'}{\partial y} \\ \frac{\partial Y'}{\partial x} & \frac{\partial Y'}{\partial y} \end{pmatrix} = \begin{pmatrix} -1 & 0 \\ 0 & 1 \end{pmatrix},$$

8 so that we obtain  $\text{Ind}(\mathbf{W}') = -1$ , the same as  $\text{Ind}(\mathbf{W})$ .

9 In the above discussion, we assume a sole exceptional point at the north or the  
10 south pole. If an eigenvector has several exceptional points, we have to linearize the  
11 Hamiltonian at every such point and to sum up the respective indices in order to obtain  
12 the Chern number  $c_1$ .

### 13 A.3 Delta-Chern calculation in the non-compact setting

14 We now look into the linearized Hamiltonian at the north pole of  $\mathbb{S}^2(N)$ . Associating  
15 the Poisson algebra  $\text{so}(3)$  of angular momenta  $\mathbf{N}$  with the  $N$ -space  $\mathbb{R}_N^3$ , we obtain a  
16 Poisson manifold with  $\mathbb{S}^2(N)$  as its symplectic submanifold. The Poisson commuta-  
17 tion relation  $\{N_2, N_3\} = N_1$  for fixed  $N > 0$  gives rise to

$$18 \quad \left\{ \frac{N_2}{\sqrt{N}}, \frac{N_3}{\sqrt{N}} \right\} = \frac{N_1}{N}.$$

Then, on the tangent plane to  $\mathbb{S}_N^2$  at the north pole  $\{N_1 = N\}$ , we can introduce canonical variables by

$$q = \frac{N_2}{\sqrt{N}}, \quad p = \frac{N_3}{\sqrt{N}}.$$

19 Rewriting the initial Hamiltonian as

$$20 \quad H = \sqrt{\frac{N}{2}} \begin{pmatrix} \sqrt{\frac{N}{2}} \frac{N_1}{N} & \frac{N_-}{\sqrt{2\sqrt{N}}} \\ \frac{N_+}{\sqrt{2\sqrt{N}}} & -\sqrt{\frac{N}{2}} \frac{N_1}{N} \end{pmatrix} \quad (\text{A.13})$$

1 and rescaling by  $\sqrt{\frac{N}{2}}$ , we obtain the linearized Hamiltonian

$$2 \quad K_\mu = \begin{pmatrix} \mu & \frac{q-ip}{\sqrt{2}} \\ \frac{q+ip}{\sqrt{2}} & -\mu \end{pmatrix}, \quad \mu = \sqrt{\frac{N}{2}}. \quad (\text{A.14})$$

3 Although  $\mu$  is a positive number by the initial definition, we will treat  $\mu$  as a parameter  
4 taking values in  $\mathbb{R}$ . At the same time, if we linearize the Hamiltonian at the south pole  
5  $\{N_1 = -N\}$ , we obtain

$$6 \quad K'_\mu = \begin{pmatrix} -\mu & -i\frac{q+ip}{\sqrt{2}} \\ i\frac{q-ip}{\sqrt{2}} & \mu \end{pmatrix}. \quad (\text{A.15})$$

7 The eigenvalues of  $K_\mu$

$$8 \quad \nu_\pm = \pm \sqrt{\mu^2 + \frac{1}{2}(q^2 + p^2)} \quad (\text{A.16})$$

are degenerate if and only if  $\mu = 0$  and  $q = p = 0$ . The eigenvectors associated with  
 $\nu_+$  are expressed in two ways as

$$|v_{\text{up}}^+\rangle = \frac{1}{M_{\text{up}}^+} \begin{pmatrix} (q-ip)/\sqrt{2} \\ \nu_+ - \mu \end{pmatrix}, \quad M_{\text{up}}^+ = \sqrt{2\nu_+(\nu_+ - \mu)}, \quad (\text{A.17a})$$

$$|v_{\text{down}}^+\rangle = \frac{1}{M_{\text{down}}^+} \begin{pmatrix} \nu_+ + \mu \\ (q+ip)/\sqrt{2} \end{pmatrix}, \quad M_{\text{down}}^+ = \sqrt{2\nu_+(\nu_+ + \mu)}, \quad (\text{A.17b})$$

9 where the domains of  $|v_{\text{up/down}}^+\rangle$  are, respectively,

$$10 \quad V_{\text{up}}^+ = \begin{cases} \mathbb{R}^2 \setminus \{0\} & \text{if } \mu > 0, \\ \mathbb{R}^2 & \text{if } \mu < 0, \end{cases} \quad V_{\text{down}}^+ = \begin{cases} \mathbb{R}^2 & \text{if } \mu > 0, \\ \mathbb{R}^2 - \{0\} & \text{if } \mu < 0. \end{cases} \quad (\text{A.18})$$

11 On the intersection  $V_{\text{up}}^+ \cap V_{\text{down}}^+$ , the eigenvectors  $|v_{\text{up/down}}^+\rangle$  are related by

$$12 \quad |v_{\text{up}}^+\rangle = |v_{\text{down}}^+\rangle \zeta, \quad \zeta = \frac{q-ip}{\sqrt{q^2+p^2}}. \quad (\text{A.19})$$

13 In what follows, we show that delta-Chern  $\delta c_1$ , a change in the formal Chern num-  
14 ber  $c_1$  for the linearized Hamiltonian with non-compact phase space [Iwai and Zhilin-  
15 skií, 2016], provides the exact value of the Chern number for the semi-quantum eigen-  
16 state bundles of the initial Hamiltonian (A.1). The main step here is the calculation  
17 of  $\delta c_1$  for non-compact setting where it appears as a mapping degree. To simplify our  
18 notation, we introduce variables

$$19 \quad \mathbf{k} = (k_1, k_2) = (q, p)/\sqrt{2}.$$

20 Then, the model Hamiltonian  $K_\mu$  with non-compact phase space  $\mathbb{R}_{\mathbf{k}}^2$  is expressed as

$$21 \quad K_\mu = \begin{pmatrix} \mu & k_1 - ik_2 \\ k_1 + ik_2 & -\mu \end{pmatrix}, \quad \mathbf{k} \in \mathbb{R}^2, \quad (\text{A.20})$$

22 and eq. (A.19) is rewritten as

$$23 \quad |v_{\text{up}}^+(\mathbf{k})\rangle = \zeta |v_{\text{down}}^+(\mathbf{k})\rangle, \quad \text{with } \zeta = \frac{k_1 - ik_2}{k}, \quad k := \|\mathbf{k}\| = \sqrt{k_1^2 + k_2^2}. \quad (\text{A.21})$$

1 This relation determines the complex line bundle associated with  $\nu_+$ , which we call the  
 2 eigen-line bundle and denote by  $L^+$ .

3 Local connection forms  $B_{\text{up}}^+$  and  $B_{\text{down}}^+$  for  $L^+$  are defined to be

$$4 \quad B_{\text{up}}^+ = \langle v_{\text{up}}^+(\mathbf{k}) | d | v_{\text{up}}^+(\mathbf{k}) \rangle, \quad B_{\text{down}}^+ = \langle v_{\text{down}}^+(\mathbf{k}) | d | v_{\text{down}}^+(\mathbf{k}) \rangle, \quad (\text{A.22})$$

5 respectively. From (A.21), they are shown to be related by

$$6 \quad B_{\text{up}}^+ - B_{\text{down}}^+ = \zeta^{-1} d\zeta, \quad (\text{A.23})$$

7 where it is to be noted that this relation is independent of  $\mu$ . The curvature form  $G^+$  is  
 8 globally defined on  $\mathbb{R}^2$  and evaluated as

$$9 \quad G^+ = dB_{\text{up}}^+ = dB_{\text{down}}^+ = \frac{i}{2} \frac{\mu dk_1 \wedge dk_2}{(k^2 + \mu^2)^{3/2}}. \quad (\text{A.24})$$

10 The Chern number can be formally defined and evaluated, by using (A.24), as

$$11 \quad \frac{i}{2\pi} \int_{\mathbb{R}^2} G^+ = -\frac{1}{2} \text{sgn}(\mu). \quad (\text{A.25})$$

While the formal Chern number (A.25) is not integer-valued, the difference between  
 the formal Chern number for  $\mu > 0$  and that for  $\mu < 0$  takes an integer value,

$$\frac{i}{2\pi} \int_{\mathbb{R}^2} G^+|_{\mu>0} - \frac{i}{2\pi} \int_{\mathbb{R}^2} G^+|_{\mu<0} = -1,$$

12 which is the same value as in Eq. (A.12).

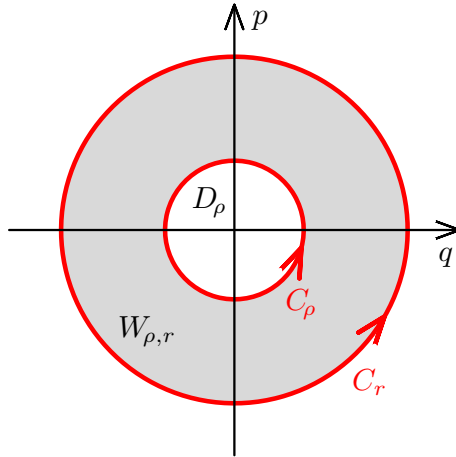


**Figure 11:** Circles  $C_\rho$  and  $C_r$  of respective radii  $\rho$  and  $r$  form the boundary of the annulus  $W_{\rho,r}$ , and  $C_\rho$  is also the boundary of disk  $D_\rho$ .

In what follows, we show that the difference makes sense as a topological quantity. For  $\mu > 0$ , the origin  $\mathbf{k} = 0$  is the exceptional point for  $|v_{\text{up}}^+(\mathbf{k})\rangle$  but not so for  $|v_{\text{down}}^+(\mathbf{k})\rangle$ . With this in mind, we integrate the curvature form  $G^+$  on the regions  $D_\rho$

and  $W_{\rho,r}$  shown in Fig. 11 to obtain

$$\begin{aligned}
\int_{\mathbb{R}^2} G^+ &= \int_{D_\rho} dB_{\text{down}}^+ + \lim_{r \rightarrow \infty} \int_{W_{\rho,r}} dB_{\text{up}}^+ \\
&= \int_{C_\rho} B_{\text{down}}^+ + \lim_{r \rightarrow \infty} \left( \int_{-C_\rho} B_{\text{up}}^+ + \int_{C_r} B_{\text{up}}^+ \right) \\
&= - \int_{C_\rho} \zeta^{-1} d\zeta + \lim_{r \rightarrow \infty} \int_{C_r} B_{\text{up}}^+ \quad \text{for } \mu > 0, \tag{A.26}
\end{aligned}$$

where use has been made of the relation (A.23) and the Stokes theorem. For  $\mu < 0$ , the origin is the exceptional point of  $|v_{\text{down}}^+(\mathbf{k})\rangle$  but not so for  $|v_{\text{up}}^+(\mathbf{k})\rangle$ . A similar calculation to the above provides

$$\int_{\mathbb{R}^2} G^+ = \int_{C_\rho} \zeta^{-1} d\zeta + \lim_{r \rightarrow \infty} \int_{C_r} B_{\text{down}}^+ \quad \text{for } \mu < 0. \tag{A.27}$$

1 Although eqs. (A.26) and (A.27) contain locally-defined terms,  $B_{\text{up}}^+$  and  $B_{\text{down}}^+$ , their  
2 difference may give a characteristics of the eigen-line bundle  $L^+$  depending on  $\mu$ . In  
3 fact, using (A.23) and the equality  $\int_{C_r} \zeta^{-1} d\zeta = \int_{C_\rho} \zeta^{-1} d\zeta$ , one can verify that

$$\frac{i}{2\pi} \int_{\mathbb{R}^2} G^+|_{\mu>0} - \frac{i}{2\pi} \int_{\mathbb{R}^2} G^+|_{\mu<0} = -\frac{i}{2\pi} \int_{C_\rho} \zeta^{-1} d\zeta. \tag{A.28}$$

5 Equation (A.28) implies that a jump  $\delta c_1$  in the formal Chern number accompanying the  
6 variation of the parameter  $\mu$  is a topological invariant which is given by winding  
7 number associated with the mapping defined through the transition function  $\zeta : C_\rho \rightarrow$   
8  $U(1)$ . We note also that (A.28) holds for any  $\mu$ -independent function  $\zeta$ .

#### 9 A.4 Delta-Chern as the index of the $\Delta$ -bundle

10 We turn to the relation between the delta-Chern index  $\delta c_1$  which is introduced in  
11 eq. (A.28) of sec. A.3 and the index  $c_1$  of the eigenvector bundle  $\Delta$  over the sphere  
12  $\mathbb{S}^2$  surrounding the origin in the parameter space. The  $\Delta$  bundle arises naturally in  
13 all geometric phase systems [Simon, 1983, Avron et al., 1988, Wilczek and Shapere,  
14 1989] when no distinction of control parameters as dynamical and formal (sec. 1.1) is  
15 made. The relation of the two indices is suggested in sec. 1.2 and is further discussed  
16 and exploited in the analysis of concrete systems, notably in sec. 2.2, sec. 3.1.1 and  
17 footnote 10, secs. 4.3 and 5.3. In this section, we uncover this relation explicitly using  
18 the results of sec. A.1 and A.3.

19 Let us consider a generic semi-quantum  $2 \times 2$  Hermitian matrix Hamiltonian  $H_m$   
20 with one tuning control parameter  $m \in \mathbb{R}$  and dynamical control parameters defining  
21 points  $\mathbf{p}$  on a two-dimensional classical phase space  $P$  of the slow subsystem. The total  
22 parameter space  $\mathbb{R} \times P$  is of dimension 3. The eigenvalues  $\lambda_{1,2}$  of  $H_m$  are functions  
23  $\mathbb{R} \times P \rightarrow \mathbb{R}$ . In a generic system, they become degenerate [von Neumann and Wigner,  
24 1929, Arnold, 1995] at isolated points  $\zeta_0 = (m_0, \mathbf{p}_0)$  of  $\mathbb{R} \times P$ . Let us assume that  
25  $\lambda_{1,2}$  become degenerate for  $m_0 = 0$ . If other isolated non-regular values of  $m$  exist, we  
26 can always work on a sufficiently small open regular neighbourhood  $M \ni 0$ , otherwise  
27  $M = \mathbb{R}$ . Similarly, we can always work on an open neighbourhood of  $\mathbf{p}_0 \in P$  where  
28  $\mathbf{p}_0$  remains a unique degeneracy point, but for simplicity, let us assume for now that  
29  $\mathbf{p}_0$  is unique on  $P$ . Shifting energy by  $\lambda_0(m, \mathbf{p}) = \frac{1}{2}(\lambda_1 + \lambda_2)$  can always make  $H_m$

1 traceless on  $M \times P$ . Since  $\lambda_{1,2}$  remain distinct on  $M \setminus 0$ , the adjusted eigenvalues  
 2  $\lambda_+$  and  $\lambda_-$  are strictly positive and strictly negative on  $(M \times P) \setminus \zeta_0$  and become 0  
 3 in the degeneracy point  $\zeta_0$ . At the same time, the derivatives  $\partial\lambda_{\pm}/\partial(m, \mathbf{p})|_{\zeta_0}$  do not  
 4 vanish in a typical system [Arnold, 1995]. Consequently, the linearization of  $H_m$  at  $\zeta_0$   
 5 is of the type (1.1) with  $\zeta_0$ -specific parameters  $\mathbf{B}(\zeta_0)$ . Furthermore, for a sufficiently  
 6 general physical interaction between the two dynamical subsystems, this linearization  
 7 results in a Dirac-oscillator-type system (sec. 2.2) with local symplectic coordinates  
 8  $(q, p)$  on  $\mathbb{R}_{q,p}^2 = T_{\mathbf{p}_i}P$ ,  $\{q, p\} = 1$ . Sections 3.2 and 4.2 provide concrete illustrations.

9 For each regular  $m \in M \setminus 0$ , the eigenvectors corresponding to eigenvalues  $\lambda_{1,2}$  of  
 10  $H_m$  form two rank-1 complex line bundles over  $P$ , which we refer to as *eigenvector or*  
 11 *eigenstate bundles*, and which we denote  $\Lambda_{1,2}$  in sec. 1.2 and in the rest of the article.  
 12 Since the Chern number of the combined rank-2 bundle  $\Lambda$  over  $P$ , or the *eigenspace*  
 13 *bundle*, remains unchanged for all  $m \in M$ , it suffices to study one of the  $\Lambda_{1,2}$  compo-  
 14 nents. In what follows, we will assume that  $H_m$  is (made) traceless, and adapting the  
 15 more informative  $\pm$  notation, we will work with the  $\Lambda_+$  bundle.  $\Lambda_+$  constitutes two  
 16 *continuous* one-parameter families of bundles  $\Lambda_{+,m<0}$  and  $\Lambda_{+,m>0}$ . In other words,  
 17 bundles  $\Lambda_{+,m}$  over  $P$  have a certain fixed topology on each disconnected component of  
 18  $M \setminus 0$ . The delta-Chern index  $\delta c_1$  characterizes the change of this topology at  $m = 0$ .  
 19 For a compact  $P$  (with sole point  $\mathbf{p}_0$ ), this index can be computed simply as

$$20 \quad \delta c_1(\Lambda_+) = c_1(\Lambda_{+,m>0}) - c_1(\Lambda_{+,m<0}). \quad (\text{A.29})$$

21 In the non-compact setting, we can either use formal Chern numbers (A.25) [Iwai and  
 22 Zhilinskií, 2011, 2015] or rely directly on (A.28). Since (A.28) defines a local number  
 23 its application does, generally, require linearization at  $\zeta_0$ .

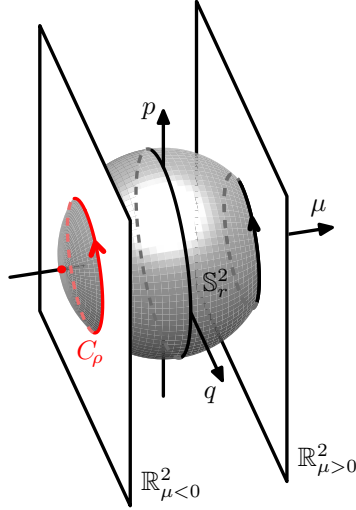


**Figure 12:** Base spaces  $\mathbb{R}_\mu^2$  and  $\mathbb{S}_r^2$  of the  $\Lambda_{\pm}$  and  $\Delta_{\pm}$  eigenvector bundles, respectively, in the parameter space  $\mathbb{R}^3$  of the Dirac oscillator (sec. 2.2). The spaces intersect on the  $\mathbb{S}^1$  circle  $C_\rho$  involved in the Chern index calculus, see sec. A.4 for details, and compare to fig 11.

24 At the same time, we consider *local eigenvector bundles*  $\Delta_+$  over sphere  $\mathbb{S}_{r,\zeta_0}^2$   
 25 of sufficiently small radius  $r$  surrounding  $\zeta_0$  in the combined control parameter space  
 26  $M \times P$ . In this space, as illustrated in fig. 12, typical non-empty intersections of  $P$  and

1  $\mathbb{S}_{r, \mathbf{p}_i}^2$  are circles of radius  $\rho = (r^2 - m^2)^{1/2} > 0$

$$2 \quad C_{\rho, m} := \mathbb{S}_\rho^1 = (m, P) \cap \mathbb{S}_{r, \zeta_0}^2 \quad \text{with fixed } m, |m| < r. \quad (\text{A.30})$$

3 Indeed, the existence of  $\partial\lambda/\partial\mathbf{p}$  at  $\mathbf{p}_0$  already requires that  $\mathbf{p}_0$  is contained in  $P$  together  
4 with an open saturated disk  $D_\epsilon = \{\mathbf{p} \in P; \|\mathbf{p}_0 - \mathbf{p}\| < \epsilon\}$  of some, possibly small,  
5 finite radius  $\epsilon > 0$ . Taking  $r < \epsilon$ , we make sure that  $\mathbb{S}_{r, \zeta_0}^2 \subset M \times P$  and consequently,  
6 that typical non-empty constant- $m$  sets  $C_{\rho, m}$  on  $\mathbb{S}_{r, \zeta_0}^2$  lie entirely within  $D_\epsilon$ . We have  
7 seen across sec. A.1 and A.3 that Chern and delta-Chern numbers  $c_1$  and  $\delta c_1$  of line  
8 bundles  $\Lambda_+$  are computed (for fixed regular values of the tuning parameter  $m$ ) using  
9 integrals (A.9) and (A.28) over certain circles in the base space  $P$ . This makes  $C_{\rho, m}$   
10 central to our analysis here.

11 Consider the  $\Delta$  and  $\Lambda$  bundles of the Dirac oscillator (sec. 2.2), the most basic  
12 typical  $2 \times 2$  semi-quantum system. It has traceless Hamiltonian (2.10) with tuning  
13 control parameter  $\mu \in M = \mathbb{R}$  and dynamical control parameters  $(q, p) \in P = \mathbb{R}^2$ . Its  
14 eigenvalues have a sole degeneracy point  $\mathbf{p}_0 = (0, (0, 0))$ . The following lemma lays  
15 the corner stone of our analysis.

16 **Lemma A.1** ( $\delta c_1$  and  $c_1(\Delta)$  in the noncompact local setup): *The Chern number  $c_1$  of*  
17 *the local eigenvalue bundle  $\Delta_+$  of the Dirac oscillator (sec. 2.2) equals the delta-Chern*  
18 *index  $\delta c_1$  of its one-parameter family of bundles  $\Lambda_{+, \mu}$ ,*

$$19 \quad c_1(\Delta_+) = \delta c_1(\Lambda_+) = 1 .$$

20 *Proof.* As pointed out in sec. 2.2, the local bundle  $\Delta$  of the Dirac oscillator can be  
21 identified with that of the Berry spin system (1.1) and of the spin-orbit system (2.1)–  
22 (2.3)–(A.1) through a simple GL(3) parameter rescaling

$$23 \quad (2\mu, \sqrt{2}q, -\sqrt{2}p) \mapsto \mathbf{B} \mapsto \mathbf{N} .$$

24 Since the determinant of this map (cf. [Iwai and Zhilinskiĭ, 2017, eq. (107)]) is negative,  
25 the index (A.10) and the Chern number  $c_1(\Delta_+)$  are of opposite signs, i.e.,

$$26 \quad c_1(\Delta_+) = 1 .$$

27 Further comparing to sec. A.1, we note that now the radius of the base space  $\mathbb{S}_N^2$  be-  
28 comes  $r$ , and that the transition function in (A.5) equals

$$29 \quad \eta = \frac{q + ip}{\sqrt{q^2 + p^2}} = \exp(i\varphi) \quad \text{with } \varphi = \arg(q + ip) = -\phi .$$

30 As pointed out in sec. A.2, the integration (A.9) may follow any constant level set of  
31  $N_1 = 2\mu$  with  $|2\mu| < r$ , such as

$$32 \quad C_\rho = \mathbb{S}_\rho^1 \subset \mathbb{R}_{\mu < 0}^2 \cap \mathbb{S}_r^2 = \left\{ (\mu, q, p); 2(q^2 + p^2) = \rho^2, 2\mu = -\sqrt{r^2 - \rho^2} \right\}$$

33 shown in fig. 12. Comparing to the delta-Chern computation in sec. A.3, we note that  
34 its matrix Hamiltonian (A.14) is made identical to (2.10) through

$$35 \quad (\mu, q, p) \mapsto (-\sqrt{2}\mu, -q, -p) .$$

36 It follows that (A.28) and the delta-Chern of (2.10) are of opposite signs, i.e.,

$$37 \quad \delta c_1(\Lambda_+) = 1 .$$



1 In more detail, we can see that in our coordinates, the transition function

$$2 \quad \zeta = -\frac{q - ip}{\sqrt{q^2 + p^2}} = -\frac{1}{\eta}$$

3 differs in sign from its original form in (A.19) while the direction on  $C_\rho$  is preserved.  
 4 The sign gets trivially cancelled in (A.28). On the other hand, the inversion of the  
 5 parameter space  $\mathbb{R}^3$ , which can be seen otherwise as flipping the energy-axis, is im-  
 6 portant. The positive-energy bundle  $\Lambda_+$  of (A.14) corresponds to the negative-energy  
 7 bundle  $\Lambda_-$  of the Dirac oscillator (2.10). Therefore, computing the delta-Chern number  
 8 for the  $\Lambda_+$  bundle of (2.10), we should use (A.28) with an additional factor of  $-1$

$$9 \quad \delta c_1(\Lambda_+) = \frac{i}{2\pi} \int_{C_\rho} \zeta^{-1} d\zeta = \frac{i}{2\pi} \int_{C_\rho} \eta d\eta^{-1} = \frac{1}{2\pi} \int_{C_\rho} d\varphi = 1. \quad \square$$

10 A similar lemma can be formulated and proven for systems with compact phase  
 11 space  $P$ . We turn to the particular system in sec. 3 with  $P = \mathbb{S}_N^2$  and tuning control  
 12 parameter  $\gamma \in (0, 1)$  because, like the Dirac oscillator in lemma A.1, it has a sole  
 13 degeneracy point

$$14 \quad (\gamma, \mathbf{p}_0) = \left(\frac{1}{2}, (-N, 0, 0)\right) \in [0, 1] \times \mathbb{S}_N^2.$$

15 **Lemma A.2** ( $\delta c_1$  and  $c_1(\Delta)$  in the compact local setup): *The Chern number  $c_1$  of the*  
 16 *local bundle  $\Delta_+$  of the basic spin-orbit system in sec. 3 with tuning and dynamical*  
 17 *control parameters  $\gamma \in [0, 1]$  and  $\mathbf{p} = \{N, \|N\| = N\} \in \mathbb{S}_N^2$ , respectively, equals the*  
 18 *delta-Chern index  $\delta c_1$  of its one-parameter family of bundles  $\Lambda_{+, \gamma}$  over  $\mathbb{S}_N^2$ .*

19 *Proof.* The Chern numbers  $c_1(\Lambda_\pm)$  equal zero for  $\gamma = 0$  and are computed in sec. A.1  
 20 for  $\gamma = 1$ . Continuing from these limits, we find  $\delta c_1(\Lambda_+) = -1 - 0 = -1$ . We can  
 21 also rely on sec. A.1 and footnote 10 to compute  $c_1(\Delta_+)$  like we did in the proof of  
 22 lemma A.1. The circle  $C_\rho = \mathbb{S}_{N, \mu < 0}^2 \cap \mathbb{S}_{(\mu, N_2, N_3)}^2$  parameterized by  $(N_2, N_3)$  is at the  
 23 centre of the analysis. Omitting the details,  $c_1(\Delta_+) = -1$ .  $\square$

24 *Remark A.1* (linearization). By itself, lemma A.2 does not imply any linearization of the semi-  
 25 quantum Hamiltonian  $H_\gamma$  defined on  $\mathbb{S}_N^2$ . However, the radius  $r < N$  of the base space  $\mathbb{S}_r^2$  of  
 26 the local bundle  $\Delta$  can be chosen sufficiently small  $r \ll N$  for linearizing  $H_\gamma$  at the degeneracy  
 27 point  $N = (-N, 0, 0)^T$  to be viable (see sec. 3.2) and for the Chern index computation to take  
 28 advantage of such linearization. Delta-Chern  $\delta c_1$  can as well be defined and computed locally at  
 29 the  $(-N, 0, 0)$  pole using the linearization approach in sec. A.3.

30 It remains to address the situation with several equivalent isolated degeneracy points  
 31  $(0, \mathbf{p}_i)$  on  $(0, P)$  where  $\lambda_{1,2}$  attain the same value. The existence of such points may  
 32 be related to the presence of symmetries  $P \rightarrow P$  or, more generally, of a nontrivial  
 33 isotropy group  $\text{Diff}(P)$  whose operations leave  $H_m$  invariant, see sec. 4 and [Iwai and  
 34 Zhilinskií, 2017] for the concrete examples. In a sufficiently small open neighbourhood  
 35 of each  $(0, \mathbf{p}_i)$ , the system is generic in the sense of [von Neumann and Wigner, 1929,  
 36 Arnold, 1995] and our lemmas apply. Following the ideas in sec. A.2, we can sum the  
 37 Chern numbers  $c_1$  of the local bundles  $\Delta_{+, i}$  in order to match the delta-Chern  $\delta c_1(\Lambda_+)$   
 38 for the bundle  $\Lambda_+$  over the entire  $P$ .

## 39 A.5 Spin-orbit coupling Hamiltonian in the presence of a magnetic 40 field

41 We calculate here the Chern numbers for semi-quantum Hamiltonian (3.1) using the  
 42 matrix representation (3.3) in the basis  $\{|\frac{1}{2}, \frac{1}{2}\rangle, |\frac{1}{2}, -\frac{1}{2}\rangle\}$  and with parameter  $\gamma$  replaced

1 by parameter  $t$

$$2 \quad H_t = (1-t) \begin{pmatrix} 1 & 0 \\ 0 & -1 \end{pmatrix} + \frac{t}{N} \begin{pmatrix} N_1 & N_- \\ N_+ & -N_1 \end{pmatrix}, \quad 0 \leq t \leq 1. \quad (\text{A.31})$$

3 The eigenvalues (3.5) of  $H_t$

$$4 \quad \lambda_{\pm} = \pm \sqrt{1 - 2t(1-t)(1 - N_1/N)}, \quad (\text{A.32})$$

are degenerate if and only if  $N_1 = -N$  and  $t = \frac{1}{2}$ . The eigenvector associated with  $\lambda_+$  can be expressed in two ways as

$$|u_{\text{up}}^+\rangle = \frac{1}{N_{\text{up}}^+} \begin{pmatrix} tN_-/N \\ \lambda_+ - 1 + t - tN_1/N \end{pmatrix} \quad \text{and} \quad (\text{A.33a})$$

$$|u_{\text{down}}^+\rangle = \frac{1}{N_{\text{down}}^+} \begin{pmatrix} \lambda_+ + 1 - t + tN_1/N \\ tN_+/N \end{pmatrix}, \quad (\text{A.33b})$$

where the normalization factors  $N_{\text{up/down}}^+$  are given, respectively, by

$$N_{\text{up}}^+ = \sqrt{2\lambda_+(\lambda_+ - 1 + t(1 - N_1/N))} \quad \text{and} \quad (\text{A.34a})$$

$$N_{\text{down}}^+ = \sqrt{2\lambda_+(\lambda_+ + 1 - t(1 - N_1/N))}. \quad (\text{A.34b})$$

5 The exceptional points at which definitions (A.33) fail are listed below

	$t$		
	$0 \leq t < \frac{1}{2}$	$\frac{1}{2} < t \leq 1$	
excep. pts. of $ u_{\text{up}}^+\rangle$	$\{N_1 = \pm N\}$	$\{N_1 = N\}$	
excep. pts. of $ u_{\text{down}}^+\rangle$	$\emptyset$	$\{N_1 = -N\}$	

(A.35)

7 where  $\{N_1 = N\}$  and  $\{N_1 = -N\}$  denote the north and the south poles of the two-  
8 sphere  $\mathbb{S}_N^2$  of radius  $N$ .

9 According to (A.35), the eigenvector  $|u_{\text{down}}^+\rangle$  is globally defined on  $\mathbb{S}_N^2$  for  $0 \leq t <$   
10  $\frac{1}{2}$ , so that the eigenvector bundle  $\Lambda_+$  associated with  $\lambda_+$  is trivial. On the contrary, for  
11  $\frac{1}{2} < t \leq 1$ , both eigenvectors  $|u_{\text{up/down}}^+\rangle$  are only locally defined, which means that  $\Lambda_+$   
12 is non-trivial. It follows that the topology of  $\Lambda_+$  changes when the control parameter  
13  $t$  passes the critical value  $\frac{1}{2}$ . Since the Chern number  $c_1$  is piecewise constant in  $t$ , it  
14 suffices to evaluate  $c_1$  for  $t = 0$  and  $t = 1$ . For  $t = 0$ , the Chern number is, of course,  
15  $c_1 = 0$ . For  $t = 1$ , we have already evaluated the Chern number  $c_1 = -1$  for the  
16 eigenvector bundle associated with  $\lambda_+$ .

## 17 A.6 A family of $\mathcal{T}$ -invariant Hamiltonians $H_\alpha$

18 In this section, we work with the semi-quantum Hamiltonian (4.2) written in the matrix  
19 representation (4.3) with the basis  $\{|\frac{1}{2}, \frac{1}{2}\rangle, |\frac{1}{2}, -\frac{1}{2}\rangle\}$

$$20 \quad H_\alpha = \frac{\alpha}{N} \begin{pmatrix} N_1 & N_- \\ N_+ & -N_1 \end{pmatrix} - i \frac{\varepsilon}{N} \begin{pmatrix} 0 & N_- \\ -N_+ & 0 \end{pmatrix}, \quad -1 \leq \alpha \leq 1, \quad (\text{A.36})$$

21 where  $0 < |\varepsilon| < 1$  is a small non-zero constant. The eigenvalues (4.4) of  $H_\alpha$

$$22 \quad \lambda_{\pm} = \pm \sqrt{\alpha^2 + \varepsilon^2 \sin^2 \theta}, \quad (\text{A.37})$$

1 where  $(\theta, \phi)$  are spherical coordinates on  $\mathbb{S}_N^2$ , become degenerate if and only if

$$2 \quad \alpha = 0, \quad \theta = 0, \pi. \quad (\text{A.38})$$

For  $\alpha \neq 0$ , the eigenvectors associated with  $\lambda_+$  are expressed in two ways as

$$|u_{\text{up}}^+\rangle = \frac{1}{N_{\text{up}}^+} \begin{pmatrix} (\alpha - i\varepsilon)e^{-i\phi} \sin \theta \\ \lambda_+ - \alpha \cos \theta \end{pmatrix} \text{ and} \quad (\text{A.39a})$$

$$|u_{\text{down}}^+\rangle = \frac{1}{N_{\text{down}}^+} \begin{pmatrix} \lambda_+ + \alpha \cos \theta \\ (\alpha + i\varepsilon)e^{i\phi} \sin \theta \end{pmatrix}, \quad (\text{A.39b})$$

3 where the normalization factors  $N_{\text{up/down}}^+$  are given, respectively, by

$$4 \quad N_{\text{up}}^+ = \sqrt{2\lambda_+(\lambda_+ - \alpha \cos \theta)} \quad \text{and} \quad N_{\text{down}}^+ = \sqrt{2\lambda_+(\lambda_+ + \alpha \cos \theta)}. \quad (\text{A.40})$$

5 The exceptional points at which the eigenvectors fail to be defined are as follows

	$\alpha$	$\alpha < 0$	$\alpha > 0$	
6	exc. pts. of $ u_{\text{up}}^+\rangle$	$\{N_1 = -N\}$	$\{N_1 = N\}$	(A.41)
	exc. pts. of $ u_{\text{down}}^+\rangle$	$\{N_1 = N\}$	$\{N_1 = -N\}$	

7 In other words, the domains of  $|u_{\text{up/down}}^+\rangle$  are  $\mathbb{S}_N^2$  without the respective exceptional  
8 points. On the intersection of those domains, the eigenvectors are related by

$$9 \quad |u_{\text{up}}^+\rangle = |u_{\text{down}}^+\rangle \eta, \quad \eta = \frac{\alpha - i\varepsilon}{\sqrt{\alpha^2 + \varepsilon^2}} e^{-i\phi}. \quad (\text{A.42})$$

10 The local connection forms  $A_{\text{up/down}}^+$  are defined to be

$$11 \quad A_{\text{up}}^+ = \langle u_{\text{up}}^+ | d | u_{\text{up}}^+ \rangle, \quad A_{\text{down}}^+ = \langle u_{\text{down}}^+ | d | u_{\text{down}}^+ \rangle. \quad (\text{A.43})$$

12 Combining eq. (A.42) and the above definition yields the relation

$$13 \quad A_{\text{up}}^+ = A_{\text{down}}^+ + \eta^{-1} d\eta. \quad (\text{A.44})$$

14 The local curvature forms are defined to be

$$15 \quad F_{\text{up}}^+ = dA_{\text{up}}^+ \quad \text{and} \quad F_{\text{down}}^+ = dA_{\text{down}}^+. \quad (\text{A.45})$$

On account of (A.44), one has  $F_{\text{up}}^+ = F_{\text{down}}^+$ , so that the curvature form  $F^+$  is globally defined on  $\mathbb{S}_N^2$ . We integrate the curvature form  $F^+$  over  $\mathbb{S}_N^2$  both for  $\alpha < 0$  and  $\alpha > 0$ . In the case of  $\alpha < 0$ , after dividing  $\mathbb{S}_N^2$  into the north hemisphere  $\mathbb{S}_{N+}^2$  and the south hemisphere  $\mathbb{S}_{N-}^2$ , the integration is performed as follows:

$$\begin{aligned} \int_{\mathbb{S}_N^2} F^+ &= \int_{\mathbb{S}_{N-}^2} F_{\text{down}}^+ + \int_{\mathbb{S}_{N+}^2} F_{\text{up}}^+ = \int_{\mathbb{S}_{N-}^2} dA_{\text{down}}^+ + \int_{\mathbb{S}_{N+}^2} dA_{\text{up}}^+ \\ &= - \int_{\mathbb{S}_N^1} A_{\text{down}}^+ + \int_{\mathbb{S}_N^1} A_{\text{up}}^+ = \int_{\mathbb{S}_N^1} (A_{\text{up}}^+ - A_{\text{down}}^+) \\ &= \int_{\mathbb{S}_N^1} \eta^{-1} d\eta = -2\pi i, \end{aligned}$$

1 where  $\mathbb{S}_N^1$  denotes the equator of  $\mathbb{S}_N^2$  and where the Stokes theorem and eq. (A.44) have  
 2 been used. It then follows that the first Chern number for the eigenvector bundle  $\Lambda_+$   
 3 associated with  $\lambda_+$  is given by

$$4 \quad c_1^+ = \frac{i}{2\pi} \int_{\mathbb{S}_N^2} F^+ = +1 \quad \text{for } \alpha < 0. \quad (\text{A.46})$$

In the case of  $\alpha > 0$ , calculation runs in parallel to give

$$\begin{aligned} \int_{\mathbb{S}_N^2} F^+ &= \int_{\mathbb{S}_{N-}^2} F_{\text{up}}^+ + \int_{\mathbb{S}_{N+}^2} F_{\text{down}}^+ = \int_{\mathbb{S}_{N-}^2} dA_{\text{up}}^+ + \int_{\mathbb{S}_{N+}^2} dA_{\text{down}}^+ \\ &= - \int_{\mathbb{S}_N^1} A_{\text{up}}^+ + \int_{\mathbb{S}_N^1} A_{\text{down}}^+ = - \int_{\mathbb{S}_N^1} (A_{\text{up}}^+ - A_{\text{down}}^+) \\ &= - \int_{\mathbb{S}_N^1} \eta^{-1} d\eta = 2\pi i, \end{aligned}$$

5 It then follows that

$$6 \quad c_1^+ = \frac{i}{2\pi} \int_{\mathbb{S}_N^2} F^+ = -1 \quad \text{for } \alpha > 0. \quad (\text{A.47})$$

In a similar manner, the Chern number for the eigenspace bundle  $\Lambda_-$  associated with  
 the negative eigenvalue  $\lambda_-$  is evaluated to be

$$c_1^- = \frac{i}{2\pi} \int_{\mathbb{S}_N^2} F^- = -1 \quad \text{for } \alpha < 0, \quad (\text{A.48a})$$

$$c_1^- = \frac{i}{2\pi} \int_{\mathbb{S}_N^2} F^- = +1 \quad \text{for } \alpha > 0. \quad (\text{A.48b})$$

## 7 A.7 Delta-Chern analysis for the linearized Hamiltonians

We calculate now the Chern numbers for the time-reversal invariant semi-quantum  
 Hamiltonians (4.7) and (4.7b), which correspond to the linearization of (4.3) at the  
 north and south poles of the  $\mathbb{S}_N^2$  sphere, respectively. We rewrite them using the  $a^- =$   
 $z = q + ip$  representation as

$$K_\alpha^{(+)} = \begin{pmatrix} -\alpha & -i \frac{(\alpha - i\varepsilon)}{\sqrt{N}} z \\ i \frac{(\alpha + i\varepsilon)}{\sqrt{N}} \bar{z} & \alpha \end{pmatrix}, \quad (\text{A.49a})$$

$$K_\alpha^{(-)} = \begin{pmatrix} \alpha & \frac{(\alpha - i\varepsilon)}{\sqrt{N}} \bar{z} \\ \frac{(\alpha + i\varepsilon)}{\sqrt{N}} z & -\alpha \end{pmatrix}, \quad (\text{A.49b})$$

8 and find the eigenvalues of  $K^{(+)}$

$$9 \quad \nu_\pm = \pm \sqrt{\alpha^2 + \frac{\alpha^2 + \varepsilon^2}{N} |z|^2}. \quad (\text{A.50})$$

The eigenvectors associated with  $\nu_+$  are expressed in two ways as

$$|v_{\text{up}}^{(+)}\rangle = \frac{1}{N_{\text{up}}^{(+)}} \begin{pmatrix} \frac{\alpha - i\varepsilon}{\sqrt{N}} \bar{z} \\ \nu_+ - \alpha \end{pmatrix}, \quad (\text{A.51a})$$

$$|v_{\text{down}}^{(+)}\rangle = \frac{1}{N_{\text{down}}^{(+)}} \begin{pmatrix} \nu_+ + \alpha \\ \frac{\alpha + i\varepsilon}{\sqrt{N}} z \end{pmatrix}, \quad (\text{A.51b})$$

1 where  $N_{\text{up/down}}^{(+)}$  are normalization factors given, respectively, by

$$2 \quad N_{\text{up}}^{(+)} = \sqrt{2\nu_+(\nu_+ - \alpha)}, \quad N_{\text{down}}^{(+)} = \sqrt{2\nu_+(\nu_+ + \alpha)}. \quad (\text{A.52})$$

3 The exceptional points at which the eigenvectors fail to be defined are listed as follows:

4	$\alpha$	$\alpha < 0$	$\alpha > 0$	5
6	excep. pt. of $ v_{\text{up}}^{(+)}\rangle$	$\emptyset$	$0$	(A.53)
7	excep. pt. of $ v_{\text{down}}^{(+)}\rangle$	$0$	$\emptyset$	

6 Outside of the exceptional points, the eigenvectors  $|v_{\text{up/down}}^{(+)}\rangle$  are related by

$$7 \quad |v_{\text{up}}^{(+)}\rangle = |v_{\text{down}}^{(+)}\rangle \zeta, \quad \zeta = \frac{\alpha - i\varepsilon}{\sqrt{\alpha^2 + \varepsilon^2}} \frac{\bar{z}}{|z|}, \quad \bar{z} = q - ip. \quad (\text{A.54})$$

8 The local connection forms are defined to be

$$9 \quad B_{\text{up}}^{(+)} = \langle v_{\text{up}}^{(+)} | d | v_{\text{up}}^{(+)} \rangle, \quad B_{\text{down}}^{(+)} = \langle v_{\text{down}}^{(+)} | d | v_{\text{down}}^{(+)} \rangle, \quad (\text{A.55})$$

10 and are related by

$$11 \quad B_{\text{up}}^{(+)} - B_{\text{down}}^{(+)} = \zeta^{-1} d\zeta. \quad (\text{A.56})$$

12 The local curvature forms are defined, accordingly, to be

$$13 \quad G^{(+)} = dB_{\text{up}}^{(+)} = dB_{\text{down}}^{(+)}. \quad (\text{A.57})$$

14 In the same manner as discussed in the subsection A.3, we obtain

$$15 \quad \frac{i}{2\pi} \int_{\mathbb{R}^2} G^{(+)}|_{\alpha>0} - \frac{i}{2\pi} \int_{\mathbb{R}^2} G^{(+)}|_{\alpha<0} = \frac{1}{2\pi i} \int_C \zeta^{-1} d\zeta = -1. \quad (\text{A.58})$$

16 We need further delta-Chern analysis for  $K_{\alpha}^{(-)}$ . The eigenvalues of  $K_{\alpha}^{(-)}$  are easily  
17 evaluated as

$$18 \quad \nu_{\pm} = \pm \sqrt{\alpha^2 + \frac{\alpha^2 + \varepsilon^2}{N} |z|^2}. \quad (\text{A.59})$$

The eigenvectors associated with  $\nu_+$  are expressed in two ways as

$$|v_{\text{up}}^{(-)}\rangle = \frac{1}{N_{\text{up}}^{(-)}} \begin{pmatrix} -i \frac{\alpha - i\varepsilon}{\sqrt{N}} z \\ \nu_+ + \alpha \end{pmatrix}, \quad (\text{A.60a})$$

$$|v_{\text{down}}^{(-)}\rangle = \frac{1}{N_{\text{down}}^{(-)}} \begin{pmatrix} \nu_+ - \alpha \\ i \frac{\alpha + i\varepsilon}{\sqrt{N}} \bar{z} \end{pmatrix}, \quad (\text{A.60b})$$

19 where  $N_{\text{up/down}}^{(-)}$  are the normalization factors given, respectively, by

$$20 \quad N_{\text{up}}^{(-)} = \sqrt{2\nu_+(\nu_+ + \alpha)}, \quad N_{\text{down}}^{(-)} = \sqrt{2\nu_+(\nu_+ - \alpha)}. \quad (\text{A.61})$$

21 The exceptional points at which the eigenvectors fail to be defined are listed as follows:

22	$\alpha$	$\alpha < 0$	$\alpha > 0$	23
24	excep. pt. of $ v_{\text{up}}^{(-)}\rangle$	$0$	$\emptyset$	(A.62)
25	excep. pt. of $ v_{\text{down}}^{(-)}\rangle$	$\emptyset$	$0$	

1 Outside of the exceptional points, the eigenvectors  $|v_{\text{up/down}}^{(-)}\rangle$  are related by

$$2 \quad |v_{\text{up}}^{(-)}\rangle = |v_{\text{down}}^{(-)}\rangle \xi, \quad \xi = -i \frac{\alpha - i\varepsilon}{\sqrt{\alpha^2 + \varepsilon^2}} \frac{z}{|z|}, \quad z = q + ip. \quad (\text{A.63})$$

3 The local connection forms are defined to be

$$4 \quad B_{\text{up}}^{(-)} = \langle v_{\text{up}}^{(-)} | d | v_{\text{up}}^{(-)} \rangle, \quad B_{\text{down}}^{(-)} = \langle v_{\text{down}}^{(-)} | d | v_{\text{down}}^{(-)} \rangle, \quad (\text{A.64})$$

5 and are related by

$$6 \quad B_{\text{up}}^{(-)} - B_{\text{down}}^{(-)} = \xi^{-1} d\xi. \quad (\text{A.65})$$

7 The local curvature forms are defined, accordingly, to be

$$8 \quad G^{(-)} = dB_{\text{up}}^{(-)} - dB_{\text{down}}^{(-)}. \quad (\text{A.66})$$

In order to evaluate the delta-Chern, a similar method with small modification runs in parallel. For the sake of a review of the method, we reproduce the evaluation procedure. For  $\alpha > 0$ , the origin is the exceptional point for  $|v_{\text{down}}^{(-)}\rangle$  but not so for  $|v_{\text{up}}^{(-)}\rangle$ . With this in mind, we integrate the curvature form  $G^{(-)}$  on the regions  $D_\rho$  and  $W_{\rho,r}$  shown in Fig. 11 to obtain

$$\begin{aligned} \int_{\mathbb{R}^2} G^{(-)} &= \int_{D_\rho} dB_{\text{up}}^{(-)} + \lim_{r \rightarrow \infty} \int_{W_{\rho,r}} dB_{\text{down}}^{(-)} \\ &= \int_{C_\rho} B_{\text{up}}^{(-)} + \lim_{r \rightarrow \infty} \left( \int_{-C_\rho} B_{\text{down}}^{(-)} + \int_{C_r} B_{\text{down}}^{(-)} \right) \\ &= \int_{C_\rho} \xi^{-1} d\xi + \lim_{r \rightarrow \infty} \int_{C_r} B_{\text{down}}^{(-)} \quad \text{for } \alpha > 0, \end{aligned} \quad (\text{A.67})$$

where use has been made of the relation (A.65) and the Stokes theorem. For  $\alpha < 0$ , the origin is the exceptional point of  $|v_{\text{up}}^{+}\rangle$  but not so for  $|v_{\text{down}}^{+}\rangle$ . A similar calculation to the above provides

$$\int_{\mathbb{R}^2} G^{(-)} = - \int_{C_\rho} \xi^{-1} d\xi + \lim_{r \rightarrow \infty} \int_{C_r} B_{\text{up}}^{(-)} \quad \text{for } \alpha < 0. \quad (\text{A.68})$$

9 Though Eqs. (A.67) and (A.68) contain locally-defined terms,  $B_{\text{up}}^{(-)}$  and  $B_{\text{down}}^{(-)}$ , the difference between them may have a characteristic of the eigenvector bundle depending on  $\alpha$ . In fact, one can verify that

$$12 \quad \frac{i}{2\pi} \int_{\mathbb{R}^2} G^{(-)}|_{\alpha>0} - \frac{i}{2\pi} \int_{\mathbb{R}^2} G^{(-)}|_{\alpha<0} = \frac{-1}{2\pi i} \int_{C_\rho} \xi^{-1} d\xi = -1, \quad (\text{A.69})$$

13 where use has been made of the relation (A.65) and the fact that  $\int_{C_r} \xi^{-1} d\xi = \int_{C_\rho} \xi^{-1} d\xi$ .  
14 Eqs. (A.58) and (A.69) imply that the respective jumps in the formal Chern number accompanying the variation of the parameter  $\alpha$  make sense as topological invariants. For  
15  $\zeta : C_\rho \rightarrow U(1)$ , it is a winding number, but for  $\xi : C_\rho \rightarrow U(1)$ , it is the negative of the  
16 winding number.  
17

18 The Chern number of the eigenvector bundle associate with the positive eigenvalues  
19 of the initial Hamiltonian  $H_\alpha$  is  $c_1 = -1$  for  $\alpha > 0$  and  $c_1 = +1$  for  $\alpha < 0$ . Hence,  
20 the change in the Chern number in the positive direction of  $\alpha$  is  $-1 - (+1) = -2$ .  
21 The initial semi-quantum Hamiltonian  $H_\alpha$  has two degeneracy points at the north and  
22 the south poles of  $\mathbb{S}_N^2$ . We have evaluated the change in the formal Chern number for  
23 each of the linearized Hamiltonians. The totality of the change is  $-1 + (-1) = -2$ ,  
24 the same result as above.

## A.8 Chern number calculation for spin-quadrupole Hamiltonian

We begin with Hamiltonian (5.1) in the matrix form

$$H_\mu = \begin{pmatrix} \mu \mathbf{G} & \mathbf{M} \\ \mathbf{M}^\dagger & -\mu \mathbf{G} \end{pmatrix} \quad (\text{A.70})$$

with tuning control parameter  $\mu$ ,

$$\mathbf{G} = \frac{N^2 - 3N_1^2}{2} \begin{pmatrix} 1 & 0 \\ 0 & -1 \end{pmatrix}, \text{ and } \mathbf{M} = \begin{pmatrix} (\sqrt{3}\mu + i\varepsilon)N_1N_+ & (\frac{1}{2}\sqrt{3} - i\varepsilon)N_-^2 \\ (\frac{1}{2}\sqrt{3}\mu + i\varepsilon)N_+^2 & -(\sqrt{3}\mu - i\varepsilon)N_1N_- \end{pmatrix}.$$

The eigenvalues of  $H_\mu$  are

$$\lambda_\pm = \pm \sqrt{(\mu^2 + \varepsilon^2)N^2 - \varepsilon^2N_3^2} = \pm N^2 \sqrt{\mu^2 + \varepsilon^2 \sin^2 \theta}. \quad (\text{A.71})$$

If  $N \neq 0$ , the degeneracy in eigenvalues takes place if and only if

$$\mu = 0, \quad \theta = 0, \quad \text{or} \quad \mu = 0, \quad \theta = \pi. \quad (\text{A.72})$$

To simplify the analysis, we linearize Hamiltonian (A.70) at the north pole to obtain

$$N^2 \begin{pmatrix} -\mu & 0 & \beta z & 0 \\ 0 & -\mu & 0 & -\bar{\beta} \bar{z} \\ \bar{\beta} \bar{z} & 0 & \mu & 0 \\ 0 & -\beta z & 0 & \mu \end{pmatrix} \quad \text{with } \beta = \frac{\sqrt{3}\mu + i\varepsilon}{\sqrt{N}}, \quad (\text{A.73})$$

where

$$z = \frac{N_+}{\sqrt{N}} = q + ip \quad \text{and} \quad \bar{z} = \frac{N_-}{\sqrt{N}} = q - ip \quad (\text{A.74})$$

are viewed as local coordinates on the tangent plane to  $\mathbb{S}_N^2$  at the north pole. Rescaling by  $N^2$  and reordering the basis functions as  $\{|\frac{3}{2}, \frac{3}{2}\rangle, |\frac{3}{2}, \frac{1}{2}\rangle, |\frac{3}{2}, -\frac{1}{2}\rangle, |\frac{3}{2}, -\frac{3}{2}\rangle\}$  give the linearized semi-quantum Hamiltonian at the north pole

$$K_\mu = \begin{pmatrix} \mu & \bar{\beta} \bar{z} & & \\ \beta z & -\mu & & \\ & & -\mu & -\bar{\beta} \bar{z} \\ & & -\beta z & \mu \end{pmatrix}. \quad (\text{A.75})$$

The analysis at the south pole can be done in a similar way, with two linearizations at the north and south poles being related through time-reversal transformation (2.5).

The eigenvalues of the linearized Hamiltonian (A.75)

$$\nu_\pm = \pm \sqrt{\mu^2 + |\beta|^2 |z|^2} \quad (\text{A.76})$$

have multiplicity 2 each and become totally degenerate if and only if  $\mu = 0$  and  $z = 0$ . The normalized eigenvectors associated with  $\nu_+$  are expressed in two ways as

$$|w_{1,\text{up}}^+\rangle = \frac{1}{N_{1,\text{up}}^+} \begin{pmatrix} \bar{\beta} \bar{z} \\ \nu_+ - \mu \\ 0 \\ 0 \end{pmatrix}, \quad |w_{2,\text{up}}^+\rangle = \frac{1}{N_{2,\text{up}}^+} \begin{pmatrix} 0 \\ 0 \\ -\bar{\beta} \bar{z} \\ \nu_+ + \mu \end{pmatrix}, \quad (\text{A.77a})$$

$$|w_{1,\text{down}}^+\rangle = \frac{1}{N_{1,\text{down}}^+} \begin{pmatrix} \nu_+ + \mu \\ \beta z \\ 0 \\ 0 \end{pmatrix}, \quad |w_{2,\text{down}}^+\rangle = \frac{1}{N_{2,\text{down}}^+} \begin{pmatrix} 0 \\ 0 \\ \nu_+ - \mu \\ -\beta z \end{pmatrix}, \quad (\text{A.77b})$$

with normalization factors

$$N_{1,\text{up}}^+ = \sqrt{2\nu_+(\nu_+ - \mu)}, \quad N_{2,\text{up}}^+ = \sqrt{2\nu_+(\nu_+ + \mu)}, \quad (\text{A.78a})$$

$$N_{1,\text{down}}^+ = \sqrt{2\nu_+(\nu_+ + \mu)}, \quad N_{2,\text{down}}^+ = \sqrt{2\nu_+(\nu_+ - \mu)}. \quad (\text{A.78b})$$

1 On the intersection of their respective domains

$$2 \quad \begin{array}{ccccc} \mu & |w_{1,\text{up}}^+\rangle & |w_{1,\text{down}}^+\rangle & |w_{2,\text{up}}^+\rangle & |w_{2,\text{down}}^+\rangle \\ \mu < 0 & \mathbb{R}^2 & \mathbb{R}^2 \setminus \{0\} & \mathbb{R}^2 \setminus \{0\} & \mathbb{R}^2 \\ \mu > 0 & \mathbb{R}^2 \setminus \{0\} & \mathbb{R}^2 & \mathbb{R}^2 & \mathbb{R}^2 \setminus \{0\} \end{array}, \quad (\text{A.79})$$

3 eigenvectors (A.77) are related by

$$4 \quad (|w_{1,\text{up}}^+\rangle, |w_{2,\text{up}}^+\rangle) = (|w_{1,\text{down}}^+\rangle, |w_{2,\text{down}}^+\rangle) \begin{pmatrix} \zeta_1 & 0 \\ 0 & \zeta_2 \end{pmatrix}, \quad \zeta_1 = \frac{\bar{\beta}\bar{z}}{|\beta||z|} = -\zeta_2. \quad (\text{A.80})$$

5 This transition relation determines the eigenspace bundle of rank two over  $\mathbb{R}^2$  associ-  
6 ated with the eigenvalue  $\nu_+$  of  $K_\mu$ .

7 The projection map onto the eigenspace associated with  $\nu_+$

$$8 \quad P_+ = \sum_{k=1}^2 \langle w_{k,\text{up}}^+ | \langle w_{k,\text{up}}^+ | = \sum_{k=1}^2 \langle w_{k,\text{down}}^+ | \langle w_{k,\text{down}}^+ |.$$

9 defines the covariant differential operator  $P_+d$  with which the basis eigenvectors are  
10 operated on in order to define local connection forms. We obtain

$$11 \quad \mathcal{A}_{\text{up/down}}^+ = \begin{pmatrix} A_{1,\text{up/down}}^+ & \\ & A_{2,\text{up/down}}^+ \end{pmatrix}, \quad (\text{A.81})$$

12 where

$$13 \quad A_{k,\text{up/down}}^+ = \langle w_{k,\text{up/down}}^+ | d | w_{k,\text{up/down}}^+ \rangle, \quad k = 1, 2. \quad (\text{A.82})$$

14 On the intersection of their respective domains,  $A_{k,\text{up/down}}^+$  are related by

$$15 \quad A_{k,\text{up}}^+ - A_{k,\text{down}}^+ = \zeta_k^{-1} d\zeta_k, \quad k = 1, 2. \quad (\text{A.83})$$

16 The local curvature forms

$$17 \quad \mathcal{F}_{\text{up/down}}^+ = \begin{pmatrix} F_{1,\text{up/down}}^+ & \\ & F_{2,\text{up/down}}^+ \end{pmatrix} = \begin{pmatrix} dA_{1,\text{up/down}}^+ & \\ & dA_{2,\text{up/down}}^+ \end{pmatrix}$$

18 coincide on the intersection of their respective domains and can be combined to define  
19 the global curvature form

$$20 \quad \mathcal{F}^+ = \begin{pmatrix} F_1^+ & \\ & F_2^+ \end{pmatrix}. \quad (\text{A.84})$$

21 The Chern form is defined through

$$22 \quad \text{Det}\left(t\mathbb{1} + \frac{i}{2\pi}\mathcal{F}\right) = t^2 + \frac{i}{2\pi}t(F_1^+ + F_2^+), \quad (\text{A.85})$$



1 where  $t$  is a real parameter,  $\mathbb{1}$  denotes the  $2 \times 2$  identity matrix, and where use has been  
 2 made of  $F_1^+ \wedge F_2^+ = 0$ . Thus, the first Chern form is defined to be

$$3 \quad C_1 = \frac{i}{2\pi} (F_1^+ + F_2^+), \quad (\text{A.86})$$

4 and the first Chern number is formally defined to be

$$5 \quad c_1 = \int_{\mathbb{R}^2} C_1. \quad (\text{A.87})$$

We are to observe a change in the Chern number against the control parameter  $\mu$ .  
 On account of (A.79), under the procedure we have frequently performed, we obtain

$$\frac{i}{2\pi} \int_{\mathbb{R}^2} F_1^+|_{\mu>0} - \frac{i}{2\pi} \int_{\mathbb{R}^2} F_1^+|_{\mu<0} = \frac{1}{2\pi i} \int_{\Gamma} \zeta_1^{-1} d\zeta_1 = -1, \quad (\text{A.88a})$$

$$\frac{i}{2\pi} \int_{\mathbb{R}^2} F_2^+|_{\mu>0} - \frac{i}{2\pi} \int_{\mathbb{R}^2} F_2^+|_{\mu<0} = \frac{-1}{2\pi i} \int_{\Gamma} \zeta_2^{-1} d\zeta_2 = +1, \quad (\text{A.88b})$$

6 where  $\Gamma$  denotes a circle with the center at the origin of  $\mathbb{R}^2$ . It then follows that the  
 7 change in the Chern number for the eigenspace bundle associated with the eigenvalue  
 8  $\nu_+$  of the linearized Hamiltonian  $K_\mu$  at the north pole is zero;

$$9 \quad c_1|_{\mu>0} - c_1|_{\mu<0} = 0. \quad (\text{A.89})$$

10 Similar result can be obtained for the linearization at the south pole. This means that for  
 11 the Hamiltonian (5.1) there is no modification of the Chern numbers for superbands.  
 12 This result is consistent with the conservation of the number of energy levels in su-  
 13 perbands. Nevertheless the rearrangement of superbands clearly occurs because of the  
 14 modification in the decomposition of the superbands into individual irreps demonstrated  
 15 by correlation diagrams (see Fig 8, 10). In order to see topological modifications it  
 16 is sufficient to add small perturbation breaking the Kramers degeneracy of superbands  
 17 caused by  $\mathcal{T}_S$  symmetry and to discuss the modifications of Chern numbers for indi-  
 18 vidual components of superbands like it is done in the main text.

## 19 Notes

20 <sup>1</sup>A particularly instructive example with *formal* control parameters  $q$  of dynamical origin is the phase  
 21 of the electronic wavefunctions  $\Psi_{\text{el}}$  in the Jahn–Teller systems. Herzberg and Longuet-Higgins [1963]  
 22 considered such systems within the Born-Oppenheimer approximation, where nuclear coordinates  $q$  play  
 23 the role of control parameters of the separated electronic Hamiltonian  $H_{\text{el}}$ . Their work anticipated the  
 24 geometrical phase analysis by Berry [1984] and is widely known in molecular physics [Mead and Truhlar,  
 25 1979]. The nontrivial topological contribution to the phase of  $\Psi_{\text{el}}$  is associated with the close loop around  
 26 the degeneracy point of two electronic potential energy surfaces in the  $q$ -space. While being plain control  
 27 parameters of  $H_{\text{el}}$ , the nuclear coordinates  $q$  are dynamical variables for the complete electronic-nuclear  
 28 Hamiltonian or, equally, for the separated Hamiltonian  $H_{\text{nucel}}$  describing the slow vibrations of the nuclei.  
 29 We like to stress that  $q$  are formal and *not* dynamical control parameters of the fast electronic subsystem  
 30 because  $H_{\text{el}}$  has no influence on their evolution. In other words,  $q$  get no feedback from the fast system. On  
 31 the other hand, the reason why dynamical parameters remain influenced explicitly by the fast system in the  
 32 semi-quantum description of our systems (sec. 2, 3, 4, and 5) is in the nature of their slow-fast separation  
 33 which applies only on the complement to the open saturated neighbourhood of the degeneracy point (bounded  
 34 by the base space of  $\Delta$ , see sec. 1.3) in the formal-dynamical control parameter space.

35 <sup>2</sup>Dynamical variables of slow-fast systems fall in two categories with strongly different rates of variation  
 36 and respective time scales. Under certain conditions, this allows separation into slow and fast subsystems.  
 37 There is a vast literature on slow-fast dynamical systems which are ubiquitous in applications, see, for  
 38 example, [Berglund and Gentz, 2006, Neishtadt and Vasiliev, 2006, Neishtadt, 2008].  
 39

<sup>3</sup>In this work, unless indicated explicitly, we shall assume  $N \gg 1$  and imply  $\|\mathbf{N}\| = \hbar N$  instead of the quantum relation  $\|\mathbf{N}\| = \hbar\sqrt{N(N+1)}$ , or the semiclassical formula  $\|\mathbf{N}\| = \hbar(N + \frac{1}{2})$ . Furthermore, atomic units with  $\hbar = 1$  will be used throughout the paper.

<sup>4</sup>One pertinent example is the reduced phase space  $\mathbb{S}^2$  of the Euler top, the freely rotating rigid body.

<sup>5</sup>The operation  $\mathcal{T}$  has the same effect on the trajectories of the classical system as reversing time in the equations of motion. A more exact terminology, however, may be *momentum reversal*. In classical mechanics, we consider normal and reversing (or reversal) isotropy symmetries of the Hamiltonian function  $H$ , depending whether the symplectic form  $\omega$  remains invariant or covariant [Lamb, 1992, Lamb and Roberts, 1998, Baake, 2018]. In quantum mechanics, time reversal action on the Hilbert space [Wigner, 1932, Avron et al., 1989] involves complex conjugation  $C_*$  times a unitary transformation. So it can be seen that in the concrete example of Pauli matrices, i.e., for spin- $\frac{1}{2}$  wavefunctions,  $\mathcal{T}$  in (2.5) is realized as  $C_* \circ C_2^y$ , where  $C_2^y$  is rotation by  $\pi$  about axis  $y$  (axis 3 in our notation). Although the whole class of reversing symmetries may match Wigner's definition of quantum time-reversal symmetry operation, we like to distinguish our concrete realization of time-reversal proper  $\mathcal{T}$  from other reversing symmetries.

<sup>6</sup>Here again we use the same notation for the classical action  $I$  and the oscillator quantum number  $n$ , thus simplifying the exact quantum expression  $I = n + \frac{1}{2}$  in the limit  $n \gg 1$ , see footnote 3.

<sup>7</sup>Another possibility is to consider two fast doublet states, for example a doublet electronic state  ${}^2E$  or  ${}^2\Pi$  for Jahn-Teller or Renner-Teller systems, respectively

<sup>8</sup>The only other symmetric powers of degree 2, the rank-0 scalars  $\mathbf{S} \cdot \mathbf{S}$  and  $\mathbf{N} \cdot \mathbf{N}$  are of no interest.

<sup>9</sup>The components of  $\mathbf{S}$  are labeled in [Avron et al., 1989] as  $(x, y, z) := (2, 3, 1)$ .

<sup>10</sup>As pointed out in sec. 1.4, all bundle constructions and index computations for the systems in sec. 3 come back to those in the original plain setup with Hamiltonian (1.1). Specifically, substituting

$$N_1 = -\sqrt{N^2 - N_2^2 - N_3^2}, \quad \gamma = \frac{1}{2} - \frac{\mu}{4N}, \quad \text{and} \quad \frac{1}{2NS}(\mu, N_2, N_3) =: (B_1, B_2, B_3)$$

into Hamiltonian (3.1), and Taylor expanding to the principal order in  $\mathbf{B}$  result in (1.1) which we analyze in the standard way [Simon, 1983, Wilczek and Shapere, 1989]. All local bundles  $\Delta$ , including those discussed in sec. 2.2 (with noncompact slow phase space  $\mathbb{R}_{q,p}^2$ ), 4, and 5 can be treated similarly. The same applies to any bundle  $\Lambda$  over  $\mathbb{S}_N^2$ , starting with sec. 2.1 where we identify  $\mathbf{N}$  with control parameters  $\mathbf{B}$  of (1.1).

<sup>11</sup>Localization in the phase space  $\mathbb{S}_N^2$  corresponds to the orientation probability of  $\mathbf{N}$ . The latter is given by the Wigner distribution  $W$  of the eigenstates and has no relation to the angular probability distribution used commonly to represent spherical functions, see, for example, [Lee Loh and Kim, 2015] and the discussion in [Faure and Zhilinskiĭ, 2000, Fontanari and Sadovskii, 2018].

<sup>12</sup>It can be thus observed that bulk states have a solid classical interpretation while the existence of the edge states remains an essentially quantum phenomenon. This is known as bulk-edge correspondence in topological insulators [Bernevig and Hughes, 2013].

<sup>13</sup>Indeed, Taylor expanding

$$N_1 = \pm\sqrt{\|\mathbf{N}\|^2 - N_2^2 - N_3^2} \approx \pm\|\mathbf{N}\| \left(1 - \frac{N_2^2 + N_3^2}{2\|\mathbf{N}\|^2}\right) = \pm\|\mathbf{N}\| \mp \frac{q^2 + p^2}{2}$$

and using the semiclassical value  $\|\mathbf{N}\| = N + \frac{1}{2}$ , we obtain

$$N_1/N \approx \pm 1 \mp I = \pm 1 \mp n$$

with oscillator action  $I = \frac{1}{2}(q^2 + p^2)$  acting as  $\hat{I}|n\rangle = (n + \frac{1}{2})|n\rangle$ .

## References

- V. I. Arnold. Remarks on eigenvalues and eigenvectors of Hermitian matrices, Berry phase, adiabatic connections and quantum Hall effect. *Select. Math.*, **1(1)**:1–19, March 1995.
- M. F. Atiyah, V. K. Patodi, and I. M. Singer. Spectral asymmetry and Riemannian geometry. I. *Math. Proc. Cambridge Phil. Soc.*, **77**:49–69, 1975a.
- M. F. Atiyah, V. K. Patodi, and I. M. Singer. Spectral asymmetry and Riemannian geometry. II. *Math. Proc. Cambridge Phil. Soc.*, **78**:405–432, 1975b.
- M. F. Atiyah, V. K. Patodi, and I. M. Singer. Spectral asymmetry and Riemannian geometry. III. *Math. Proc. Cambridge Phil. Soc.*, **79**:71–99, 1976.

- 1 J. E. Avron, L. Sadun, J. Segert, and B. Simon. Topological invariants in Fermi systems with  
2 time-reversal invariance. *Phys. Rev. Lett.*, **61**:1329–1332, Sep 1988.
- 3 J. E. Avron, L. Sadun, J. Segert, and B. Simon. Chern numbers, quaternions, and Berry’s phases  
4 in Fermi systems. *Commun. Math. Phys.*, **124**(4):595–627, Dec 1989.
- 5 M. Baake. A brief guide to reversing and extended symmetries of dynamical systems. In S. Fer-  
6 enczi, J. Kulaga-Przymus, and M. Lemanczyk, editors, *Ergodic theory and dynamical systems*  
7 *in their interactions with arithmetics and combinatorics*, volume 2213 of *Lect. Notes Math.*,  
8 pages 35–40. Springer-Verlag, Berlin, Heidelberg, July 2018. ISBN 978-3-319-74907-5. doi:  
9 10.1007/978-3-319-74908-2\_9.
- 10 N. Berglund and B. Gentz. *Noise-induced phenomena in slow-fast dynamical systems*, chap-  
11 ter Deterministic slow-fast systems, pages 17–49. Probability and its applications. Springer  
12 Verlag, London, UK, 2006. ISBN 978-1-84628-038-2. doi: 10.1007/1-84628-186-5\_2.
- 13 B. A. Bernevig and T. L. Hughes. *Topological insulators and topological superconductors*.  
14 Princeton Univ. Press, Princeton, NJ, 2013. ISBN 978-0-691-15175-5.
- 15 M. V. Berry. Quantal phase factors accompanying adiabatic changes. *Proc. Royal Soc. Lond. A*,  
16 **392**:45–57, 1984.
- 17 F. Faure and B. I. Zhilinskiĭ. Topological Chern indices in molecular spectra. *Phys. Rev. Lett.*,  
18 **85**:960–963, 2000.
- 19 F. Faure and B. I. Zhilinskiĭ. Topological properties of the Born–Oppenheimer approximation  
20 and implications for the exact spectrum. *Lett. Math. Phys.*, **55**:239–247, 2001.
- 21 F. Faure and B. I. Zhilinskiĭ. Qualitative features of intra-molecular dynamics. What can be  
22 learned from symmetry and topology. *Acta Appl. Math.*, **70**:265–282, 2002a.
- 23 F. Faure and B. I. Zhilinskiĭ. Topologically coupled energy bands in molecules. *Phys. Lett. A*,  
24 **302**:985–988, 2002b.
- 25 B. Fedosov. *Deformation quantization and index theory*. Akademie Verlag, Berlin, 1996. ISBN  
26 978-3-055-01716-2.
- 27 D. Fontanari and D. A. Sadovskii. Coherent states for the quantum complete rigid rotor. *J. Geom.*  
28 *Phys.*, **129**:70–89, Jul 2018.
- 29 J. N. Fuchs, F. Piéchon, M. O. Goerbig, and G. Montambaux. Topological Berry phase and  
30 semiclassical quantization of cyclotron orbits for two dimensional electrons in coupled band  
31 models. *Eur. Phys. J. B*, **77**(3):351–362, Sept. 2010.
- 32 F. D. M. Haldane. Model for a quantum Hall effect without Landau levels: Condensed-matter  
33 realization of the “parity anomaly”. *Phys. Rev. Lett.*, **61**:2015–2018, Oct 1988.
- 34 G. Herzberg and H. C. Longuet-Higgins. Intersection of potential energy surfaces in polyatomic  
35 molecules. *Discuss. Faraday Soc.*, **35**:77–82, 1963.
- 36 T. Holstein and H. Primakoff. Field dependence of the intrinsic domain magnetization of a  
37 ferromagnet. *Phys. Rev.*, **58**:1098–1113, 1940.
- 38 T. Iwai and B. I. Zhilinskiĭ. Energy bands: Chern numbers and symmetry. *Ann. Phys. (NY)*,  
39 **326**:3013–3066, 2011.
- 40 T. Iwai and B. I. Zhilinskiĭ. Qualitative feature of the rearrangement of molecular energy spectra  
41 from a wall-crossing perspective. *Phys. Lett. A*, **377**:2481–2486, 2013.

- 1 T. Iwai and B. I. Zhilinskiĭ. Local description of band rearrangements. Comparison of semi-  
2 quantum and full quantum approach. *Acta Appl. Math.*, **137**:97–121, 2015.
- 3 T. Iwai and B. I. Zhilinskiĭ. Band rearrangement through the 2D-Dirac equation: Comparing the  
4 APS and the chiral bag boundary conditions. *Indagationes Math.*, **27**(5):1081–1106, 2016.
- 5 T. Iwai and B. I. Zhilinskiĭ. Chern number modification in crossing the boundary between  
6 different band structures: Three-band model with cubic symmetry. *Rev. Math. Phys.*, **29**:  
7 1750004/1–91, 2017.
- 8 M. Kohmoto. Topological invariant and the quantization of the Hall conductance. *Ann. Phys.*,  
9 **160**(2):343–354, 1985. ISSN 0003-4916.
- 10 H. A. Kramers. Théorie générale de la rotation paramagnétique dans les cristaux. *Proc. Konink.*  
11 *Akad. Wetensch.*, 33:959–972, 1930. URL [http://www.dwc.knaw.nl/DL/publications/  
12 PU00015981.pdf](http://www.dwc.knaw.nl/DL/publications/PU00015981.pdf).
- 13 J. S. W. Lamb. Reversing symmetries in dynamical systems. *J. Phys. A*, **25**:925–937, 1992.
- 14 J. S. Lamb and J. A. Roberts. Time-reversal symmetry in dynamical systems: A survey. *Physica*  
15 *D*, **112**(1):1–39, 1998. ISSN 0167-2789.
- 16 Y. Lee Loh and M. Kim. Visualizing spin states using the spin coherent state representation.  
17 *Am. J. Phys.*, **83**(1):30–35, 2015.
- 18 C. A. Mead. Molecular Kramers degeneracy and non-Abelian adiabatic phase factors. *Phys.*  
19 *Rev. Lett.*, **59**:161–164, Jul 1987.
- 20 C. A. Mead and D. G. Truhlar. On the determination of Born–Oppenheimer nuclear motion wave  
21 functions including complications due to conical intersections and identical nuclei. *J. Chem.*  
22 *Phys.*, **70**(5):2284–2296, 1979.
- 23 M. Moshinsky and A. Szczepaniak. The Dirac oscillator. *J. Phys. A: Math. Gen.*, **22**(17):L817–  
24 L819, 1989.
- 25 A. I. Neishtadt and A. A. Vasiliev. Destruction of adiabatic invariance at resonances in slow-fast  
26 Hamiltonian systems. *Nucl. Instr. Meth. A*, **561**(2):158–165, 2006. ISSN 0168-9002.
- 27 A. I. Neishtadt. Averaging method and adiabatic invariants. In W. Craig, editor, *Hamiltonian*  
28 *dynamical systems and applications*, NATO science for peace and security series B: Physics  
29 and Biophysics, pages 53–66. Springer Science, Netherlands, 2008. ISBN 978-1-4020-6963-  
30 5. doi: 10.1007/978-1-4020-6964-2.
- 31 V. B. Pavlov-Verevkin, D. A. Sadovskii, and B. I. Zhilinskiĭ. On the dynamical meaning of the  
32 diabolic points. *Europhysics Letters*, **6**:573–8, Aug 1988.
- 33 D. A. Sadovskii and B. I. Zhilinskiĭ. Monodromy, diabolic points, and angular momentum  
34 coupling. *Phys. Lett. A*, **256**:235–44, Jun 1999.
- 35 B. Simon. Holonomy, the quantum adiabatic theorem, and Berry’s phase. *Phys. Rev. Lett.*, **51**  
36 (24):2167–2170, Dec 1983.
- 37 D. J. Thouless. *Topological Quantum Numbers in Nonrelativistic Physics*. World Scientific,  
38 Singapore, 1998. ISBN 978-9-810-23025-8.
- 39 D. J. Thouless, M. Kohmoto, M. P. Nightingale, and M. den Nijs. Quantized hall conductance in  
40 a two-dimensional periodic potential. *Phys. Rev. Lett.*, **49**:405–408, Aug 1982.
- 41 J. von Neumann and E. P. Wigner. Über merkwürdige diskrete Eigenwerte. Über das Verhalten  
42 von Eigenwerten bei adiabatischen Prozessen. *Physicalische Z.*, 30:467–470, 1929.

- 1 E. P. Wigner. Über die Operation der Zeitumkehr in der Quantenmechanik. *Nachr. Akad. Ges.*  
2 *Wiss. Göttingen*, 31:546–559, 1932. URL [http://www.digizeitschriften.de/dms/img/?PPN=](http://www.digizeitschriften.de/dms/img/?PPN=GDZPPN002509032)  
3 [GDZPPN002509032](http://www.digizeitschriften.de/dms/img/?PPN=GDZPPN002509032).
- 4 F. Wilczek and A. Shapere, editors. *Geometric Phases in Physics*, volume 5 of *Advanced Series*  
5 *in Mathematical Physics*. World Scientific, July 1989. doi: [10.1142/0613](https://doi.org/10.1142/0613).
- 6 R. N. Zare. *Angular momentum: understanding spatial aspects in chemistry and physics*. Wiley,  
7 New York, 1988. ISBN 978-0-471-85892-8.
- 8 W.-M. Zhang, D. H. Feng, and R. Gilmore. Coherent states: theory and some applications. *Rev.*  
9 *Mod. Phys.*, [62\(4\):867–927](https://doi.org/10.1022/1522-2480(1990)62(4)867::AID-REMP867), 1990.